THE DESIGN AND SYNTHESIS OF MIXED LIGAND METAL ORGANIC FRAMEWORKS FOR XYLENE INCLUSION.

By:
Nonhlanhla Fortunate Dhlamini
Student Number: 11618249

Thesis Submitted in Partial Fulfilment for the Degree:
MSc in Chemistry

School of Mathematical and Natural Sciences
Department of Chemistry

UNIVERSITY OF VENDA
Thohoyandou, Limpopo
South Africa

Supervisor: Dr. E Batisai

Co-supervisor: Prof. L. J Barbour

March 2022

DECLARATION

I, Nonhlanhla Fortunate Dhlamini, student number 11618249, assert that the thesis titled, THE DESIGN AND SYNTHESIS OF MIXED LIGAND METAL ORGANIC FRAMEWORK FOR XYLENE INCLUSION, has not been submitted, in part or in whole for a degree at any institution. I declare that the conclusions drawn are the results of my research project except where states otherwise by acknowledgement and reference.

Student signature: .....  ..... Date: 01/07/2022

ABSTRACT

Host-guest chemistry, also known as inclusion chemistry, is an important subfield of supramolecular chemistry where there is great current interest owing to its great promise in the areas of separation of small molecules, sensors, and chiral separation. The term 'inclusion compounds' refers to the association between large compounds (host) that is able to enclose a smaller molecule (guest). This association utilizes non-covalent interactions, and the supramolecular entity is known as a "host-guest complex" or supermolecule.

The aim of the study is to design and synthesize mixed ligands metal organic frameworks (MOFs) for xylene inclusion. The first part of the study involves the synthesis and characterisation of five pyridine N-donor and O-donor ligands, namely: 2,7-di(pyridin-4-yl)benzo[lmn][3,8]phenthroline-1,3,6,8(2H,7H)tetraone(Lig1), 2,7-bis(pyridin-3-ylmethyl)benzo[lmn][3,8]phenthroline-1,3,6,8(2H,7H)tetraone(Lig2), 2-(pyridin-4-yl)-1H-benzo[de]isoquinoline-1,3(2H)-dione (Lig3), 2-(pyridin-4-ylmethyl)-1H-benzo[de]isoquinoline-1,3(2H)-dione (Lig4) and *N,N'*-bis(glycinyl)pyromellitic diimide (Lig5).

The second part involves the synthesis and characterization of MOFs. The MOFs will be synthesized by reacting the pyridine N-donor ligands, carboxylate O-donor co-ligands (fumaric acid; 2.2-bipyridine; 2.2-bipyridine-4.4'-dicarboxylic acid, 4.4'-oxybis(benzoic acid) and 2.6-naphthalenedicarboxylic acid) and transition metal salts in DMF under solvothermal conditions. The synthesized MOFs were characterized using thermogravimetric analysis (TGA), single crystal X-ray diffraction (SCXRD) and powder X-ray diffraction (PXRD). Xylene inclusion experiments were performed on the MOFs and the resulting inclusion compounds were characterized using TGA, SCXRD and PXRD.

Key words: Supramolecular Chemistry; Metal-Organic Frameworks; Xylene inclusion.

ACKNOWLEDGEMENTS

To God be the glory for none of this would have happened if it was not for him strengthening me every single day.

I appreciate my supervisor Dr. E Batisai for her patience, her willingness to help and support me throughout this whole research and giving me the opportunity to be part of this wonderful project.

My special thanks to my co-supervisor Prof. L.J Barbour from Stellenbosch University for his availability during the times of need.

I am grateful to the chemistry department in the University of Venda for allowing the opportunity to be part of their team.

My special thanks to NRF/ Sasol Inzalo for their funding.

I would also like to express my gratitude to Stellenbosch University for their characterization techniques such as TGA, SCXRD, PXRD and Vapour Sorption.

Lastly, I would like to send my warm regards to my friends and family for the support they have given me throughout this incredible journey, thank you.

DEDICATION

I devote this project to my dearest mother, Angeline Sengithule Sibongile Dhlamini; my beautiful sister, Nomalungelo and my lovely kids, Unarine and Thendo.

TABLE OF CONTENTS

LIST OF FIGURES

LIST OF TABLES

LIST OF SCHEMES

ABBREVIATIONS

Ortho-xylene – **ox**

Meta- xylene – **mx**

Para-xylene -- **px**

1-dimensional – **1D**

2-dimensional – **2D**

3-dimensional – **3D**

Linker – **L**

Metal – **M**

Asymmetric unit– **ASU**

Dimethylformamide – **DMF**

Fumaric acid- **FUM**

2,2-Bipyridine- **BPy**

2,2-Bipyridine-4,4-dicarboxyilic acid- **BPDC**

2,6_-naphthalenedicarboxylic acid – **NDC**

4,4_-oxybis(benzoic acid) – **OXB**

Single crystal X-ray diffraction – **SCXRD**

Thermogravimetric analysis – **TGA**

Powder X-ray diffraction – **PXRD**

Dynamic Vapour Sorption- **DVS**

Nuclear magnetic resonance spectroscopy - **NMR**

Metal-organic frameworks – **MOFs**

Deuterated dimethylsulfoxide – **DMSO-d6**

Deuterated chloroform – **$CDCl_3$**

Crystallographic Information File – **CIF**

2,7-di(pyridin-4-yl)benzo[lmn][3,8]phenthroline-1,3,6,8(2H,7H)tetraone – **Lig1**

2,7-bis(pyridin-3-ylmethyl)benzo[lmn][3,8]phenthroline-1,3,6,8(2H,7H)tetraone – **Lig2**

2-(pyridin-4-ylmethyl)-1H-benzo[de]isoquinoline-1,3(2H)-dione – **Lig3**

N,N'-bis(glycinyl)pyromellitic diimide – **Lig4**

Figure - **Fig**

CHAPTER 1

INTRODUCTION

1.1. SUPRAMOLECULAR CHEMISTRY

Supramolecular chemistry is an area of chemistry that specializes in the study of non-covalent interactions within and between molecules.[1] Jean-Marie Lehn introduced the term "supramolecular chemistry" and described it as "the domain of chemistry beyond that of molecules".[1] Supramolecular chemistry is amongst the advances in science that emerged by chance. The history of supramolecular chemistry dates to the 1970s, when Charles J. Pedersen synthesized crown ethers.[2] Jean-Marie Lehn and other researchers then showed interested and started synthesizing receptors.[2]

Supramolecular chemistry has two subgroups, namely host-guest chemistry and self-assembly. These two subgroups can be differentiated by the size and the shape of molecules involved. In host-guest chemistry systems, a large 'host' compound encloses a smaller 'guest' molecule in the binding region.[2] The resulting host-guest complex is known as an inclusion compound. If the guest is enclosed on all the corners of the host so that it is 'trapped', the compound is referred to as a clathrate.[3]

Self-assembly is the process whereby atoms interacting have no outstanding contrast in their sizes.[4] In this process, it does not matter whether the components are small or large[5], there is no significant difference between the sizes of the components involved.[6] The sizes may be from the molecular to the macroscopic.[6]

Molecular recognition refers to the intermolecular forces between molecules. Molecular recognition is the pillar of supramolecular chemistry[7] and, it is said that supramolecular chemistry originates from molecular chemistry.[7]

1.1.1 Host-guest chemistry

Host-guest chemistry, also known as inclusion chemistry, is a subset of supramolecular chemistry whereby a host molecule encompasses a guest molecule, and the host component is the larger molecule while the guest is the smaller molecule.[1] The host and guest are bound together by intermolecular forces, such as hydrogen bonding (Fig 1.1), pi-pi interactions, and Van der Waals forces.[8] Molecular recognition plays an important part in the formation of host-guest complexes and catalysis reactions.[1] Molecular recognition is best illustrated by the enzyme-substrate interactions in

biological systems (Fig 1.2). The binding between the host and guest species is defined by the two moieties involved and is illustrated in the equation below.[8]

$$H + G \leftrightarrow HG$$, H= "Host", G= "Guest" and HG= "Host-guest complex".

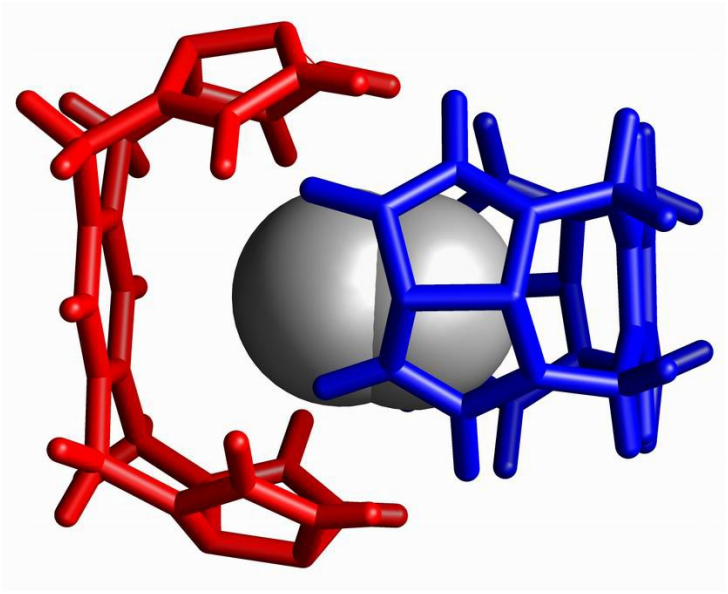

Figure 1.1. A guest is bound within a host hydrogen-bonded capsule.[9]

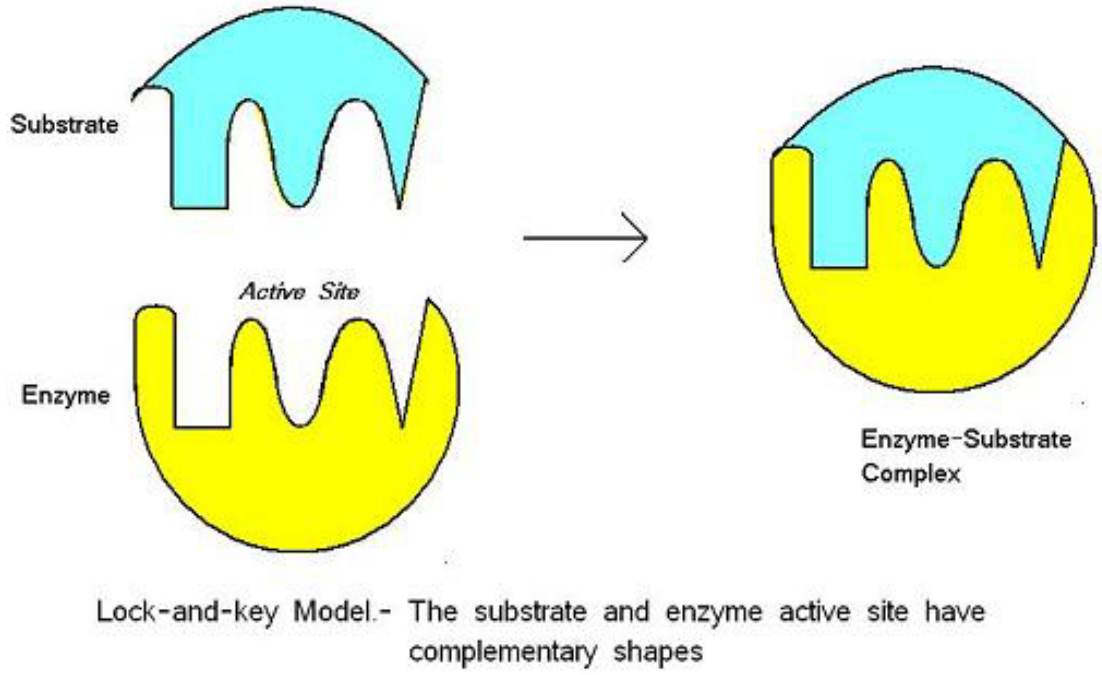

Figure 1.2. An example of a "Lock and Key "model of enzyme and substrate in biological systems.[10]

1.2. INTERMOLECULAR INTERACTIONS

Intermolecular interactions or non-covalent interactions are the force that connects different molecules. In host-guest systems, intermolecular interactions also organize molecules in an ordered manner to form a crystal or a supermolecule.[5] These intermolecular interactions include electrostatic, van der Waals forces, π-effects, and coordinate bonds.[2] Electrostatic interactions involve ionic, hydrogen bonding, and halogen bonding. Ionic interactions are the strongest and their strength is almost the same as that of covalent bonds, and they can occur in any orientation. Van der Waals forces, unlike electrostatic, are directionally dependent.[6] Types of π-effects, include π- π interactions, cation- π, and anion- π interactions. The different types of non-covalent interactions, their strength, and their examples are given in Table 1.1.

Table 1.1. Types of non-covalent interactions, their strength, and examples.[11]

Interaction	Strength bond energy (kJ mol^{-1})	Example
Ion-ion	100-350	Sodium chloride
Ion-dipole	50-200	Crown ethers and alkaline metal ions
Dipole-dipole	5-50	Acetone
Hydrogen bonding	4-120	Amino acids
π-π interaction	0-50	Benzene and graphite
Van der Waals	<5 kJ mol^{-1} but variable depending on the surface area	Argon, molecular crystals
Hydrophobic effect	Related to solvent- solvent interaction.	Cyclodextrin inclusion compounds

1.2.1. Hydrogen bonding

Hydrogen bonding may be defined as an attraction formed between a lone pair of an electronegative atom (nitrogen, oxygen, or fluorine) and a hydrogen atom.[3] Hydrogen bonding is a strong electrostatic interaction which has some features of covalent bonding.[12] This interaction has three classes, namely, very strong (15-40 kcal/mol), strong (4-15 kcal/mol), and weak (0-4 kcal/mol) according to strength and directionality (Table 1.2).[13-15]

Hydrogen bonding serves as the backbone for the development of some synthetic receptors, artificial enzymes, and the design of supramolecular crystals. An example of hydrogen bonding interaction is shown in Fig 1.3.

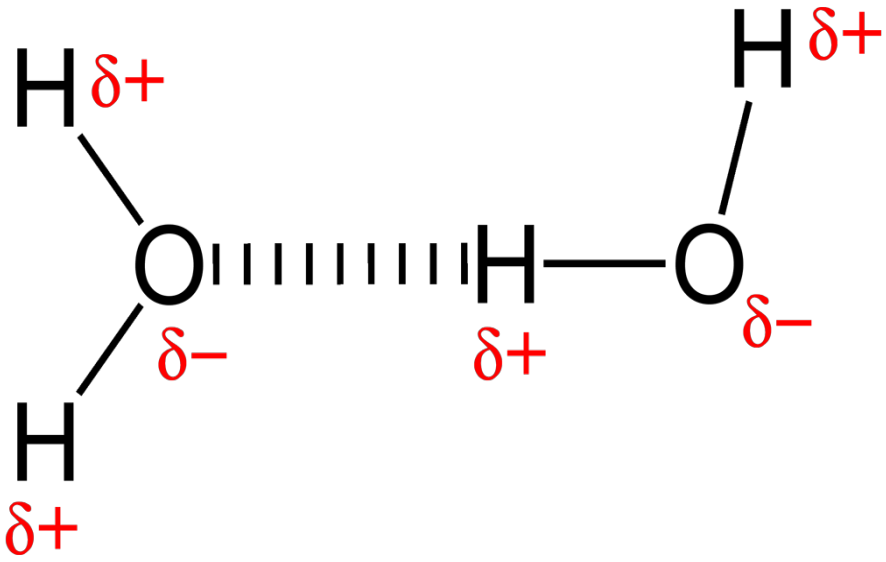

Figure 1.3. A hydrogen bond between a partially positive hydrogen atom and partially negative oxygen in water 2D.[18]

Table 1.2. Properties of very strong, strong, and weak hydrogen bonds.[19]

	Very Strong	Strong	Weak
Type of interaction	Covalent	Electrostatic	Dispersive
Bond Energy/kcal mol^{-1}	15-40	4-15	<4
Examples	$[F{---}H{---}F]^-$	O-H---O=C	C-H---O

	$[N---H---N]^+$	O-H---O-H	O-H---π
Bond Lengths / Å			
H---A	1.2-1.5	1.5-2.2	2.0-3.0
Lengthening of D-H/ Å	0.08-0.25	0.02-0.08	$<$0.02
D-H versus H---A	D-H~ H---A	D-H$<$H---A	D-H$<<$ H---A
D---A / Å	2.2-2.5	2.5-3.2	3.0-4.0
Bond shorter than Van Der Waals radii	100%	About 100%	30-80%
Directionality	Strong	Moderate	Weak
Bond angles, θ/°	170-180	$>$130	$>$90
Effect on crystal packing	Strong	Distinctive	Variable
Utility in crystal engineering	Unknown	Useful	Partly useful

1.2.2. Pi-pi interactions

Pi-pi interactions take place between two or more neighbouring aromatic rings whereby one of the rings is electron-rich while the other one is electron-deficient.[4] The attractive force behind this stacking phenomena is electrostatic.[5] Aromatics may interact with one another in two common ways which are, face-to-face (displaced & sandwich) and edge-to-face (T-shaped) interactions. The face-to-face or pi-pi stacking is responsible for the 'slick texture' of the graphite.[5] The pi-pi interactions that hold together the covalently bonded lattice sheets in the graphite structure, tend to easily slide over each other. The T-shaped or edge-to-face interactions are responsible for the herringbone packing pattern of small aromatic hydrocarbons in some structures.[2] The different types of pi- pi stacking are shown in Fig 1.4.

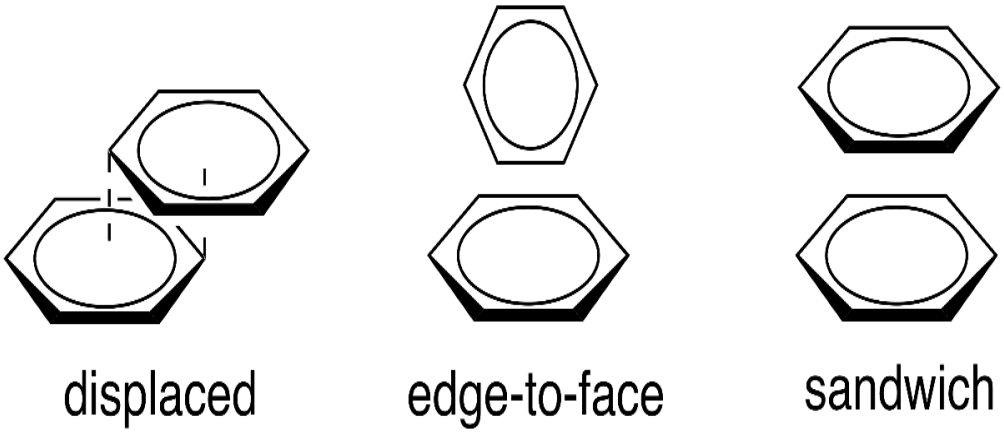

Figure 1.4. Three different types of π-stacking confirmations of benzene dimer.[5]

1.2.3. Van der Waals forces

Van der Waals are forces of attraction and repulsion between atoms or molecules. They are caused by correlation in the fluctuating polarizations of neighbouring particles.[2] These forces depend on the distance between atoms or molecules and are weaker than ionic or covalent bonds.[2,20] They play a significant role in the field of supramolecular chemistry. They are liable to disturbance and quickly disappear at longer distances between interacting molecules.[2]

1.2.4. Coordinate Bonds

A coordinate bond is a bond that is formed between two atoms where one of the atoms (a ligand) donates a pair of electrons to an empty metal orbital to form a coordinate bond.[21] This bond is basically a covalent bond, the only difference is that in the coordinate bond, the shared pair of electrons is provided by one atom.[21] The coordinate bond plays a vital role in the formation of coordination polymers.[22] The coordinate bond is considered the strongest among all the intermolecular forces with the strength ranging from 20 to 45 Kcal/mol.[22]

1.3. CRYSTAL ENGINEERING

Crystal engineering refers to the study of intermolecular forces and their utilization in the synthesis and preparation for compounds that have desired properties.[23] Crystal engineering utilizes the concepts

of molecular recognition, self-organization, and supramolecular synthons as design strategies. There are two types of intermolecular interactions commonly used in crystal engineering of new solid forms with desired properties, i.e., hydrogen bonding and coordinate bonding.[24]

1.3.1. Supramolecular synthons

A supramolecular synthon, according to Desiraju, "is a recurring pattern that often occurs between the same functional groups in the solid state".[6] Though supramolecular synthons act as a connection between molecules, they are different from functional groups of a molecule.[6] The difference lies in the kind of bond used to connect the molecules. Functional groups are bonded *via* covalent bonding whereas supramolecular synthons are moieties containing hydrogen-bonded complementary functional groups.[6] Synthons are divided into two groups; homosynthons and heterosynthons. Homosynthons include acid dimers, amide dimers and urea dimers. Heterosynthons form between different but complementary functional groups. Examples of heterosynthons include acid-amide dimer, acid-pyridine dimer and naphthyridine- acid dimer (Fig. 1.5).[6]

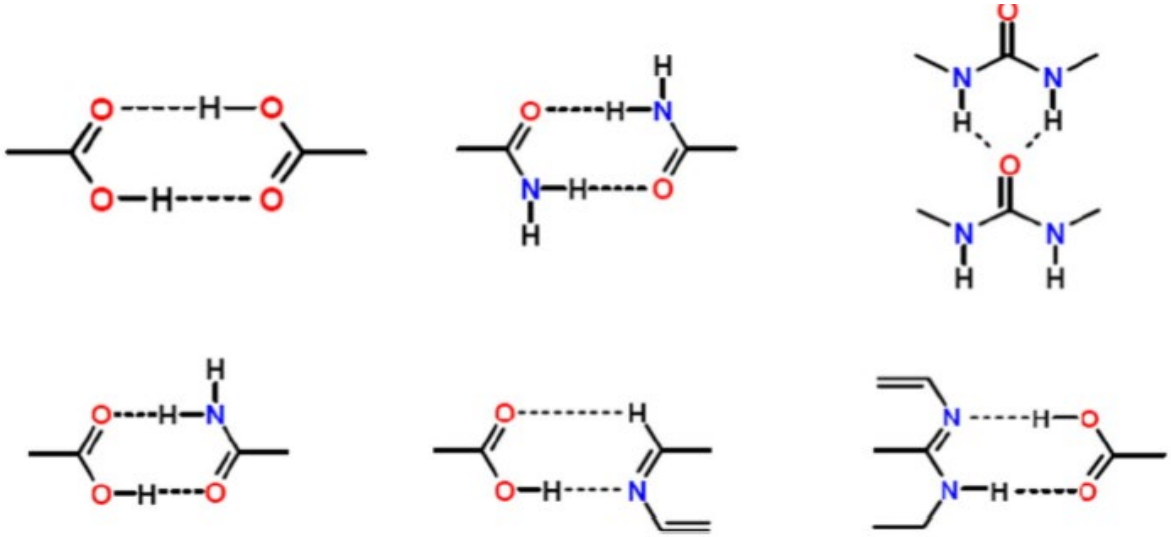

Figure 1.5. Common examples of supramolecular synthons (the first three dimers at the top are examples of HOMO-synthons: far left is acid dimer; in the middle is amide dimer; far right is urea dimer, and the last three at the bottom are examples of HETERO-synthons: on the left is acid-amide dimer; in the middle is acid-pyridine; on the right is naphthyridine-acid dimer).[6]

1.4. COORDINATION COMPOUNDS

A coordination compound is a complex that contains a central metal ion, also known as a coordination centre, surrounded by molecules or ions that are referred to as ligands.[25] The coordinate covalent bond joining the ligands and metal centre involves the donation of a lone pair of electrons from the ligand to the vacant orbital of a metal centre.[26] Coordination compounds are usually formed by the process of self-assembly during the crystallization of a metal salt with a ligand. The methods used to prepare coordination compounds may include slow evaporation, solvent layering, slow cooling and solvothermal.[27]

1.5. METAL ORGANIC FRAMEWORKS (MOFs)

MOFs are compounds that comprise organic linkers and metal ions joined to form one-, two-, or three-dimensional structures.[28]. In one-dimension, the coordination bonds are spread over the compound in one direction, while in a two-dimension are spread over two directions and lastly, in a three-dimension, the coordination bonds run through all three directions. The voids in a one-dimension structure can only take small guests.[28] In a two-dimension structure, layers are connected through an edge-to-face kind of stacking whereas, in a three-dimensional structure, the frameworks are very stable and porous due to the coordination bonds spread in all three directions.[28]

MOFs contain potential voids that remain stable during the removal of the guest molecules. Due to their high porosity, crystallinity, large surface area, ultra-low densities, tunable pore functionality and thermal stability[29,30], MOFs have many potential applications.[29] These applications include gas storage, gas separation, gas purification, gas adsorption, sensing, bio-medical, ion-exchange, separation of isomers and catalysis.

The study of MOFs originated from zeolites. Zeolite's synthesis uses ions that influence the structure of the growing inorganic framework. Those ions are called "templates". The porous structure of zeolites can accommodate as many cations as possible such as Mg^{2+}, Ca^{2+}, K^{+}, etc. These cations are loosely held and can be readily substituted by other cations in a contact solution.[31]

MOFs can be synthesized by numerous methods such as solvent evaporation, mechanochemical synthesis, electrochemical, microwave-assisted, microfluidic synthesis, solvothermal, and hydrothermal.[32] The most common methods are solvothermal and hydrothermal. These methods

involve slowly growing crystals under high pressure and temperature. Solvothermal method is a chemical reaction that takes place in a solvent at a temperature higher than the solvent's boiling point in a sealed flask. Hydrothermal method is defined as a chemical reaction that occurs in an aqueous solution above the boiling point of water in a sealed pressure flask. The structure of the resulting MOF is influenced by factors such as pH, molar ratio, temperature, and solvent.[28][32]

1.6. LITERATURE REVIEW

1.6.1. Metal-organic frameworks (MOFs) in xylene isomers separation.

MOFs are potential candidates for xylene separation due to their porosity.[29] Xylene isomers separation is achieved by immersing a porous MOF in a mixture of xylene isomers or exposing an activated MOF to a mixture of xylene vapours using a microbalance. The resulting clathrates can be characterized using single crystal X-ray diffraction (SCXRD), thermogravimetric analysis (TGA), and gas chromatography (GC), to determine the amount of xylene included in the framework.

Metal-organic frameworks with the ability to selectively include one xylene isomer over the other two isomers have been reported. For instance, Mukherjee, S, *et al* successfully synthesized a novel dynamic MOF using a ligand with two flexible ether linkages. Due to the ether linkages functioning as adjustable nodes, the MOF showed high degree of framework flexibility and could selectively adsorb *para* xylene over *meta* and *ortho* xylene.[33]

MOFs can be used as energy efficient adsorbents in industrial feedstocks separations.[34] Chen et al synthesized a MOF containing an expanded porous network of alkali metal salts and γ-cyclodextrin (γ-CD), CD-MOF. The ability of the CD-MOF-1 to separate xylene isomers was investigated using a batch vapor-phase and a liquid-phase adsorption method.[34] The MOF showed preferable adsorption of *o*-xylene over the para and meta-xylene isomers, with adsorption strength in the order *o*-xylene (*o*X) > *m*-xylene (*m*X) > *p*-xylene (*p*X). It was also reported that, at high temperatures, adsorption capacities of *o*X and *m*X over *p*X are higher. Nevertheless, a decrease in the separation factors of *oX*/*p*X and *m*X/*p*X was also detected. The authors concluded that CD-MOF-1 is a reliable and efficient alternative adsorbent for the separation of xylene isomers compared to other methods that are presently utilised in the petrochemical industry.[34]

MIL-53 metal-organic frameworks have become interesting potential adsorbents for separation of xylene isomers.[35] Three materials - MIL-53(Al), MIL-53(Cr), and MIL-53(Fe) - were chosen for comprehensive quaternary liquid advance measurements.[35] These MOFs are made up of terephthalic acid as the linker and the combination of three metal salts (Al, Cr, Fe). All the MIL-53 materials showed high o-xylene quaternary selectivity, with MIL-53(Al) being the most selective. The high o-xylene selectivity is attributed to the interactions of o-xylene with the MIL-53 (Al) framework and better packing efficiency.[36] Good overall agreement of the predictions from flexible-structure multicomponent adsorption simulations with the experiment were obtained.[36]

1.6.2. Werner complexes in xylenes separation.

Werner complexes are octahedral zero-dimensional (0-D) compounds with the general formula MX_2L_4, where M is a metal salt (M= Co, Ni, Mn, Fe, Cd, Cu), X is an anion (X= Cl, SCN, NO_2, CN, NO_3) and L is an organic ligand (L= Substituted pyridine, α-arylalkylamine, isoquinoline).[37] These complexes can enclathrate aromatic guests and can therefore be employed in the separation of mixtures of aromatic compounds.[37] The most commonly studied compounds have the general formula $[Ni(NCS)_2(4\text{-}RPy)_4]$, where RPy is an alkyl or aryl substituted pyridyl group.[37] The most commonly utilised method for the synthesis of Werner complexes is the mechanochemical method. Werner complexes can be characterized using SCXRD, TGA and PXRD.[38] Werner complexes have earned a place in the separation of hydrocarbons with similar boiling points such as xylenes, because they can trap guest molecules in their lattice. [38-39]

The Werner host $[Ni(NCS)_2(para\text{-}phenylpyridine)_4]$ was used to selectively enclathrate *ortho* xylene over *para* xylene and *meta* xylene from an equimolar ternary mixture. The Werner host was also utilized to separate *meta* xylene over *para* xylene from a binary mixture of the xylene vapours.[40] Schaeffer, W.D, separated *o*-xylene from its isomers by preferential clathrate formation.[41] Using ultraviolet analysis, the following isomer distributions were obtained (isomer, % in mixed isomers): *p*-xylene, 19.9; *m*-xylene, 45.5.[41]

McCandless, F.P, *et al* investigated the separation of xylene isomers using a poly(vinylidene fluoride) membrane modified with $Ni(SCN)_2(4\text{-methylpyridine})_4$ and $Ni(SCN)_2(\alpha\text{-methylbenzylamine})_4$ Werner complexes.[42] Their results show that $Ni(SCN)_2(4\text{-methylpyridine})_4$ and $Ni(SCN)_2(\alpha\text{-methylbenzylamine})_4$ enhanced the selectivity of the poly(vinylidene fluoride) membrane for *p*-xylene over *m*-xylene and *o*-xylene.[42] Nassimbeni L. R, *et al* separated xylene isomers by enclathration involving three organic host compounds; 9.9'-bianthryl (H1), 9.9'-spirobifluorene (H2)

and trans-2.3-dibenzoylspiro[cyclopropane-1.9-fluorene] (H3). It was concluded that the three hosts H1, H2, and H3 can distinguish between the three xylene isomers by forming clathrates. H1 encloses both *ortho* xylene and *para* xylene but favours *ortho* xylene, on the other hand, H2 and H3 enclathrate both *para* and *ortho* xylene respectively.[43]

Wicht et *al* synthesised and elucidated a Werner host [Ni(NCS)$_2$ (isoquinoline)$_4$]. The host did not favour any of the xylene isomers, indicating that this Werner host has poor selectivity. The poor selectivity is due to the lack of torsional flexibility of the isoquinoline ligands.[44]

1.6.3. Ligand- Exchange

A ligand is defined as an ion or a molecule that forms a coordination complex by binding to a central metal atom.[45] A ligand can be replaced by another in a compound, and that chemical reaction is referred to as ligand- exchange, also known as ligand substitution. Ligand- exchange occurs via associative substitution or by dissociative substitution. Both the associative and dissociative substitutions are pathways whereby compounds interchange ligands but differs in a way that the associative substitution is comparable to SN_2 pathway, and the dissociative substitution resembles the SN_1 mechanism.[46]

1.7. MOTIVATION

There are three isomers of xylene; *ortho*- (*o*-), *meta*- (*m*-), and *para*- (*p*-).[47] Xylene isomers are important reagents in the industry; *para*-xylene can be oxidized to terephthalic acid, *ortho*-xylene can be used to synthesize phthalic anhydride, and *meta*-xylene can be converted to isophthalic acid.[48] Xylenes can also be used as solvents and to make baths with dry ice in the laboratory.[49] Each of the isomers has a boiling point of about 140 °C (*ortho* 144 °C, *meta* 139 °C and *para* 138 °C) (Table 1.3), but different melting points ranging from -48 °C to 13 °C.[50] Xylene isomers have similar physical and chemical properties.[51] Due to the xylene isomer's properties, it is very difficult to separate them into their pure forms.[52-54] Fractional distillation can be used to remove *para*-xylene and *meta*-xylene from the less volatile *ortho*-xylene because of their similar boiling points.[55- 65] Though they can be separated by fractional distillation[54], the process is inefficient, very expensive and it involves the use of about 150 theoretical plates, therefore, there is a great need for much cheaper alternative methods.

This aim of this project is to design and synthesize MOFs for xylene inclusion. In this project, we plan to separate the xylene isomers from the mixture into their pure forms. The mixture of the xylene is originally from catalytic reforming of crude oil [48], and it is well known that each one of these isomers plays a vital role individually in the industry. The MOFs will be synthesized by reacting transition metal salts, carboxylate ligands (Scheme 1.1) and pyridine donor naphthalene diimide ligands: 2,7-di(pyridin-4-yl)benzo[lmn][3,8]phenthroline-1,3,6,8(2H,7H)tetraone(Lig1), 2,7-bis(pyridin-3-ylmethyl)benzo[lmn][3,8]phenthroline-1,3,6,8(2H,7H)tetraone(Lig2), 2-(pyridin-4-yl)-1H-benzo[de]isoquinoline-1,3(2H)-dione (Lig3), 2-(pyridin-4-ylmethyl)-1H-benzo[de]isoquinoline-1,3(2H)-dione (Lig4) and *N,N'*-bis(glycinyl)pyromellitic diimide (Lig5) (Scheme 1.2). The MOFs are expected to enclathrate xylene isomers via pi-pi interactions between the xylene and the naphthalene diimide moiety. Skeletal structures of *ortho*-, *meta*-, and *para*-xylene are displayed in Fig 1.6 and a table of the boiling points, and the melting points of the xylene isomers is also displayed in table 1.3.

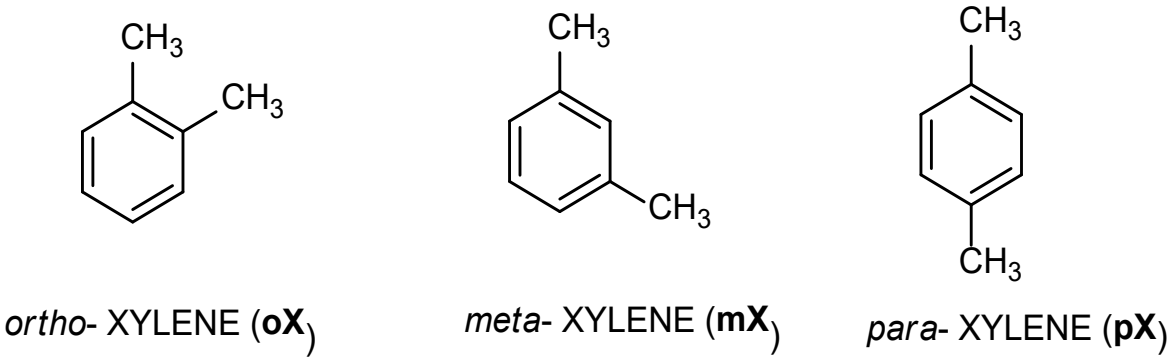

Figure 1.6. Structures of the three xylene isomers.[47]

Table 1.3. A table displaying xylene isomer's boiling and melting points.[50]

Xylene Isomers	*ortho*	*meta*	*para*
Melting points/ ºC	-25	-48	+13
Boiling points/ ºC	144	139	138

1.8. AIM AND OBJECTIVES

AIM:

The aim of this study is to synthesise and characterize porous MOFs for xylene inclusion.

OBJECTIVES:

- To synthesize and characterize the pyridine N-donor ligands.
- To synthesize MOFs by reacting pyridine N-donor ligands, carboxylate O-donor co-ligands and transition metal salts.
- To characterize the MOFs using thermogravimetric analysis (TGA), single crystal X-ray diffraction (SCXRD), and powder X-ray diffraction (PXRD).
- To test for the porosity of MOFs by xylene inclusion.

Co-ligands

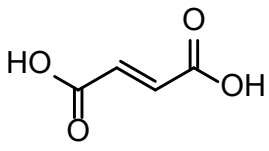

Fumaric acid

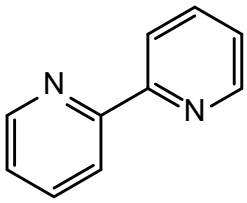

2,2'-bipyridine

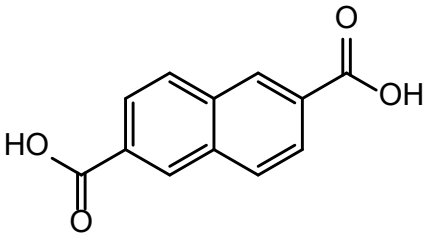

2,6-naphthalenedicarboxylic acid

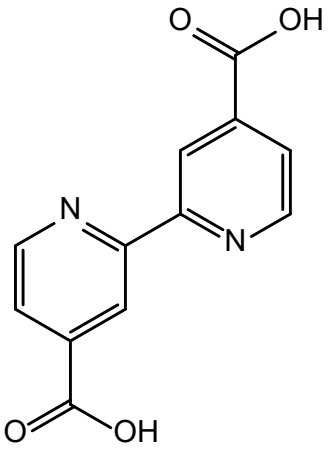

[2,2'-bipyridine]-4,4'-dicarboxylic acid

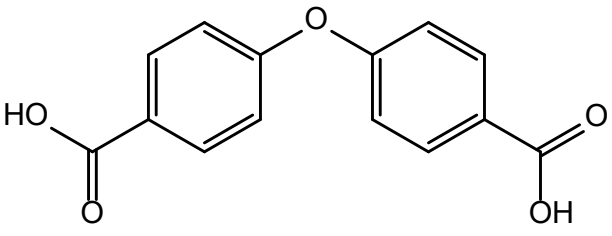

4,4'-oxydibenzoic acid

Scheme 1.1. The schematic diagrams of the co-ligands

MAIN LIGANDS

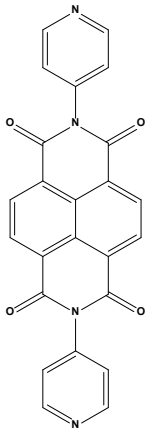

2,7-di(pyridin-4-yl)benzo[*lmn*][3,8] phenanthroline-1,3,6,8(2*H*,7*H*)-tetraone **(Lig 1)**

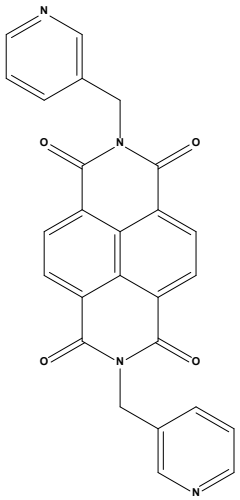

2,7-bis(pyridin-3-ylmethyl)benzo[*lmn*][3,8] phenanthroline-1,3,6,8(2*H*,7*H*)-tetraone **(Lig2)**

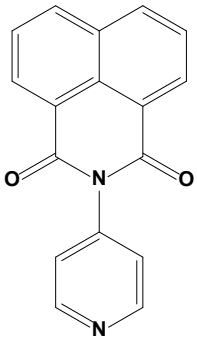

2-(pyridin-4-yl)-1H-benzo[de] isoquinoline-1,3(2H)-dione **(Lig3)**

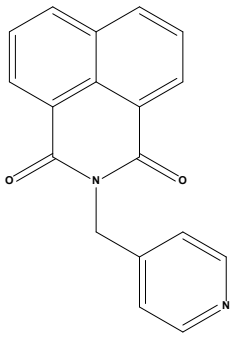

2-(pyridin-4-ylmethyl)-1*H*-benzo[*de*] isoquinoline-1,3(2*H*)-dione **(Lig4)**

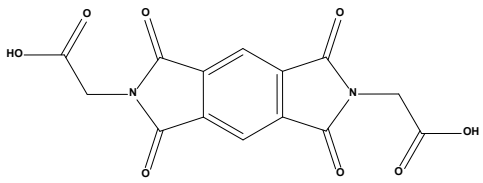

N,N'-bis(glycinyl)pyromellitic diimide **(Lig5)**

Scheme 1.2. The schematic diagrams of the successfully synthesized ligands.

REFERENCES

1. Lehn, J.M. 1995. “Supramolecular Chemistry”. Concepts and Perspectives. New York.
2. Steed, J.W. Atwood, J.L. 2009. “Supramolecular Chemistry”. 2nd edn. Wiley. United Kingdom.
3. ANON. Comendium of Chemical Terminology, 2nd ed. (the “Gold Book”). 1997. Online corrected version: 2006. “Hydrogen bond”.
4. Desiraju, G.R. 2013. *J. Am. Chem. Soc*. **135**: 9952.
5. Hunter, C.A. Sanders, J.K.M. 1990. *J. Am. Chem. Soc.* **112**: 5525.
6. Desiraju, G.R. 1996. eds. MacNicol, D.D, Toda, F and Bishop, R. Pergamon. 1996. *Cryst. Eng. Comm.* **6**: 4.
7. Gellman, S.H. 1997. *Chemical Reviews.* **97**: 1231.
8. Lodish, H. Berk, A. Kaiser, C. 2008. Molecular Cell Biology. ISBN 978-0-7167-7601-7.
9. Valdés, C. Toledo, L.M. Spitz, U. Rebek, J. 1996. "Structure and Selectivity of a Small Dimeric Encapsulating Assembly". *Chem. Eur. J.* **2**: 989.
10. Anslyn, E.V. Dougherty, D.A. 2005. Modern Physical Organic Chemistry. MacMillan. ISBN 978-1-891389-31-3.
11. Matsumoto, K. Hayashi, N. 2009. “Hetorocyclic Supramolecules II”. Springer. New York.
12. Lindh, U. 2012. “Biological functions of the elements”. Essentials of Medical Geology. Springer. Dordrecht.129-177.
13. Shattock, T.R. Arora, K.K. Vishweshwar, P. Zaworotko, M.J. 2008. *Cryst. Growth. Des*. **8**: 4533.
14. Kirby, A. J. 1996. *Angew. Chem. Int. Ed. Engl*. **35**: 707.
15. Anslyn, E. 2004. Modern Physical Organic Chemistry. Sausalito, CA: University Science. ISBN 978-1-891389-31-3.
16. Desiraju, G.R. 1989. *Crystal Engineering: The Design of Organic Solids*, Elsevier: Amsterdam.
17. MacDonald, J.C. Whitesides G.M. 1994. *Chem Rev.* **94**: 2383.
18. Luning, U. Kuhl, C. 1998. *Tetrahedron Lett.* **39**: 5735.
19. Desiraju, G.R. Steiner, T. 2006. “The Weak Hydrogen Bond in Structural Chemistry and Biology”. Oxford University Press. New York.
20. Leite, F.L, Buen, C.C, Da Roz, A.l, Zeimath, E.C. Oliverira, O.N. 2012. *Int. J. Mol. Sci.* **13**: 12773.
21. Nangia, A. 2010. *J. Chem. Sci.* **122**: 295.
22. Hosseini, M. 2003. *Coord. Chem. Rev*. **240**: 157
23. Desiraju, G.R, Vittal, J.J. Ramanan, A. 2011. “Crystal Engineering Textbook”. World Scientific. India.
24. Dunitz, J.D. 1991. *Pure. Appl. Chem*. **63**: 177.

25. Geoffrey, A.L. 2009- 2010. “Introduction to Coordination Chemistry”. John Wiley & Sons. University of Newcastle.
26. Cotton, F.A. Geoffrey, W. Murillo, C.A. 1999. “Advanced Inorganic Chemistry”. Wiley. University of Michigan.
27. Werner, A. 1893. *Z. Anorg. Chem*. **3**: 267.
28. Batten, S.R. Champness, N.R. Chen, X.M. Garcia- Martinez, J. Kitagawa, S, Ohrstrom, L. Cejka, J. 2011. “Metal- Organic Frameworks”. Wiley. Germany.
29. Cejka, J. ed. 2011. Metal-Organic Frameworks Applications from Catalysis to Gas Storage. Wiley-VCH. ISBN 978-3-527-32870-3.
30. Murray, L.J. Dincă, M. Long, J.R. 2009. "Hydrogen storage in metal-organic frameworks". *Chem. Soc. Rev*. **38**: 1294.
31. Bucar, D.K. Papaefstathiou, G.S. Hamilton, T.D. Chu, Q.L. Georgiev, I.G. MaGillivray, L.R. 2007. *Eur. J. Inorg. Chem.* **2007**: 4559.
32. Cheetham, A.K. Ferey, G. Loiseau, T. 1999. *Angew. Chem. Int. Ed.* **38**: 3268.
33. Mukherjee, S. Joarder, B. Manna, B. Desai, A.V. Chaudhari, A. K. Ghosh, S. K. 2014. *Sci. Rep*. **4**: 5761.
34. Chen, L. Zhu, D. Ji, G. Yuan, S. Qian, J. He, M. Chen, Q. Zhang, Z. 2018. *J. Chem. Tech. and Biotech*. **93**: 2898.
35. Agrawal, M. Bhattacharyya, S. *et al.* 2018. *J. Phys. Chem*. **122**: 387.
36. Wu, X. Wei, W. Jiang, J. Caro, J. Huang, A. 2018. *Int. Edition*. **57**: 15354.
37. Batisai, E. Lusi, M. Jacobs, T. Barbour, L.J. 2012. *Chem. Commun*. **48**: 12171
38. Atwood, J.L. 2012. Inclusion Compounds. Wiley- VCH.
39. Schaeffer, W.D. 1959. Werner Complexes of Metal Cyanides. United States.
40. Lusi, M. Barbour, L.J. 2012. *Angew. Chem. Int. Ed*. **51**: 3931
41. Schaeffer, W.D. McKinnis, A.C. Dorsey, W. S. 1958. Separation of Organic Compounds by Clathrate Formation. United States.
42. Sikonia, J.G; McCandless, F. P. 1978. *J. Membrane. Sci*. **4**: 229.
43. Nassimbeni, L.R. Bathori, N.B. Patel, L.D. Su, Hong. Weber, E. 2015. *Chem.Commun*. **51**: 3627.
44. Wicht, M.M. Bathori, N.B. Nassimbeni, L.R.2015. *Dalton Trans*. **44**: 6863.
45. Burdge, J. Overby, J. 2020. Chemistry- Atoms first. *4th ed*. New York. McGraw Hill.
46. Basolo, F. Pearson, R.G. 1967. Mechanisms of Inorganic Reactions. New York. Jonh Wiley and Son.

47. Fabri, J. Graeser, U. Simo, T.A. 2000. "Xylenes". *Ullmann's Encyclopedia of Industrial Chemistry*. doi:10.1002/14356007. Kandyala, Reena; Raghavendra, Sumanth Phani C. Rajasekharan, Saraswathi T. (2010).
48. "Xylene: An overview of its health hazards and preventive measures" (https://www.ncbi.nlm.nih.gov/pmc/articles/PMC2996004). *J Oral Maxillofac Pathol*. **14:** 1.
49. Zhou, Y.Wu, J. Lemmon, E.W. 2012. Thermodynamic properties of o-xylene, m-xylene, p-xylene, and ethylbenzene. *J. Phys. Chem*. **41**: 023103.
50. Gu, Z.Y. Yan, X.P. 2010. Metal-organic framework MIL-101 for high-resolution gas-chromatographic separation of xylene isomers and ethylbenzene. *Angew. Chem. Int. Ed.* **49**: 1477.
51. Ashraf, M.T. Chebbi, R. Darwish, N.A. 2013. Process of p-xylene production by highly selective methylation of toluene. *Ind. Eng. Chem. Res.* **52**: 13730.
52. Ma, Y. Zhang, F. Yang, S. Lively, R.P. 2018. Evidence for entropic diffusion selection of xylene isomers in carbon molecular sieve membranes. *J. Membr. Sci*. **564**: 404.
53. Yang, Y. Bai, P. Guo, X. 2017. Separation of xylene isomers: A review of recent advances in materials. *Ind. Eng. Chem. Res.* **56**: 14725.
54. Rodrigues, A.E. Pereira, C. Minceva, M. Pais, L.S. Ribeiro, A.M. Ribeiro, A. Silva, M. Graca, N. Santos, J.C. 2015. The Parex¸ Process for the Separation of p-Xylene. In Simulated Moving Bed Technology; Rodrigues, A.E. Pereira, C. Minceva, M. Pais, L.S. Ribeiro, A.M. Ribeiro, A. Silva, M. Graca, N. Santos, J.C. *Eds.* Butterworth-Heinemann: Oxford. 117–144.
55. Broughton, D.B. Neuzil, R.W. Pharis, J.M. Brearley, C.S. 1970. The Parex process for recovering paraxylene. *Chem. Eng. Prog.* **66**: 70.
56. Ash, G. Barth, K. Hotier, G. Mank, L. Renard, P. 1994. Eluxyl: a new paraxylene separation process. *Rev. Inst. Fr. Pet.* **49**: 541.
57. Jin, W. Wankat, P.C. 2007. Hybrid simulated moving bed processes for the purification of p-xylene. *Sep. Sci. Technol.* **42**: 669.
58. Minceva, M. Rodrigues, A.E. 2007. Understanding and revamping of industrial scale SMB units for p-xylene separation. *AIChE J.* **53**: 138.
59. Cottier, V. Bellat, J.P. Simonot-Grange, M.H. Méthivier, A. 1997. Adsorption of p-xylene/m-xylene gas mixtures on BaY and NaY zeolites. Coadsorption equilibria and selectivities. *J. Phys. Chem. B* **101**: 4798.

60. Bellat, J.P. Simonot-Grange, M.H. 1995. Adsorption of gaseous pxylene and m-xylene on NaY, KY, and BaY zeolites. Part 2: Modeling. Enthalpies and entropies of adsorption. Zeolites. **15**: 219.
61. Cottier, V. Pilverdier, E. Simonot-Grange, M.H. Bellat, J.P. 1999. Derivative enthalpies of adsorption of p-xylene and m-xylene onto NaY and BaY Zeolites at 150 °C: Contribution to the prediction of adsorption selectivity. *J. Therm. Anal. Calorim*. **58:** 121.
62. Daems, I. Leflaive, P. Méthivier, A. Denayer, J. Baron, G. 2005. Size and Packing Related Adsorption Effects in the Liquid Phase Adsorption of Aromatics and Alkenes on FAU Type Zeolites. In MolecularSieves: From Basic Research to Industrial Applications; cejka,ˇ J. Ž ilkova, N. Nachtigall, P. *Eds*. Elsevier. **158**: 1177.
63. Daems, I. Leflaive, P. Méthivier, A. Baron, G.V. Denayer, J.F. 2006. Influence of Si:Al-ratio of faujasites on the adsorption of alkanes, alkenes and aromatics. Microporous Mesoporous Mater. **96**: 149.
64. ICIS, *Para*xylene-*Ortho*xylene | Prices, News & Market Analysis (http://www.icis.com/chemicals/paraxylene-orthoxylene/), icis.com, 2012. Accessed 2012-4-28.
65. "Coolingbaths"(http://chemwiki.ucdavis.edu/Reference/Lab_Techniques/Cooling_baths). UC Davis Chem Wiki. 2013-10-02. Retrieved 8 February 2015.

CHAPTER 2

EXPERIMENTAL

This chapter discusses ligand and metal organic frameworks synthesis and characterization.

2.1. THE SYNTHESIS AND CHARACTERIZATION OF THE LIGANDS

2.1.1. Synthesis of ligand 1 (Lig1)

Synthesis of 2,7- di(pyridine-4-yl)benzo[lmn][3,8]phenthroline-1,3,6,8(2H, 7H)-tetraone (Lig1) involves refluxing a mixture of 1,4,5,8-naphthalenetetracarboxylic dianhydride (NTCD) (1.0 g; 3.73 mmol) and 4-aminopyridine (AMP) (0.7 g; 7.46 mmol) in dimethylformamide (DMF) (15 mL). The solution was stirred at 160 °C for 12 hours. The crude solid product was collected by filtration and washed with DMF. The ligand was analysed using nuclear magnetic resonance (NMR). The synthetic procedure of the Lig1 is presented in Scheme 2.1. Yield: 87.58%, ^{1}H-NMR (DMSO-d6, 400 MHz) δ/ppm 7.60 (d, 4H), 7.48 (d, 4H), 7.33 (d, 4H). ^{13}C-NMR (DMSO-d6, 100 MHz) δ /ppm: 149.95 (C * 4), 136.19 (CH * 4), 137.02 (C * 2), 128.19 (C * 4), 123.94 (C * 2), 113.96 (CH * 4), 129.10 (CH * 4). The spectra of Lig1 are presented in Figure 2.1. and Figure 2.2.

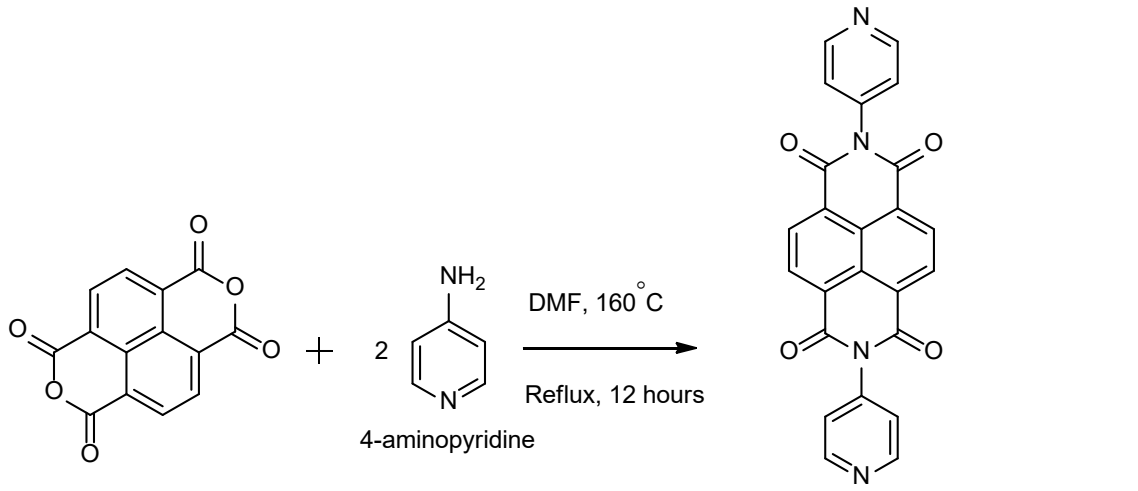

Scheme 2.1 Synthesis of 2,7- di(pyridine-4-yl)benzo[lmn][3,8]phenthroline-1,3,6,8(2H, 7H)-tetraone (Lig1).

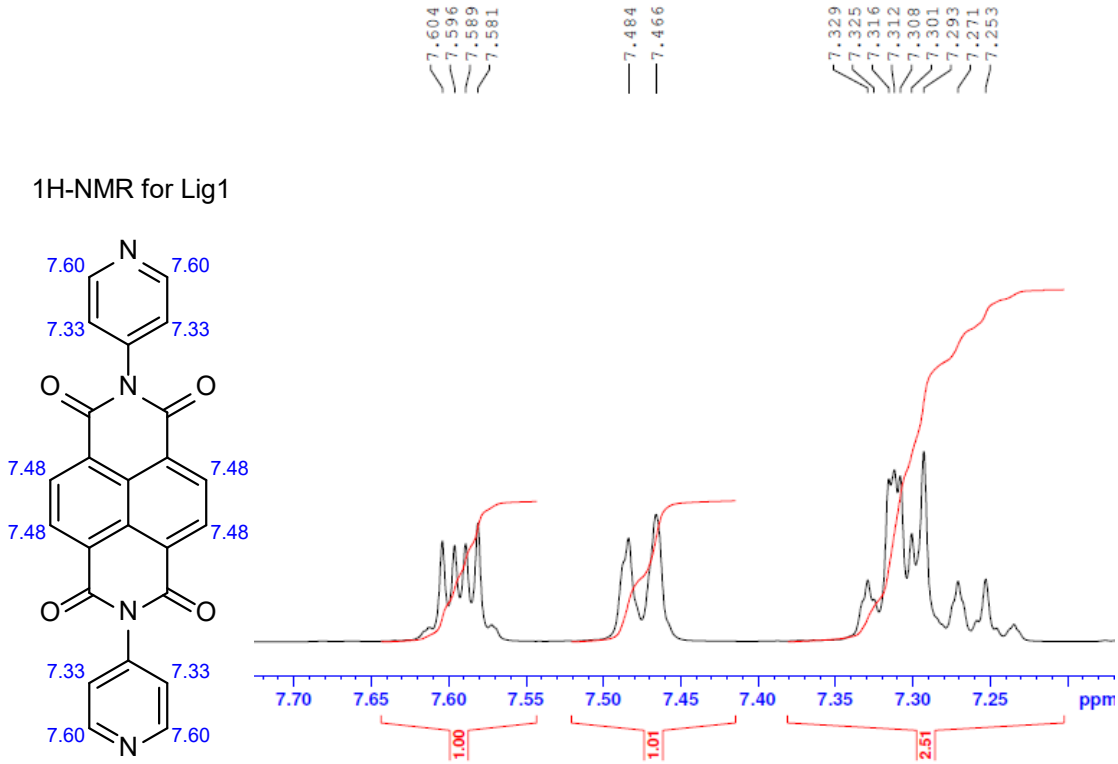

Figure 2.1. The ^{1}H-NMR spectrum for Lig1.

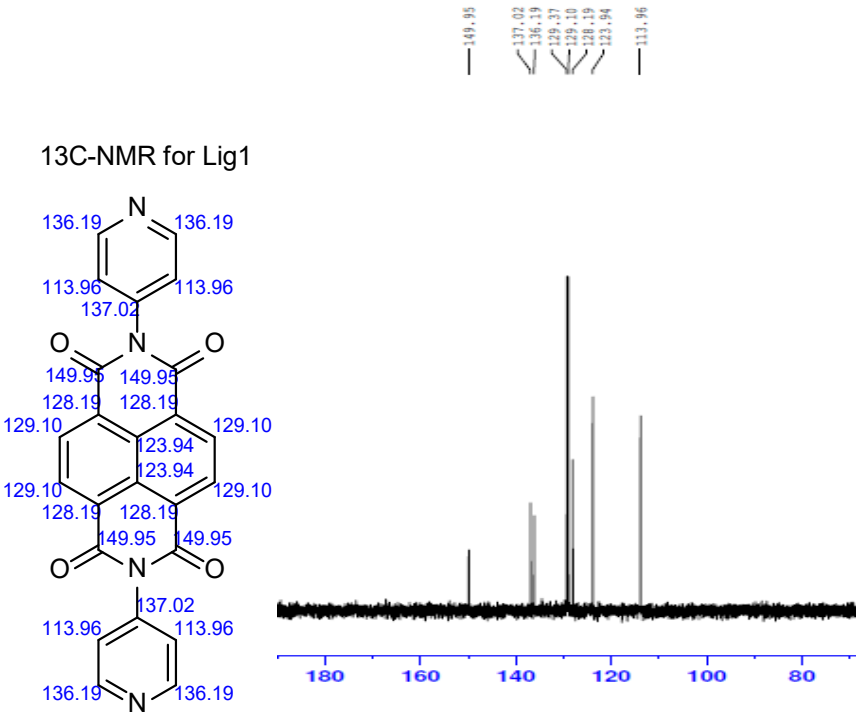

Figure 2.2. The ^{13}C NMR spectrum for Lig1.

2.1.2. Synthesis of ligand 2 (Lig2)

2,7-bis(pyridine3ylmethyl)benzo[lmn][3,8]phenanthroline1,3,6,8(2H,7H)tetraone (Lig2) was synthesised by refluxing a mixture of 1,3,5,8-naphthalenetetracarboxylic dianhydride (1.0 g; 3.73 mmol) and 3-(aminomethyl) pyridine (0.8 g; 7.46 mmol) in DMF (30 mL) at 160 °C for 12 hours. The crude solid was filtered, washed with DMF, and characterized using NMR. A reaction scheme for the synthesis of Lig2 is shown in Scheme 2.2. Yield: 51.1%, ^{1}H-NMR ($CDCl_3$, 400 MHz) δ /ppm: 8.77 (s, 2H). 8.71 (s, 4H), 8.46 (d, 2H), 7.86 (d, 2H), 7.22 (m, 2H), 5.33 (s, 4H). ^{13}C-NMR ($CDCl_3$, 100 MHz) δ /ppm: 162.69 (C * 4), 148.99 (CH * 2), 150.49 (CH * 2), 123.61 (C * 2), 132.34 (C * 4), 126.76 (C * 2), 137.43 (CH * 4), 126.59 (CH * 2), 131.37 (CH * 2), 41.61 (CH2 * 2). The ^{1}H-NMR and ^{13}C-NMR spectra are presented in Figure 2.3 and 2.4.

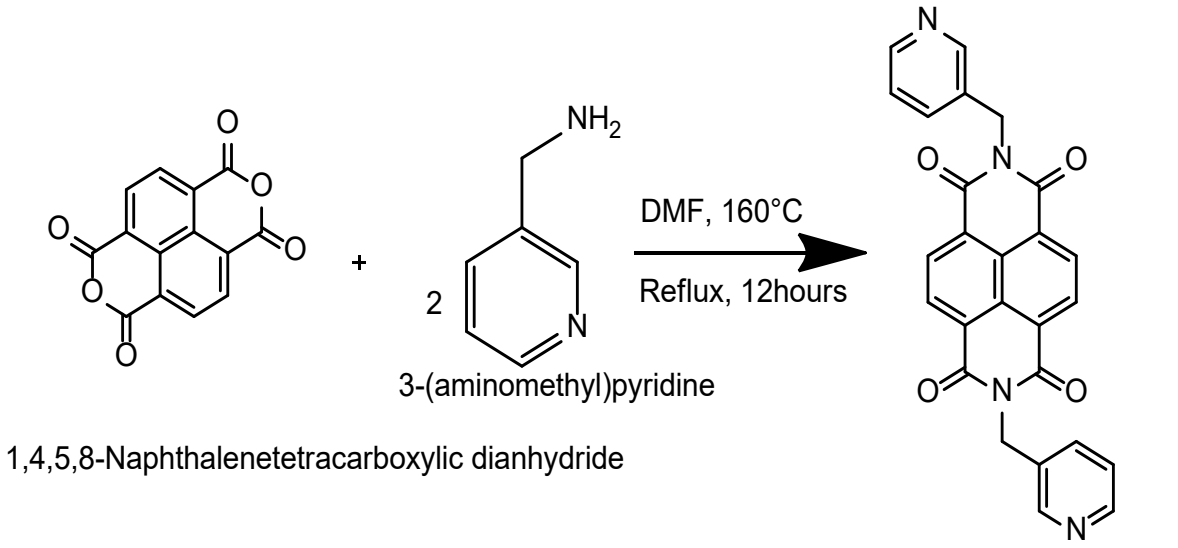

Scheme 2.2. The synthetic procedure of 2,7-bis(pyridine-3-ylmethyl)benzo[lmn][3,8]phenanthroline-1,3,6,8(2H,7H)-tetraone (Lig2).

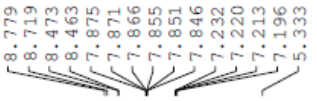

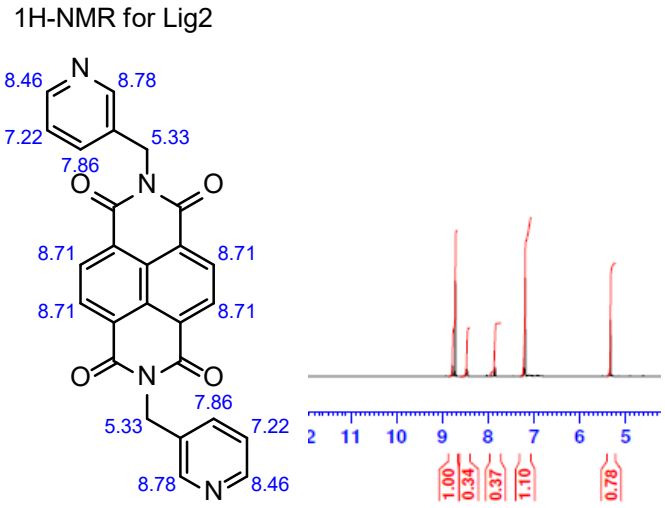

Figure 2.3. The ^{1}H-NMR spectrum for Lig2.

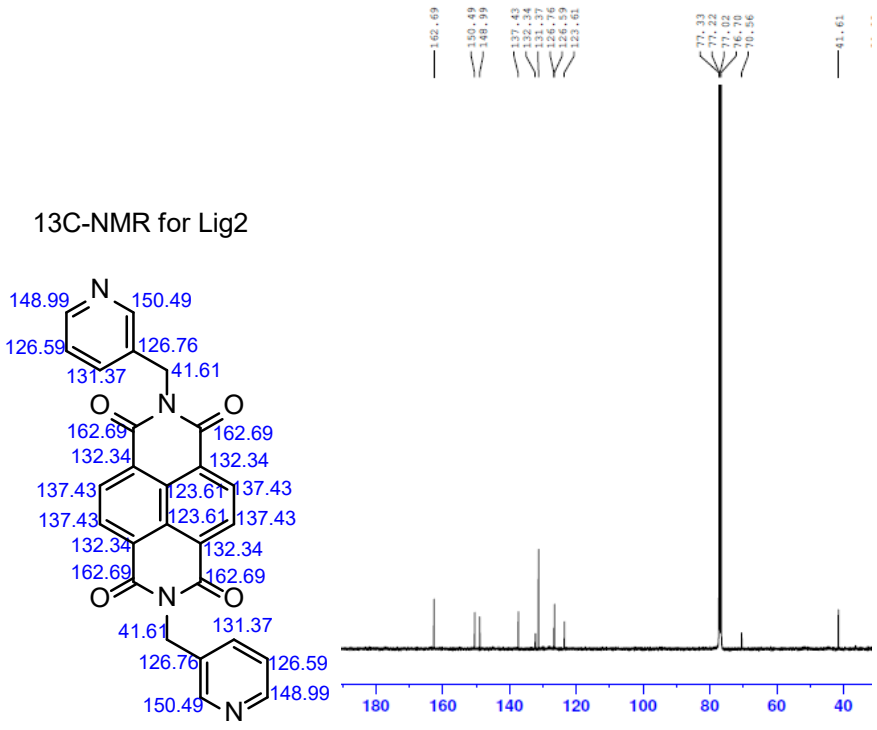

Figure 2.4. The ^{13}C-NMR spectrum for Lig2.

2.1.3. Synthesis of ligand 3 (Lig3)

2-pyridine-4-ylbenzo[de]isoquinoline-1,3-dione (Lig3) was synthesized by refluxing a mixture of 1,8-naphthalic anhydride (2.0 g; 10.09 mmol) and 4-aminopyridine (0.95 g; 10.09 mmol) in DMF (20 mL). The solution was stirred at 160 °C for 12 hours, and the resultant product was collected, filtered, and washed with DMF to remove impurities. The product was air dried and characterized using NMR. The synthetic procedure of Lig3 is presented in Scheme 2.3. Yield: 77.04%, ^{1}H-NMR (DMSO-d6, 400 MHz) δ/ppm 7.55 (d, 2H), 7.19 (d, 2H), 7.46 (d, 2H), 7.32 (d, 2H), 7.25 (dd, 2H). ^{13}C-NMR (DMSO-d6, 100, MHz) δ /ppm: 150.08 (C * 2), 137.58 (CH * 2), 127.98 (C), 122.88 (C * 2), 122.87 (C), 138.21 (C), 114.19 (CH * 2), 129.03 (CH * 2), 127.99 (CH * 2), 129.33 (CH * 2). The spectra for Lig3 are presented in Figures 2.5 and 2.6.

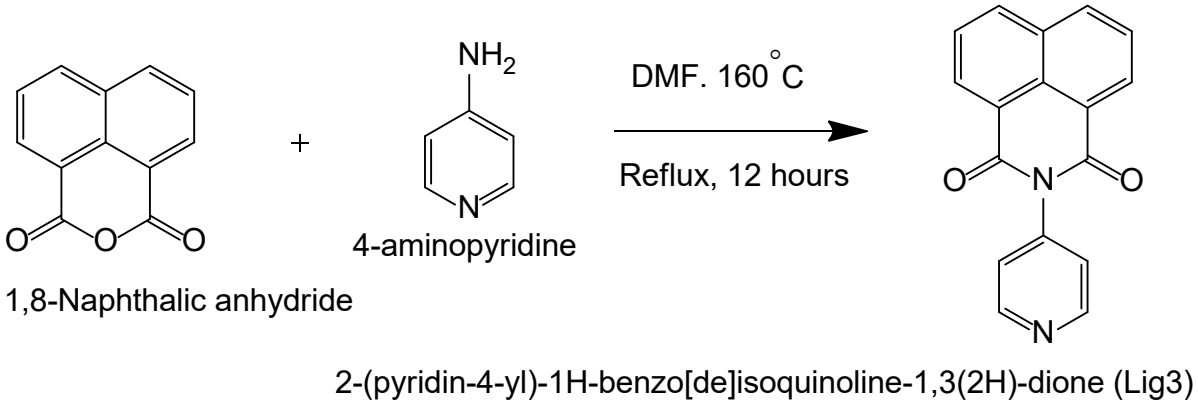

Scheme 2.3. The synthetic procedure of 2-pyridine-4-ylbenzo[de]isoquinoline-1,3-dione (**Lig3**).

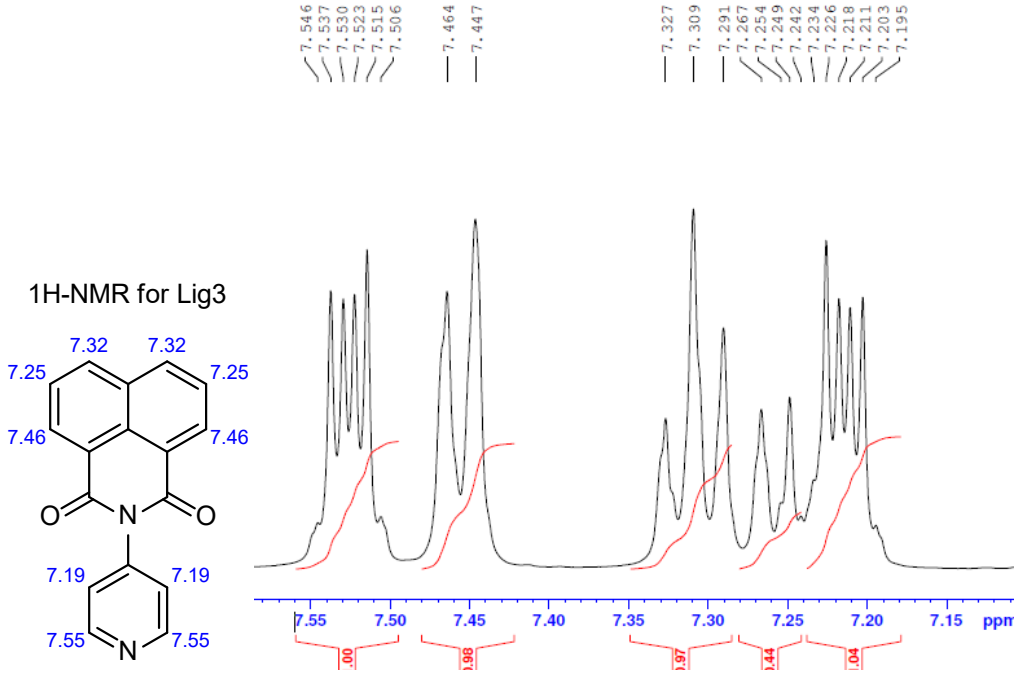

Figure 2.5. The [1]H-NMR spectrum for Lig3

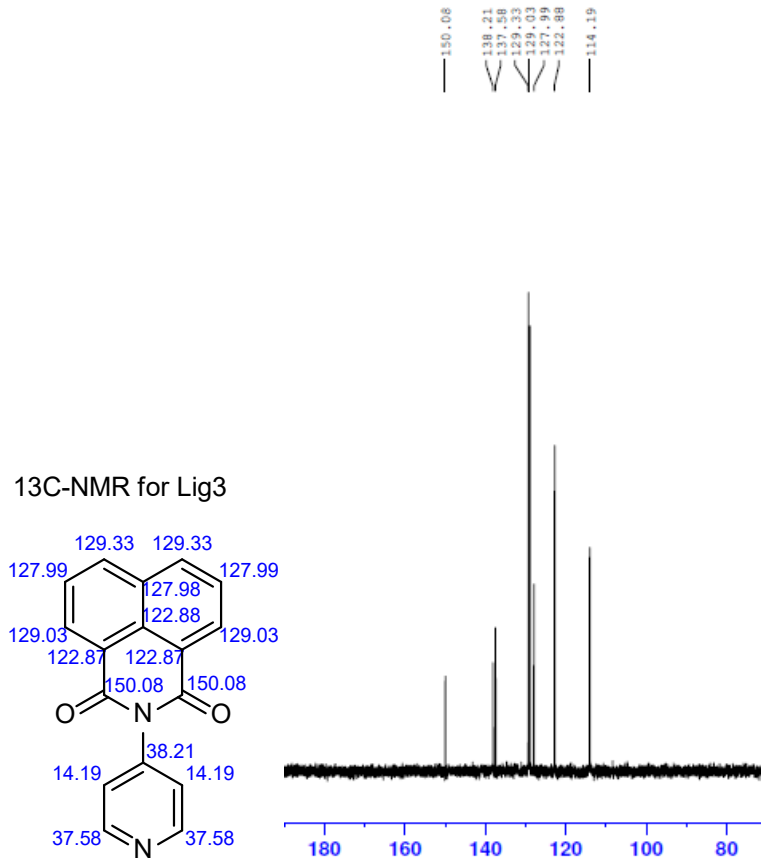

Figure 2.6. The [13]C-NMR spectrum for Lig3

2.1.4. Crystallization of Lig3

Lig3 crystallizes in the monoclinic space group *C2/c* with one Lig3 molecule in the asymmetric unit (Fig 2.7). The packing diagram showing the overall arrangement of the molecules in the crystal structure is shown in Fig 2.7.

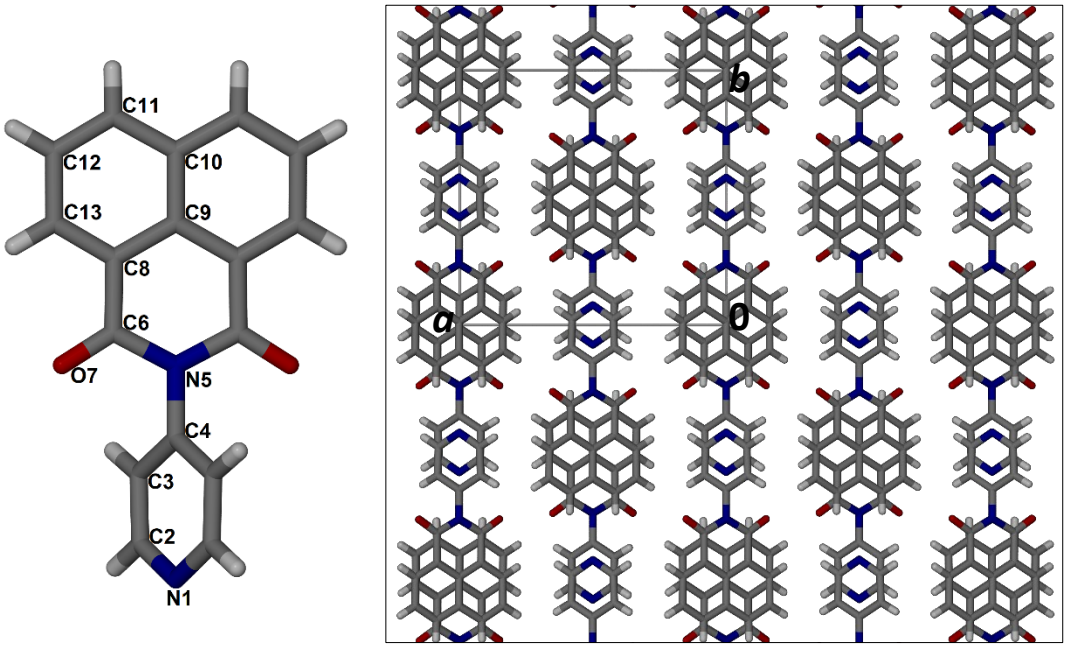

Figure 2.7. The asymmetric unit of Lig3 showing the crystallographic labelling scheme (left) and the packing diagram of Lig3 viewed in the *ab* plane.

2.1.5. Synthesis of ligand 4 (Lig4)

2-(pyridine-4-yl)-1H-benzo [de]isoquinoline-1,3(2H)-dione (Lig4) was synthesised by refluxing a mixture of 1,8-naphthalic anhydride (4.0 g; 20.0 mmol) and 4-(aminomethyl) pyridine (2.16 g; 20.0mmol) in 15 mL DMF at 160 °C for 12 hours while stirring. The product was filtered and washed with DMF to remove excess impurities. The product was air dried and analysed using NMR. The synthesis of Lig4 is presented in Scheme 2.4. Yield: 76.6%, ^{1}H-NMR (DMSO-d6, 400 MHz) δ /ppm: 7.91 (d, 2H), 7.86 (dd, 2H), 8.11 (d, 2H), 2.87 (s, 2H), 7.59 (d, 2H), 8.51 (d, 2H). ^{13}C-NMR (DMSO-d6, 100 MHz) δ /ppm: 163.68 (C * 2), 161,47 (CH * 2), 128.10 (C * 2), 130.01 (C), 136.21 (C), 125.96 (C), 133.39 (CH * 2), 134.29 (CH * 2), 118.75 (CH * 2), 132.44 (CH * 2), 39.62 (CH_2). The spectra for Lig4 are presented in Fig 2.8 and 2.9.

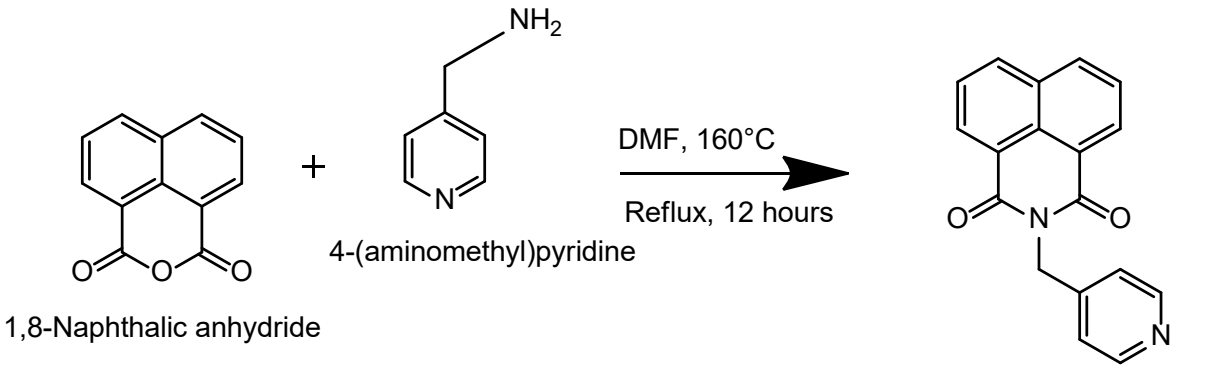

1,8-Naphthalic anhydride

4-(aminomethyl)pyridine

2-(pyridin-4-yl)-1H-benzo[de]isoquinoline-1,3(2H)-dione (Lig4)

Scheme 2.4. The synthetic procedure of 2-(pyridine-4-yl)-1H-benzo [de]isoquinoline-1,3(2H)-dione (Lig4).

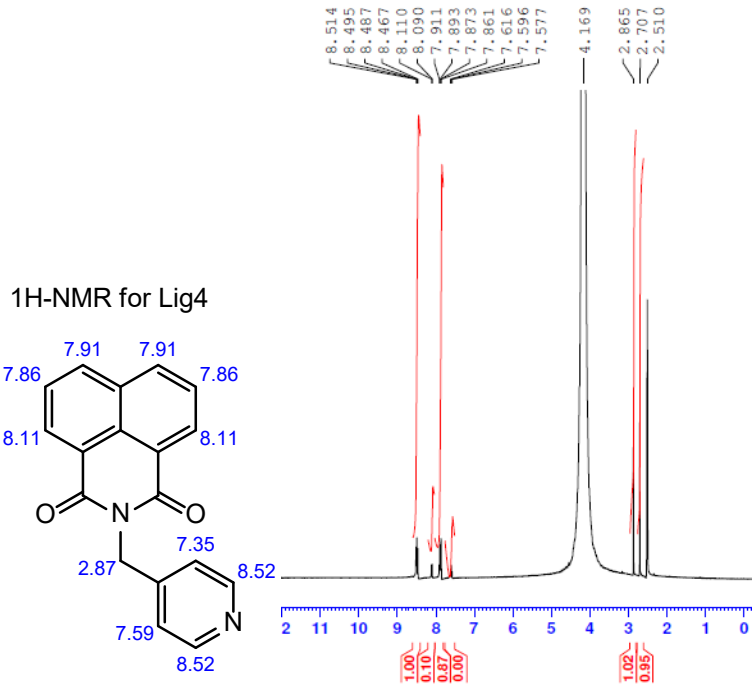

Figure 2.8. The ^{1}H-NMR spectrum for Lig4.

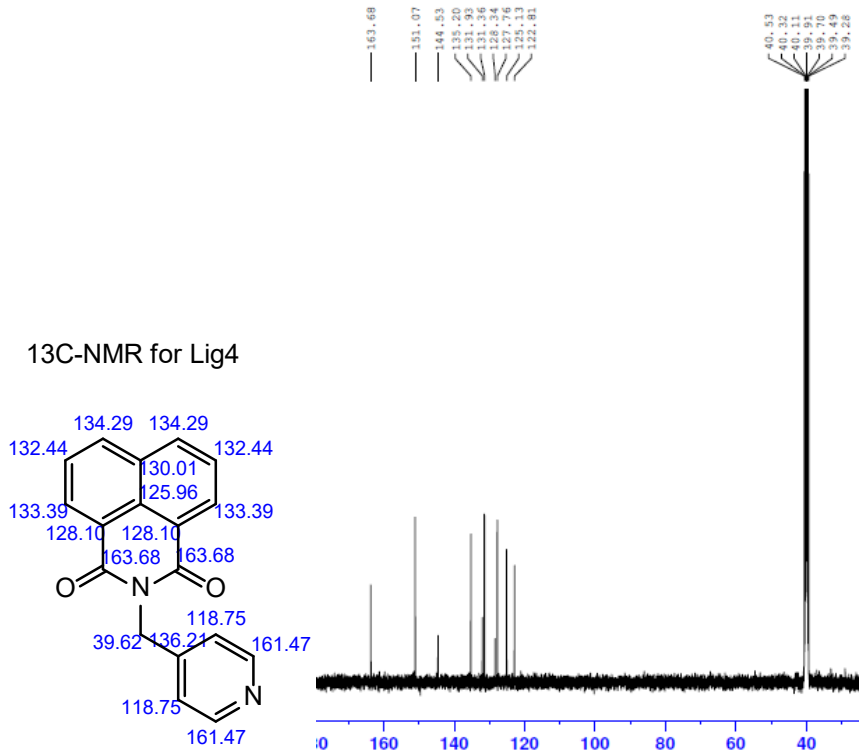

Figure 2.9. The ^{13}C-NMR spectrum for Lig4.

2.1.6. Synthesis of ligand 5 (Lig5)

N, N'-bis(glycinyl)pyromellitic diimide (Lig5) was synthesised by refluxing a mixture of pyromellitic dianhydride (2.0 g; 9.0 mmol) and glycine (1.35 g; 17.98 mmol) in acetic acid at 100 °C for 4 hours. The resultant product was washed with DMF and air dried. The synthesis of Lig5 is presented in Scheme 2.5 and the NMR spectra are presented in Fig 2.10 and Fig 2.11. Yield: 61.74%, ^{1}H-NMR (DMSO-d6, 400 MHz) δ /ppm: 4.83 (s, 4H), 7.27 (s, 2H). ^{13}C-NMR (DMSO-d6, 100 MHz) δ /ppm: 151.07 (C * 4), 135.21 (C * 4), 125.14 (CH * 2), 40.16 (CH2 * 2).

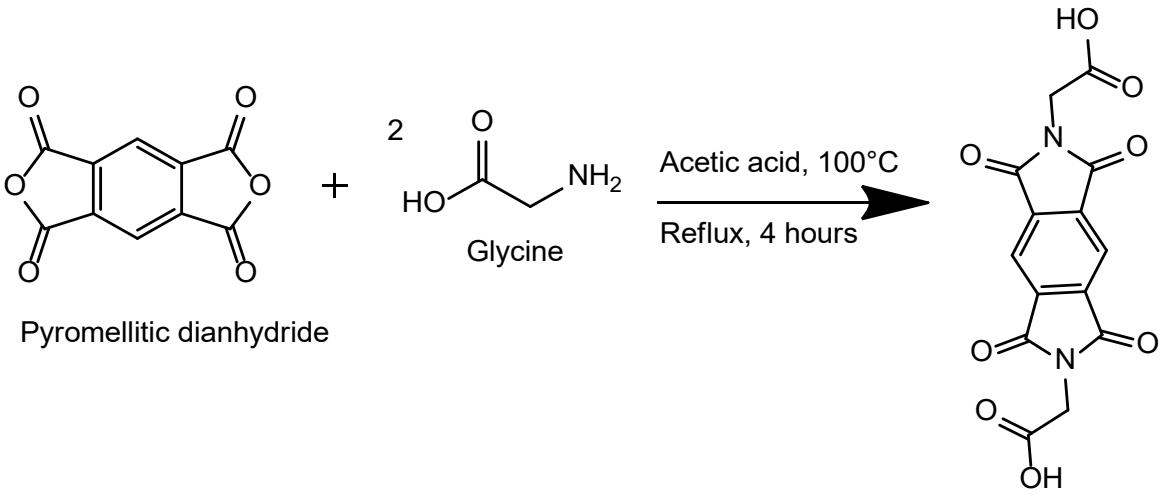

Scheme 2.5. The synthetic procedures of *N, N'*-bis(glycinyl)pyromellitic diimide (Lig5).

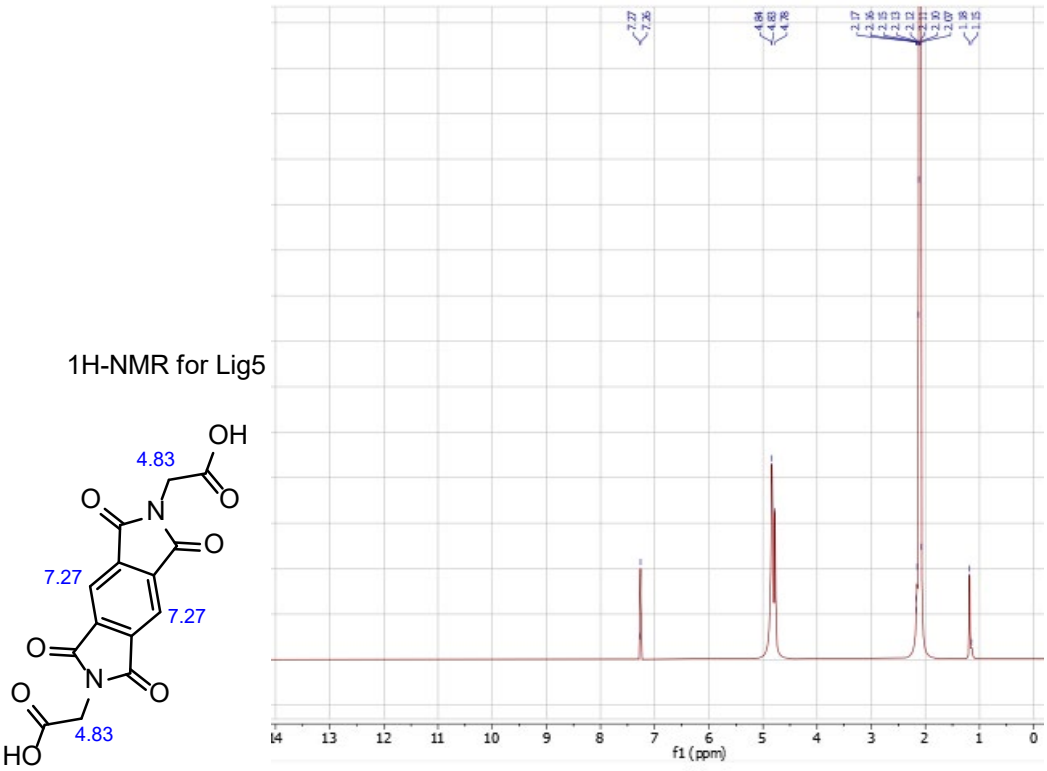

Figure 2.10. The ^{1}H-NMR spectrum for Lig5.

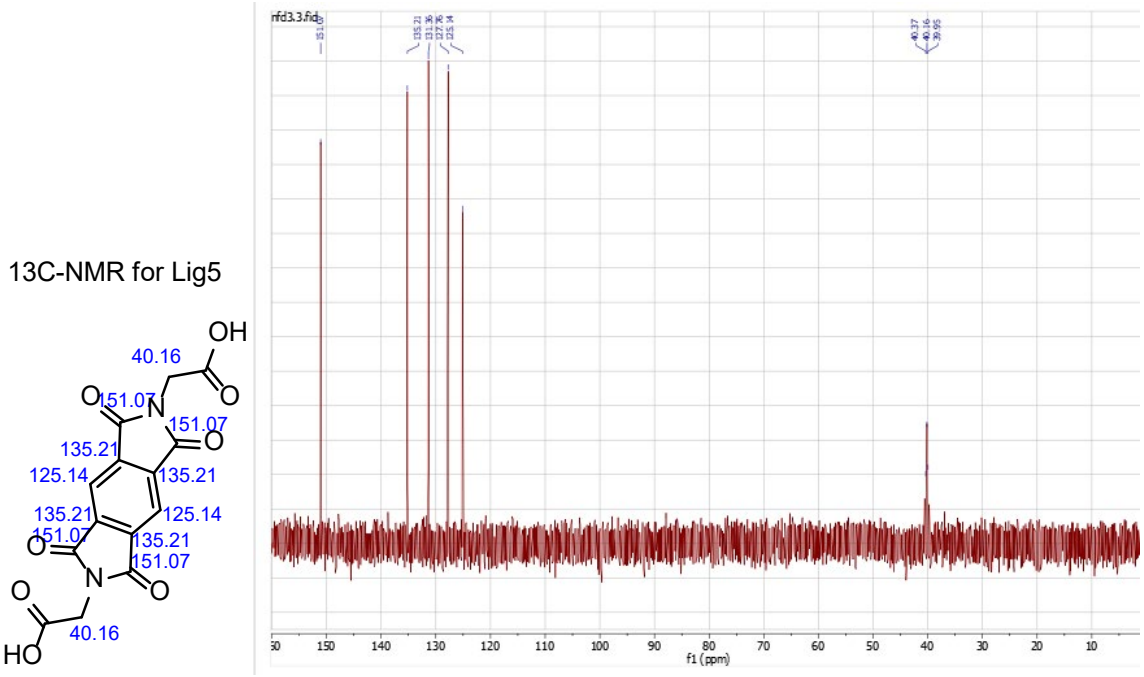

Figure 2.11. The ^{13}C-NMR spectrum for Lig5.

2.2. METAL ORGANIC FRAMEWORKS (MOFS) SYNTHESIS

MOFs were synthesized using the solvothermal technique. In general, a mixture of a nitrogen donor ligand, a carboxylate donor co-ligand, and a metal salt in DMF was heated in an oven (80°C- 100°C) for about two weeks. The resulting products were removed from the oven and washed with DMF. The crystals were characterized using thermogravimetric analysis (TGA), single crystal X-ray diffraction (SCXRD) and powder X-ray diffraction (PXRD) and subjected to an activation process overnight to remove included solvent/s. The activated crystals were analysed using TGA, SCXRD and PXRD. Table 2.2 presents resulting products for each experiment conducted in this study.

NFDMOF-1 was prepared by heating a mixture of Lig1 (20 mg; 0.048 mmol), fumaric acid (FUM) (5.5 mg; 0.048 mmol) and cobaltous(II) nitrate hexahydrate (14 mg; 0.048 mmol) in 2 mL DMF. The temperature was maintained at 100°C for seven days. The crystals were removed from the oven and washed with DMF and, characterized using TGA, SCXRD and PXRD.

NFDMOF-2 was prepared from a solvothermal reaction of Lig2 (22 mg; 0.049 mmol), 2,6-naphthalenedicarboxylic acid (NDC) (21 mg; 0.097 mmol) and zinc(II) nitrate hexahydrate (26 mg; 0.087 mmol) in 5 mL DMF. The temperature was maintained at 100 °C for three days. The resultant crystals were removed from the oven, washed with DMF, and characterized using TGA, SCXRD and PXRD.

NFDMOF-3 was prepared by heating a mixture of Lig4 (20 mg; 0.069 mmol), 2,2'-bipyridine-4,4'-dicarboxylic acid (BPDC) (8.47 mg; 0.035 mmol) and cadmium(II) nitrate tetrahydrate (42.82 mg; 0.139 mmol) in 10 mL DMF. The temperature was maintained at 100 °C for seven days. The crystals were washed with DMF and characterised using TGA, SCXRD and PXRD.

NFDMOF-4 was prepared from a solvothermal reaction of Lig2 (20 mg; 0.045 mmol), 4,4'-oxybis (benzoic acid) (OXB) (11.62 mg; 0.045 mmol) and cobaltous(II) nitrate hexahydrate (13.09 mg; 0.045 mmol) in 10 mL DMF. The temperature was maintained at 100 °C for five days. The resultant crystals were removed from the oven, washed with DMF, and characterized using TGA, SCXRD and PXRD.

NFDMOF-5 was prepared by heating a mixture of Lig2 (20 mg; 0.045 mmol), 4,4'-oxybis (benzoic acid) (OXB) (11.62 mg; 0.045 mmol) and zinc(II) nitrate hexahydrate (13.39 mg; 0.045 mmol) in 10 mL DMF. The temperature was maintained at 100 °C for five days. The resultant crystals were removed from the oven, washed with DMF, and analysed using TGA, SCXRD and PXRD.

NFDMOF-6 was synthesized from the solvothermal reaction of Lig5 (20 mg; 0.055 mmol), 2,2-bipyridine (BPy) (8.59 mg; 0.055 mmol) and zinc(II) nitrate hexahydrate (32.7 mg; 0.109 mmol) in 5 mL DMF. The temperature was maintained at 100 °C for three days. The crystals were removed from the mother liquor, washed with DMF, and characterized using TGA, SCXRD and PXRD.

Table 2.1. A table of the resultant MOFs and their building blocks.

LIGANDS	CO- LIGANDS	METAL SALTS	PRODUCT	STRUCTURE
LIG 1	**Fumaric acid**	**$Co(NO_3)_2{\cdot}6H_2O$**	**Good quality crystals**	**NFDMOF-1**
		$Zn(NO_3)_2{\cdot}6H_2O$	Powder	No structure
		$Cu(NO_3)_2{\cdot}3H_2O$	Powder	No structure
		$Cd(NO_3)_2{\cdot}4H_2O$	Powder	No structure
		$Mn(NO_3)_2{\cdot}4H_2O$	Powder	No structure
		$Mg(NO_3)_2{\cdot}6H_2O$	Powder	No structure
		$Ni(NO_3)_2{\cdot}6H_2O$	Powder	No structure

LIG 1	4,4'-Oxydibenzoic acid	$Co(NO_3)_2{\cdot}6H_2O$	Powder	No structure
		$Zn(NO_3)_2{\cdot}6H_2O$	Powder	No structure
		$Cu(NO_3)_2{\cdot}3H_2O$	Powder	No structure
		$Cd(NO_3)_2{\cdot}4H_2O$	Powder	No structure
		$Mn(NO_3)_2{\cdot}4H_2O$	Powder	No structure
		$Mg(NO_3)_2{\cdot}6H_2O$	Powder	No structure
		$Ni(NO_3)_2{\cdot}6H_2O$	Powder	No structure
LIG 1	2,6-Naphthalenedicarboxylic acid	$Co(NO_3)_2{\cdot}6H_2O$	Powder	No structure
		$Zn(NO_3)_2{\cdot}6H_2O$	Powder	No structure
		$Cu(NO_3)_2{\cdot}3H_2O$	Powder	No structure
		$Cd(NO_3)_2{\cdot}4H_2O$	Powder	No structure
		$Mn(NO_3)_2{\cdot}4H_2O$	Powder	No structure
		$Mg(NO_3)_2{\cdot}6H_2O$	Powder	No structure
		$Ni(NO_3)_2{\cdot}6H_2O$	Powder	No structure
LIG 1	2,2'-bipyridine-4,4'-dicarboxyilic acid	$Co(NO_3)_2{\cdot}6H_2O$	Powder	No structure
		$Zn(NO_3)_2{\cdot}6H_2O$	Powder	No structure
		$Cu(NO_3)_2{\cdot}3H_2O$	Powder	No structure
		$Cd(NO_3)_2{\cdot}4H_2O$	Powder	No structure
		$Mn(NO_3)_2{\cdot}4H_2O$	Powder	No structure
		$Mg(NO_3)_2{\cdot}6H_2O$	Powder	No structure
		$Ni(NO_3)_2{\cdot}6H_2O$	Powder	No structure
LIG 1	2,2-bipyridine	$Co(NO_3)_2{\cdot}6H_2O$	Powder	No structure

		$Zn(NO_3)_2{\cdot}6H_2O$	Powder	No structure
		$Cu(NO_3)_2{\cdot}3H_2O$	Powder	No structure
		$Cd(NO_3)_2{\cdot}4H_2O$	Powder	No structure
		$Mn(NO_3)_2{\cdot}4H_2O$	Powder	No structure
		$Mg(NO_3)_2{\cdot}6H_2O$	Powder	No structure
		$Ni(NO_3)_2{\cdot}6H_2O$	Powder	No structure
LIG 2	**2,6-Naphthalenedicarboxylic acid**	$Co(NO_3)_2{\cdot}6H_2O$	Powder	No structure
		$Zn(NO_3)_2{\cdot}6H_2O$	**Good quality crystals**	**NFDMOF-2**
		$Cu(NO_3)_2{\cdot}3H_2O$	Powder	No structure
		$Cd(NO_3)_2{\cdot}4H_2O$	Powder	No structure
		$Mn(NO_3)_2{\cdot}4H_2O$	Powder	No structure
		$Mg(NO_3)_2{\cdot}6H_2O$	Powder	No structure
		$Ni(NO_3)_2{\cdot}6H_2O$	Powder	No structure
LIG 2	**4,4'-Oxydibenzoic acid**	**$Co(NO_3)_2{\cdot}6H_2O$**	**Good quality crystals**	**NFDMOF-4**
		$Zn(NO_3)_2{\cdot}6H_2O$	**Good quality crystals**	**NFDMOF-5**
		$Cu(NO_3)_2{\cdot}3H_2O$	Powder	No structure
		$Cd(NO_3)_2{\cdot}4H_2O$	Powder	No structure
		$Mn(NO_3)_2{\cdot}4H_2O$	Powder	No structure
		$Mg(NO_3)_2{\cdot}6H_2O$	Powder	No structure
		$Ni(NO_3)_2{\cdot}6H_2O$	Powder	No structure

LIG 2	Fumaric acid	$Co(NO_3)_2 \cdot 6H_2O$	Powder	No structure
		$Zn(NO_3)_2 \cdot 6H_2O$	Powder	No structure
		$Cu(NO_3)_2 \cdot 3H_2O$	Powder	No structure
		$Cd(NO_3)_2 \cdot 4H_2O$	Powder	No structure
		$Mn(NO_3)_2 \cdot 4H_2O$	Powder	No structure
		$Mg(NO_3)_2 \cdot 6H_2O$	Powder	No structure
		$Ni(NO_3)_2 \cdot 6H_2O$	Powder	No structure
LIG 3		$CoCl_2$	**Good quality crystals**	**No Diffraction**
		$CuCl_2$	**Good quality crystals**	**No Diffraction**
		$NiCl_2$	**Good quality crystals**	**No Diffraction**
		$Co(NO_3)_2 \cdot 6H_2O$	**Good quality crystals**	**No Diffraction**
		$Cu(NO_3)_2 \cdot 3H_2O$	**Good quality crystals**	**No Diffraction**
		$Zn(NO_3)_2 \cdot 6H_2O$	**Good quality crystals**	**No Diffraction**
		$Ni(NO_3)_2 \cdot 6H_2O$	**Good quality crystals**	**No Diffraction**
		$Cd(NO_3)_2 \cdot 4H_2O$	**Good quality crystals**	**No Diffraction**
		$Mn(NO_3)_2 \cdot 4H_2O$	**Good quality crystals**	**No Diffraction**
		$Mg(NO_3)_2 \cdot 6H_2O$	**Good quality crystals**	**No Diffraction**
LIG 3	**4,4'-Oxydibenzoic acid**	$Co(NO_3)_2 \cdot 6H_2O$	Powder	No structure
		$Zn(NO_3)_2 \cdot 6H_2O$	Powder	No structure
		$Cu(NO_3)_2 \cdot 3H_2O$	Powder	No structure
		$Cd(NO_3)_2 \cdot 4H_2O$	**Good quality crystals**	**No Diffraction**
		$Mn(NO_3)_2 \cdot 4H_2O$	**Good quality crystals**	**No Diffraction**
		$Mg(NO_3)_2 \cdot 6H_2O$	Powder	No structure

		$Ni(NO_3)_2{\cdot}6H_2O$	Powder	No structure
	Fumaric acid	**$Co(NO_3)_2{\cdot}6H_2O$**	**Good quality crystals**	**LIG 3**
		$Zn(NO_3)_2{\cdot}6H_2O$	Powder	No structure
		$Cu(NO_3)_2{\cdot}3H_2O$	Powder	No structure
		$Cd(NO_3)_2{\cdot}4H_2O$	Powder	No structure
		$Mn(NO_3)_2{\cdot}4H_2O$	Powder	No structure
		$Mg(NO_3)_2{\cdot}6H_2O$	**Good quality crystals**	**No Diffraction**
		$Ni(NO_3)_2{\cdot}6H_2O$	Powder	No structure
LIG 4	**2,2'-bipyridine-4,4'-dicarboxyilic acid**	$Co(NO_3)_2{\cdot}6H_2O$	Powder	No structure
		$Zn(NO_3)_2{\cdot}6H_2O$	Powder	No structure
		$Cu(NO_3)_2{\cdot}3H_2O$	Powder	No structure
		$Cd(NO_3)_2{\cdot}4H_2O$	**Good quality crystals**	**NFDMOF-3**
		$Mn(NO_3)_2{\cdot}4H_2O$	Powder	No structure
		$Mg(NO_3)_2{\cdot}6H_2O$	Powder	No structure
		$Ni(NO_3)_2{\cdot}6H_2O$	Powder	No structure
LIG 5	**2,2-bipyridine**	$Co(NO_3)_2{\cdot}6H_2O$	Powder	No structure
		$Zn(NO_3)_2{\cdot}6H_2O$	**Good quality crystals**	**NFDMOF-6**
		$Cu(NO_3)_2{\cdot}3H_2O$	Powder	No structure
		$Cd(NO_3)_2{\cdot}4H_2O$	Powder	No structure
		$Mn(NO_3)_2{\cdot}4H_2O$	Powder	No structure
		$Mg(NO_3)_2{\cdot}6H_2O$	Powder	No structure
		$Ni(NO_3)_2{\cdot}6H_2O$	Powder	No structure

2.3. CHARACTERIZATION TECHNIQUES

The synthesised ligands were characterised using nuclear magnetic resonance (NMR) and the MOFs were analysed using thermogravimetric analysis (TGA), single crystal X-ray diffraction (SCXRD) and powder X-ray diffraction (PXRD).

2.3.1. Nuclear Magnetic Resonance Spectroscopy (NMR)

NMR spectroscopy is a method that is used to identify magnetic fields in the atomic nuclei. There are two well-known types of NMR spectroscopy, proton NMR (^{1}H-NMR) and carbon-13 NMR (^{13}C-NMR). This technique was used in this study to confirm the structure of the organic ligands. In general, about 3 mg of a sample was dissolved in a deuterated solvent and the proton (400MHz) and carbon (100MHz) NMR recorded. Carbon and proton spectra were recorded using Varian Unity INOVA. Linkers Lig1, Lig2, and Lig4 were immersed in DMSO-d6 and linker Lig3 was dissolved in $CDCl_3$.

2.3.2. Single Crystal X-Ray Diffraction (SCXRD)

A suitable crystal was selected for SCXRD and placed on a glass slide under paratone N oil.[1] Intensity data for **NFDMOF-1**, **NFDMOF-2**, **NFDMOF-3, NFDMOF-4, NFDMOF-5**, and **NFDMOF-6** were collected using a Bruker D8 VENTURE diffractometer equipped with Mo (λ = 0.71073 Å) radiation generated at 50 kV and 1.4 mA through a Bruker K430 generator at 173 K. The temperature was maintained using a an Oxford Cryostream 800.[2] The collection of data and the refinement of cell was carried out utilizing *SAINT-Plus*.[3-4] Absorption effects were corrected using the multi-Scan method (SADABS).[5] Space groups were then determined from systematic absences utilizing *XPREP*[6]. The crystal structures were solved using *SHELXS-97*[8] and the refinement of the structures was carried out using *SHELXL-97*[8] within the graphical user interface of the *X-Seed* program[7]. All hydrogen atoms not bonded to any carbon atoms were refined anisotropically (except for disordered atoms). All C-H hydrogen atoms were placed at calculated positions with the aid of the riding model and refined isotropically. POV-RAY and Mercury programs were used to generate images.[9-10]

2.3.3. Thermogravimetric analysis (TGA)

TGA was used to determine the percentage weight loss of guest molecules and the temperature at which the framework decomposes. TGA data were obtained using a TAQ500 thermogravimetric

analyser. About 2mg to 3mg of sample was first dried using a filter paper and placed on a sample pan. The sample was heated at a heating rate of 10 °C min^{-1} from room temperature to 400 °C / 600 °C under nitrogen gas at a flow rate of 60 mL min^{-1}.

2.3.4. Powder X-ray diffraction (PXRD)

The MOFs were characterized using PXRD. PXRD gives information on the dimensions of the unit cell and is used to identify the phase of the MOFs. The wet samples were first dried using filter paper followed by grinding until finely powdered. Ground powders were placed on the zero-background sample holder. The X-ray intensity data were collected on a Bruker D8 advance X-ray diffractometer equipped with copper radiation (Cu Kα, λ = 1.5406 Å) produced at 30 kV and 40 mA. Each of the samples was scanned between 4 and 50° 2^{θ} using a step size of 0.020° s^{-1}. During the collection of PXRD data collection the stage was rotated to correct for preferred orientations effects.

2.3.5. Dynamic-vapour Sorption (DVS)

The dynamic-vapour sorption reactions were performed on the activated MOFs using a microbalance that tracks the change in weight as a function of time under standard temperature and pressure.[11] The sample was first evacuated until a constant weight was reached and the sample was exposed to xylene vapours. Any increase in weight was tracked until a state of saturation was reached, thereafter the resultant clathrates were characterized using PXRD and TGA.

2.4. XYLENE ISOMERS INCLUSION EXPERIMENTS

Guest inclusion capabilities of the characterized MOFs were tested using xylene isomers. The successfully synthesized MOFs were immersed in xylene isomers and allowed to equilibrate at room temperature. (Equation 1). The crystals were filtered and analysed using TGA, PXRD and SCXRD.

Equation 1: H + G1(0.5) -------> H. xG1(1-x)

REFERENCES

1. Paratone N oil. (Exxon Chemical Co. Tx. USA).
2. Broker 2005. APEX2. Version 1.0-27. Bruker AXS Inc. Madison Wisconsin. USA.
3. Bruker 2007. Bruker AXS Inc. Madison. Wisconsin USA.
4. Bruker 2004. SAINT-Plus (including XPREP). Version 7.12. Bruker AXS Inc. Madison. Wisconsin. USA.
5. Sheldrick, G.M. 2001. SADABS. Bruker AXS Inc. Madison. Wisconsin. USA.
6. Bruker 2003. XPREP2. Version 6.14. Bruker AXS Inc. Madison. Wisconsin. USA.
7. Barbour, L. J. 2001. *Supramol. Chem*. **1**: 189.
8. Sheldrick, G.M. 1997. SHELXL-97. Program for Crystal Structure Solution. University of Gottingen. Germany.
9. POV-RayTM, Version 3.6. 2004. Williamstone. Persistence of Vision Raytracer (Pty)Ltd.
10. Macrae, C. F. Bruno, I. J. Chisholm, J. A. Edgington, P. R. McCabe, P. Pidcock, E. Rodriguez-Monge, L. Taylor, R. van de Streek, J. Wood, P. A. 2008. *J. Appl. Cryst*. **41**: 466.
11. Batisai, E. Lusi, M. Jacobs, T. Barbour, L. J. 2012. *Chem. Commun*. **48**: 12171.

CHAPTER 3

RESULTS AND DISCUSSION

This chapter discusses characterization and structural analysis of the following metal organic frameworks: {[Co(FUM)(Lig1)].$(DMF)_2$}n **(NFDMOF-1)**, {[Zn(NDC)$(Lig2)_{0.5}$].$(DMF)_2$}n **(NFDMOF-2)**, {[$Cd_2(BPDC)_2(DMF)_2$}n **(NFDMOF-3)**, {[Co(OBZ)$(Lig2)_{0.5}$].$(DMF)_2$}n **(NFDMOF-4)**, {[Zn(OBZ)$(Lig2)_2$].(DMF)}n **(NFDMOF-5)**, and {[Zn(BP)(Lig5)].(DMF)}n **(NFDMOF-6).** Solvent accessible volumes of the MOFs were estimated using the Mercury program (0.18 Å grid spacing, 1.2 and 1.4 Å probe radius).

3.1. NFDMOF-1

3.1.1. Single Crystal X-Ray Diffraction (SCXRD)

NFDMOF-1 was synthesized by reacting fumaric acid, cobalt(II) nitrate hexahydrate and Lig1 in DMF (2 mL) under solvothermal conditions (100 °C, 168 hours). An **NFDMOF-1** crystal was selected and analysed using single crystal diffraction analysis. **NFDMOF-1** crystallizes in the monoclinic space group *C*2/*c*. The asymmetric unit is presented in Fig 3.1 below and it consists of a complete Lig1 molecule, a fumarate anion, and a cobalt(II) cation. The guest molecules are severely disordered. An attempt to model the possible disorders of the guest was unsuccessful. A 3D packing diagram showing the overall arrangement of the molecules in the crystal structure is presented in Fig 3.2. The packing diagram viewed in the *ab* plane shows channels running along the crystallographic *c* axis. The compound has 17.3% solvent accessible volume determined using a probe radius of 1.4Å and a grid spacing of 0.8Å. A diagram showing the nature of the voids is presented in Fig 3.3. The structure possesses one dimensional channel.

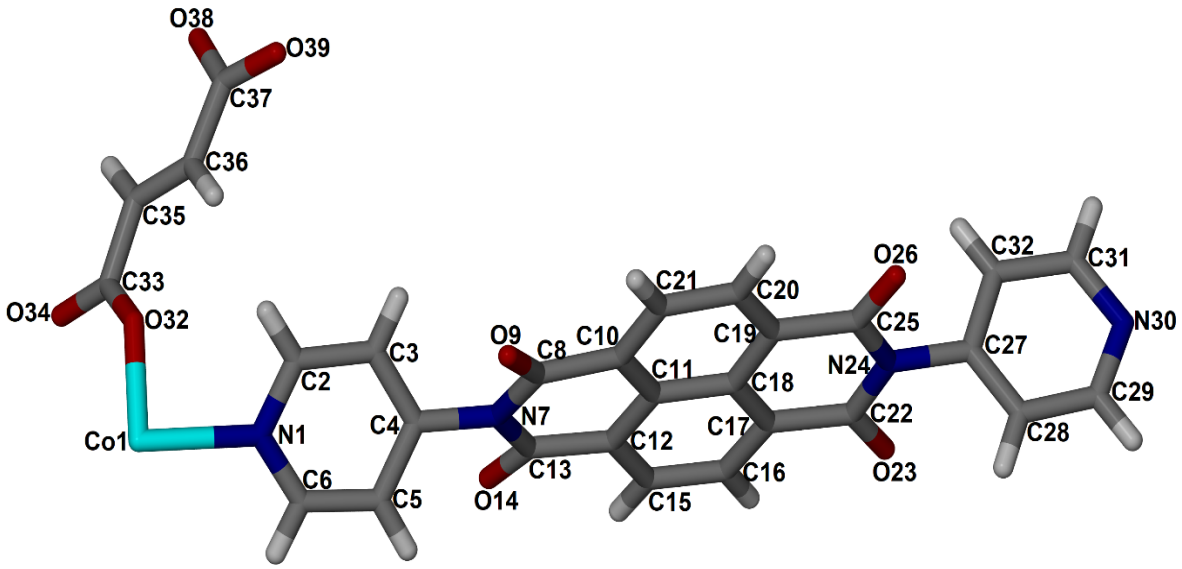

Figure 3.1. The asymmetric unit of **NFDMOF-1** showing the crystallographic labelling scheme for the asymmetric unit.

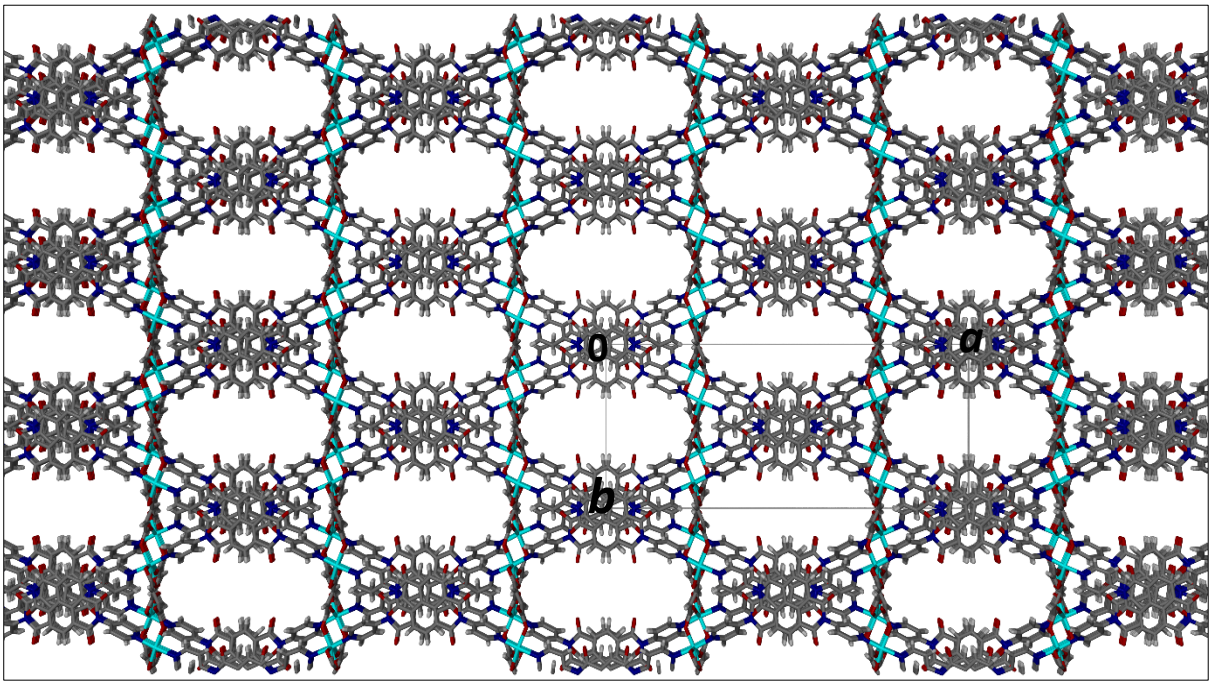

Figure 3.2. The packing diagram of **NFDMOF-1** viewed in the *ab* plane. The DMF molecules are in channels running along the *c* axis.

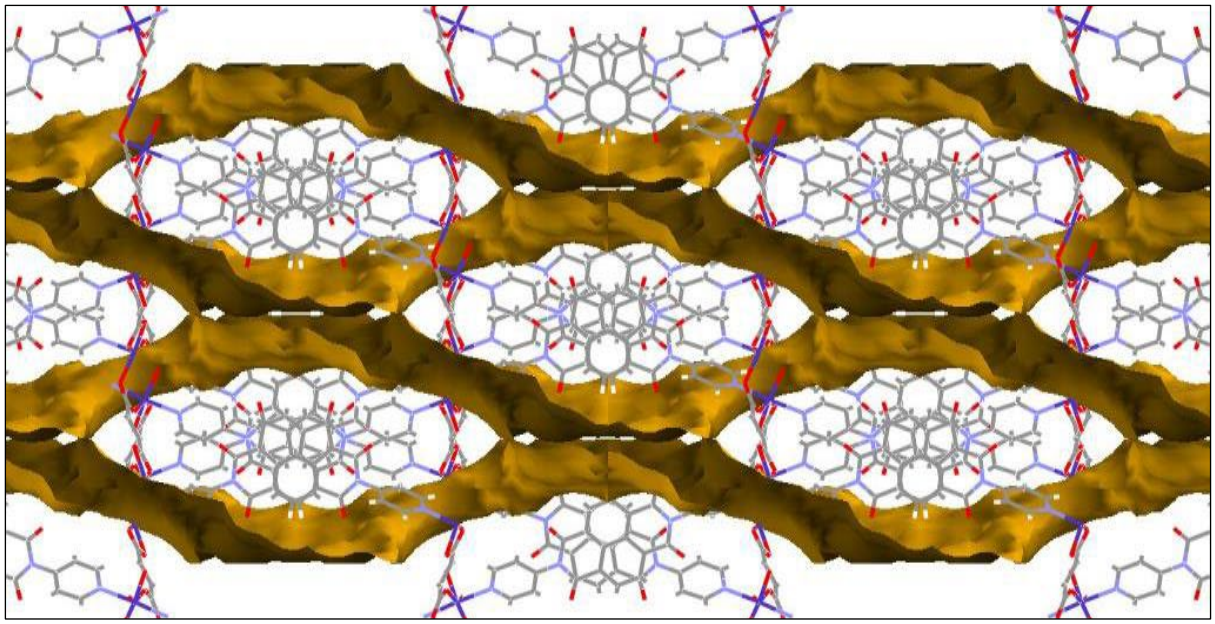

Figure 3.3. The guest accessible voids in **NFDMOF-1** generated using the Mercury program.

3.1.2. Thermogravimetric Analysis (TGA)

The thermal profile of **NFDMOF-1** was determined using TGA (Fig 3.4). The TGA traces display a mass loss of 24.29% associated with the guest molecule release within the temperature range of 22.88 °C – 192.56 °C. The 24.29% weight loss may be attributed to the loss of two DMF molecules (calculated 21.94%) and one water molecule (calculated 2.95%). There is no further significant weight loss observed within the temperature range 192.56 °C - 310.65 °C after which decomposition commences. Activation of the pores was achieved by heating the as-synthesized crystals at 100 °C for 24 hours under vacuum. The TGA trace of the activated phase shows a weight loss of 7.976% within the temperature range 0 °C -100 °C, which may be attributed to loss of moisture adsorbed after the activation process. There is evidence of guest absence within the range of 100 °C - 310.65 °C. This confirms that guest removal was successful.

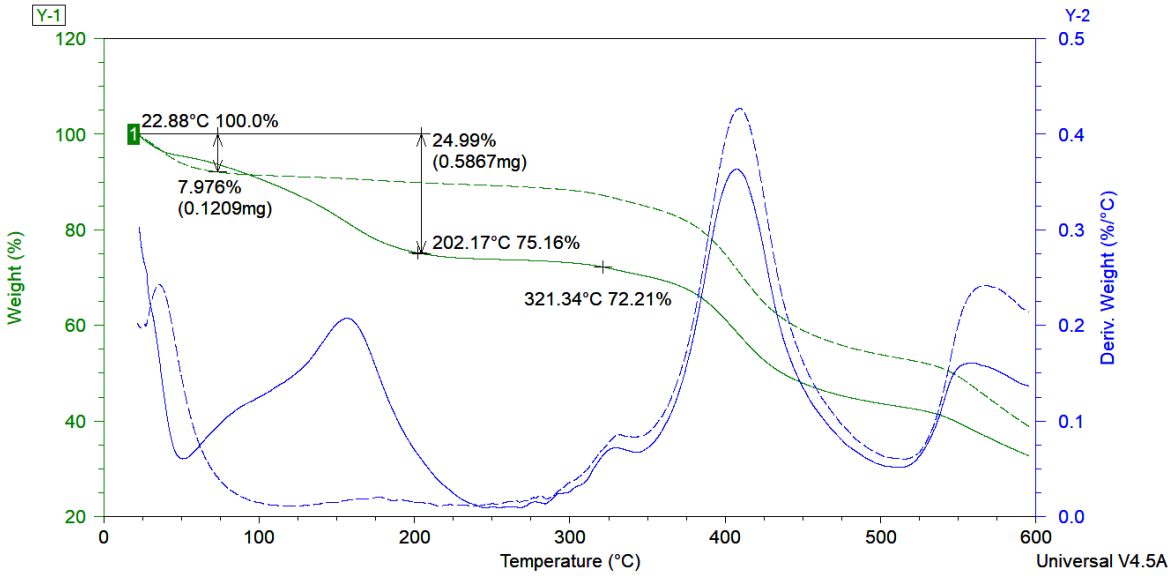

Figure 3.4. TGA profiles of the as-synthesized **NFDMOF-1** (solid green) and activated **NFDMOF-1** (dashed green) as well as the first derivatives of the weight %: as-synthesized (solid blue) and activated (dashed blue).

3.1.3. Powder X-Ray Diffraction (PXRD)

Powder X-ray diffraction was conducted on the crystals of **NFDMOF-1** (as-synthesized) and **NFDMOF-1** (activated). The **NFDMOF-1** simulated pattern was generated using the Mercury program. The PXRD patterns of **NFDMOF-1** (as-synthesised) and **NFDMOF-1** (simulated) match; this confirms purity of the bulk material. **NFDMOF-1** (activated) pattern has broad peaks (Fig 3.5) which may indicate the loss of monocrystallinity upon desolvation.

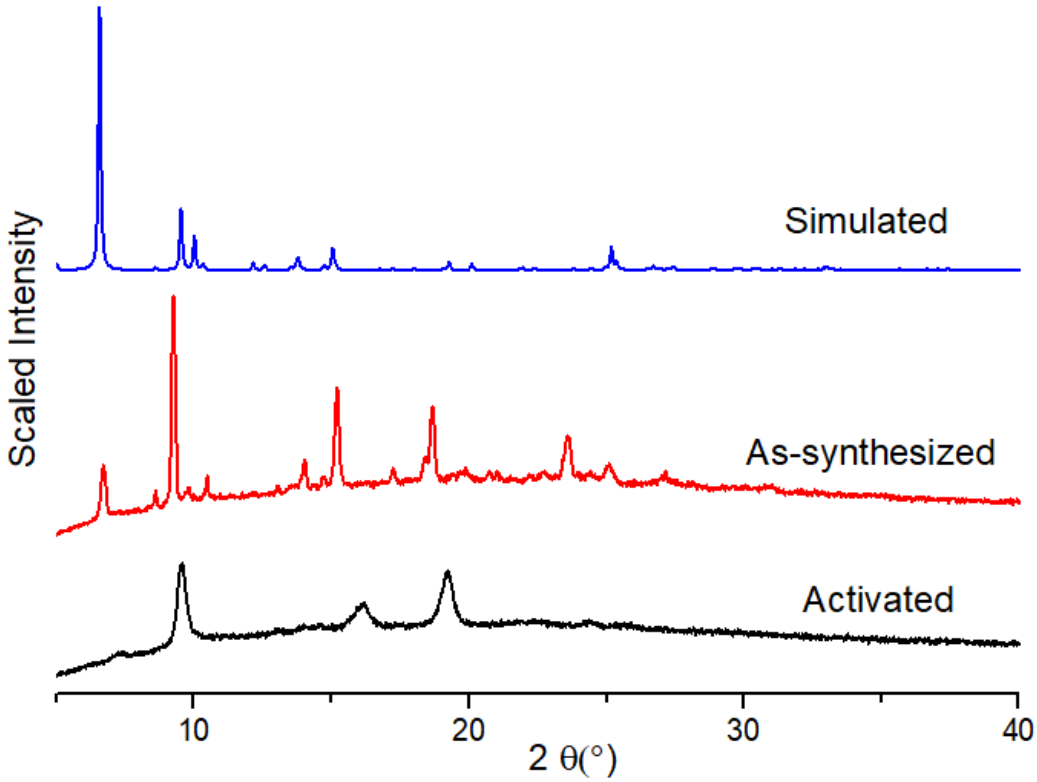

Figure 3.5. The PXRD patterns of as-synthesized **NFDMOF-1** (red), activated **NFDMOF-1** (black) and simulated **NFDMOF-1** (blue).

3.1.4. Xylene-Inclusion

To determine the porosity of **NFDMOF-1**, the as-synthesized MOF was immersed in xylene isomers separately for a week and analysed using SCXRD, PXRD and TGA.

(a). Thermogravimetric Analysis (TGA)

The TGA profiles of **NFDMOF-1-px**, **NFDMOF-1-ox**, and **NFDMOF-1-mx** (Fig 3.6) display weight loss from 40 °C, indicating the removal of the xylene isomers. A 11.49% weight loss was observed for **NFDMOF-1-px**, while the thermal profile of **NFDMOF-1-ox** shows weight loss of 12.93% and a 9.77% weight loss was also recorded for **NFDMOF-1-mx**. These weight losses are attributed to the loss of at least one xylene molecule on all the host- guest compounds. These weight losses were not included in the TGA plots for clarity. Decomposition of the framework commences at around 314.81 °C.

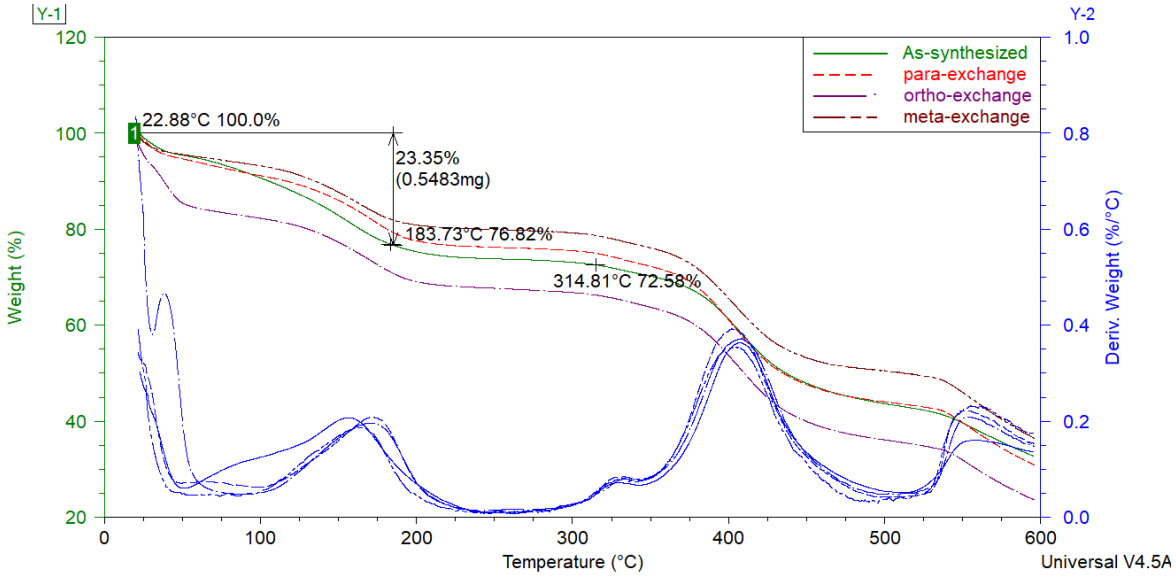

Figure 3.6. TGA profiles of the as-synthesized **NFDMOF-1** (solid green), and the as-synthesized with xylenes exchanged: **NFDMOF-1-px** (red), **NFDMOF-1-ox** (purple) and **NFDMOF-1-mx** (maroon) as well as the first derivatives of the weight %.

(b). Powder X-ray Diffraction (PXRD)

PXRD profiles of the guest-exposed phases were recorded to check any structural transformations due to xylene inclusion. There are some slight differences between the PXRD patterns of **NFDMOF-1** (as synthesized) and the xylene exchanged MOFs (**NFDMOF-1-ox**, **NFDMOF-1-mx** and **NFDMOF-1-px)** (Fig 3.7). The xylene exchanged MOFs have more peaks than the as-synthesized MOF.

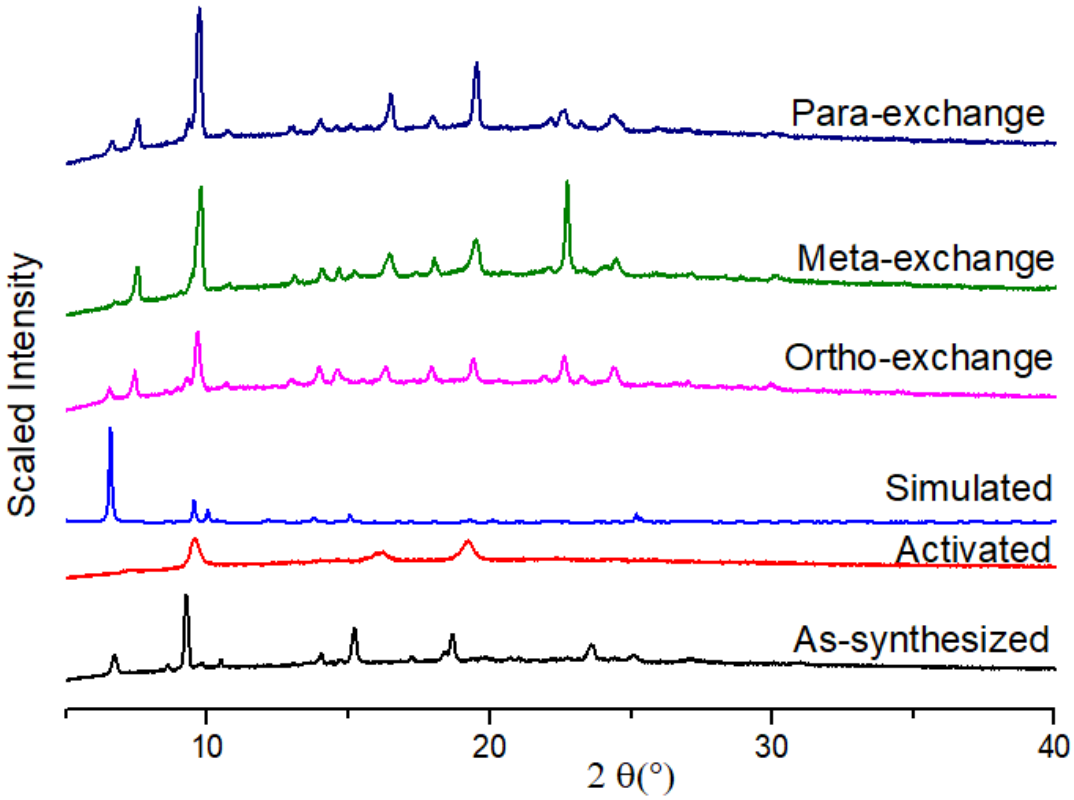

Figure 3.7. The PXRD patterns of as-synthesized **NFDMOF-1** (black), activated **NFDMOF-1** (red), simulated **NFDMOF-1** (blue) and the as-synthesized **NFDMOF-1** with xylenes exchanged: **NFDMOF-1-ox** (purple), **NFDMOF-1-mx** (green) and **NFDMOF-1-px** (navy).

3.2. NFDMOF-2

3.2.1. Single Crystal X-Ray Diffraction (SCXRD)

NFDMOF-2 was prepared from a solvothermal reaction of Lig2 (22 mg; 0.049 mmol), 2,6-naphthalenedicarboxylic acid (21 mg; 0.097 mmol) and zinc(II) nitrate hexahydrate (26 mg; 0.087 mmol) in 5 mL DMF. **NFDMOF-2** crystallizes in the monoclinic space group $P2_1/c$. The asymmetric unit of **NFDMOF-2** consists of half a Lig2 molecule, a zinc(II) cation, three DMF molecules and a 2.6-naphthalenedicarboxylate anion (Fig 3.8). The packing diagram showing the overall arrangement of the molecules in the crystal structure is presented in Fig 3.9. The packing diagram of **NFDMOF-2** viewed along the *bc* plane shows channels running along the crystallographic *a* axis. The DMF molecule is in the channels and occupies potential solvent accessible volume of 31.4%. A diagram displaying the guest accessible voids is presented in Fig 3.10. The structure contains 2D channels along the *a* axis.

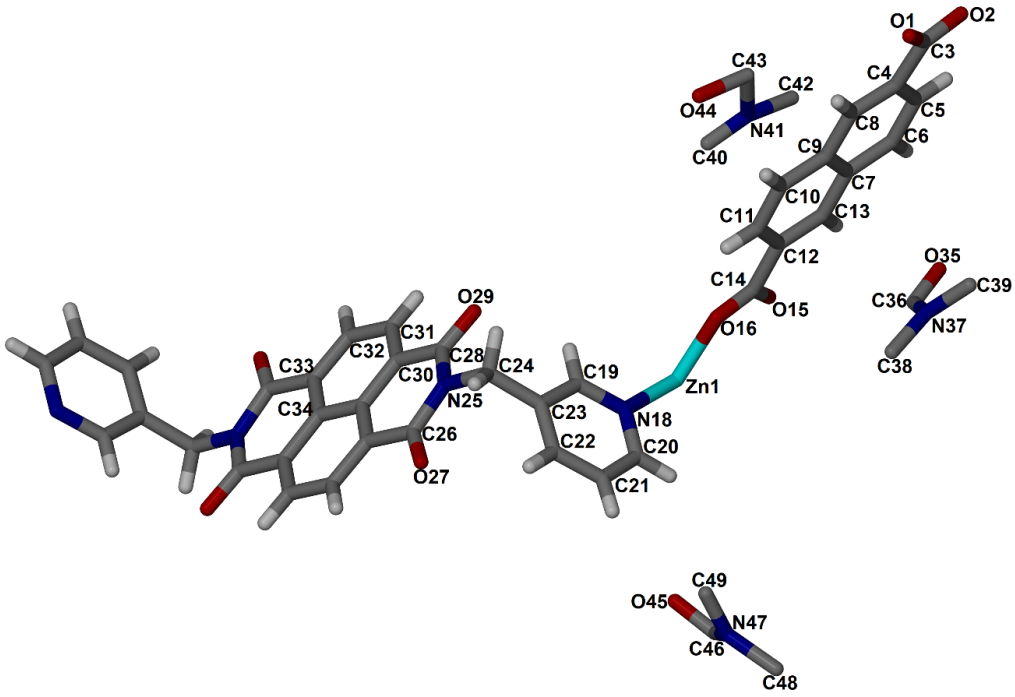

Figure 3.8. The molecular structure of NFDMOF-2 showing the crystallographic labelling for the asymmetric unit.

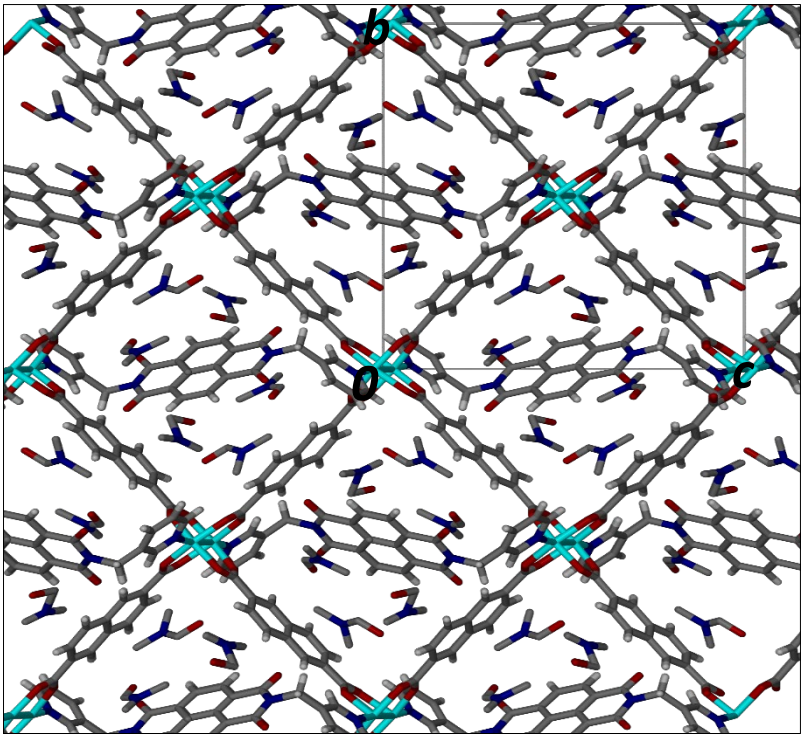

Figure 3.9. The packing diagram of NFDMOF-2 viewed in the *bc* plane. The DMF molecule is located in channels running along the crystallographic *a* axis.

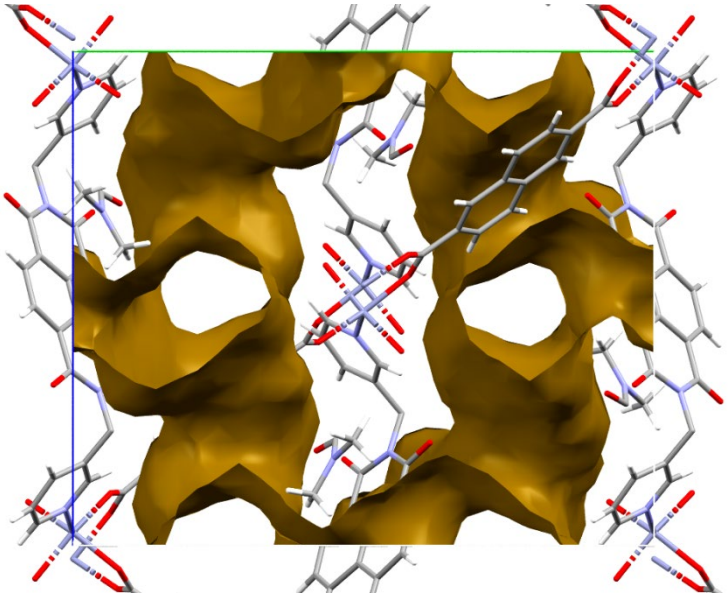

Figure 3.10. The guest accessible voids diagram of **NFDMOF-2** generated using the Mercury program.

3.2.2. Thermogravimetric Analysis (TGA)

The thermal profile of **NFDMOF-2** (Fig 3.11) shows a weight loss of 23.37% (calculated 22.60%) within the temperature range of 17.59 °C to 148.87 °C. This is attributed to the loss of three DMF molecules. The framework remains stable with no significant changes from 148.87 °C until 312.68 °C after which decomposition commences. The activated phase of **NFDMOF-2** was prepared by heating the as-synthesized crystals in an oven under vacuum at 100 °C for 24 hours. The success of the process was confirmed using TGA (Fig 3.11). The activated **NFDMOF-2** remains stable during the activation process and the framework decomposes at 312.68 °C (Fig 3.11).

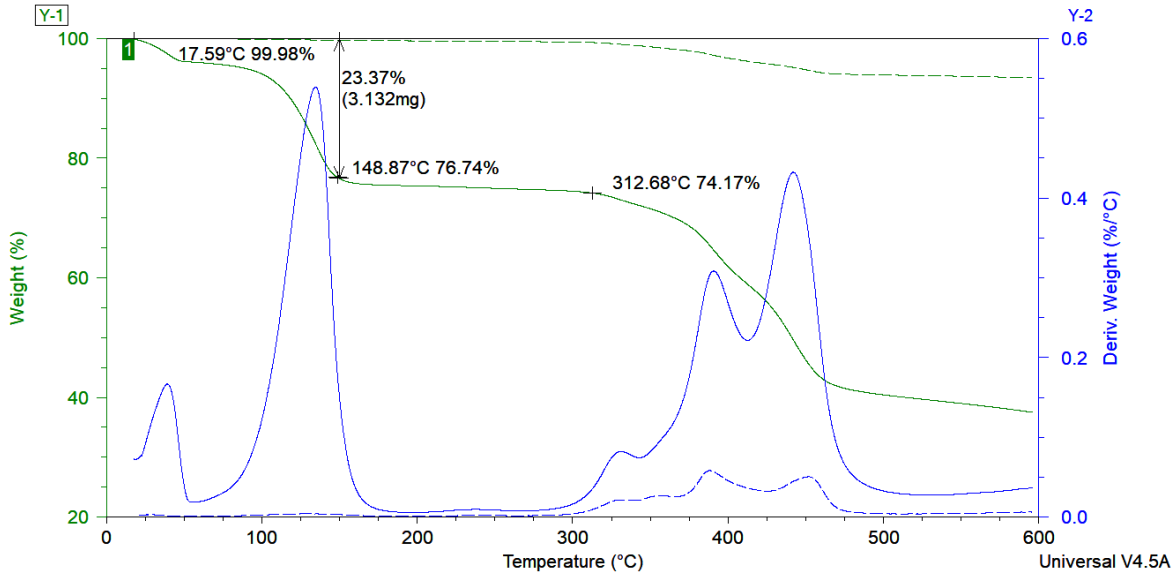

Figure 3.11. TGA profiles of the as-synthesized **NFDMOF-2** (solid green) and the activated **NFDMOF-2** (dashed green) as well as the first derivatives of the weight %: as-synthesized (solid blue) and activated (dashed blue).

3.2.3. Powder X-Ray Diffraction (PXRD)

Powder X-ray analysis was conducted on the crystals of **NFDMOF-2** (as-synthesized), and **NFDMOF-2** (activated). The PXRD patterns of **NFDMOF-2** (as-synthesised), **NFDMOF-2** (activated) and **NFDMOF-2** (simulated) are presented in Fig 3.12. The PXRD of the as-synthesized and activated plots are similar which indicates that the framework remains intact, it does not collapse during the activation process, and that the framework maintains crystallinity. The PXRD of the as-synthesized and the simulated graphs match meaning that the bulk material is pure. The slight difference observed in the PXRD patterns of the as-synthesized and the simulated may be due to presence of impurities in the as-synthesized material.

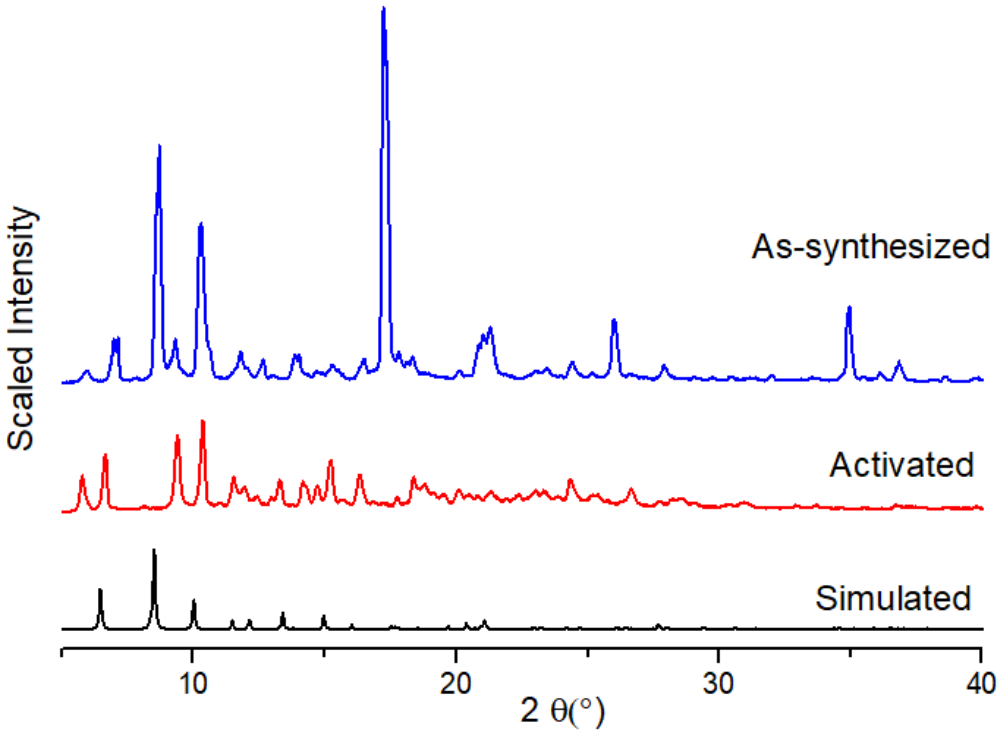

Figure 3.12. The PXRD patterns of as-synthesized **NFDMOF-2** (blue), activated **NFDMOF-2** (red) and simulated **NFDMOF-2** (black).

3.2.4. Xylene-Inclusion

The as-synthesized **NFDMOF-2** was immersed in the three xylene isomers separately for a week and analysed using SCXRD, PXRD and TGA. This was done to test for the porosity of the MOF.

(a). Thermogravimetric Analysis (TGA)

The TGA profiles of all **NFDMOF-2-ox, NFDMOF-2-mx** and exchange (Fig 3.13) show significant weight loss from 75 °C up to 138 °C, indicating the removal of the isomers of xylene. The thermal profiles show a mass loss of 27.91% for **NFDMOF-2-ox**, a mass loss of 27.50% for **NFDMOF-2-mx** and a mass loss of 27.53% for **NFDMOF-2-px.** These correspond to the mass loss of one isomer per host compound. Mass losses not shown on the TGA plot for a better view. Decomposition of the framework begins from 308.03 °C.

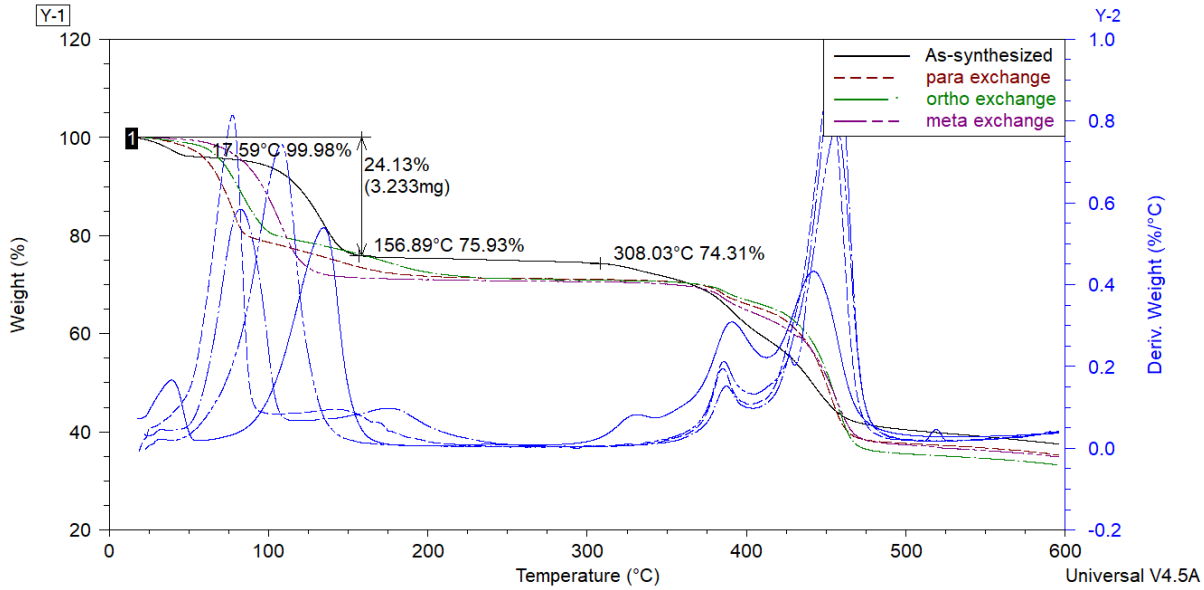

Figure 3.13. TGA profiles of the as-synthesized **NFDMOF-2** (solid black), and the as-synthesized with xylenes exchanged: **NFDMOF-2-px** (maroon), **NFDMOF-2-ox** (green) and **NFDMOF-2-mx** (purple) as well as the first derivatives of the weight %.

(b). Powder X-ray Diffraction (PXRD)

PXRD profiles of **NFDMOF-2-ox**, **NFDMOF-2-px,** and **NFDMOF-2-mx** were recorded to check any structural transformations that may have occurred due to xylene inclusion. The PXRD patterns differ from each other. **NFDMOF-2-ox**, and **NFDMOF-2-px** have more peaks than the as-synthesized **NFDMOF-2. NFDMOF-2-mx** has fewer peaks as compared to **NFDMOF-2** (Fig 3.14).

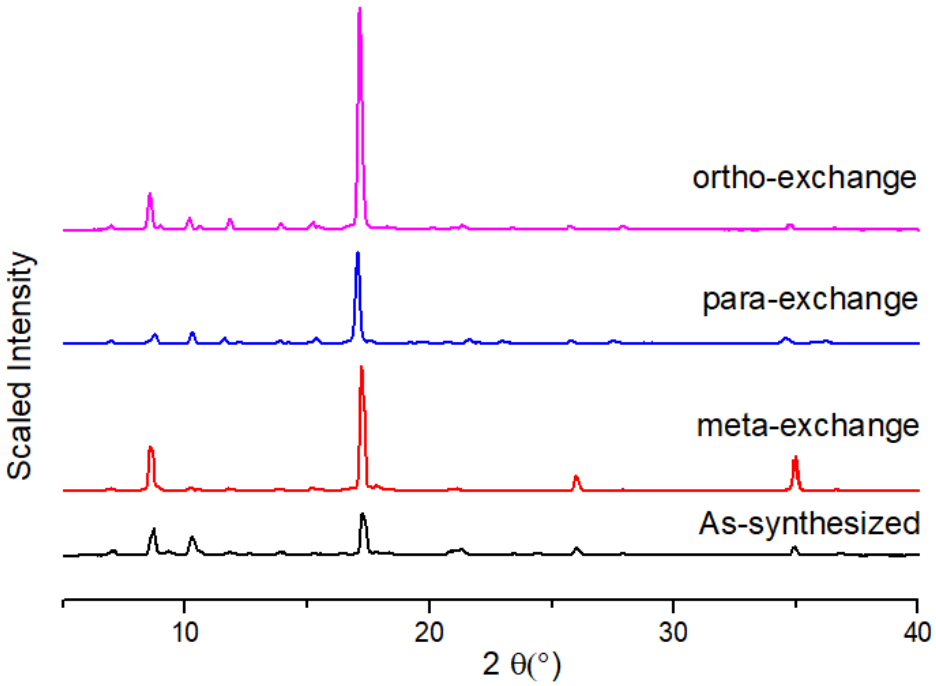

Figure 3.14. The PXRD patterns of as-synthesized **NFDMOF-2** (black), and the as-synthesized **NFDMOF-2** with xylenes exchanged: **NFDMOF-2-mx** (red), **NFDMOF-2-px** (blue) and **NFDMOF-2-ox** (purple).

3.3. NFDMOF-3

3.3.1. Single Crystal X-Ray Diffraction (SCXRD)

NFDMOF-3 was synthesized by reacting Lig4, 2.2'-Bipyridine-4.4'-dicarboxylic acid and cadmium(II) nitrate hexahydrate in 5 mL DMF under solvothermal conditions (100 °C, 72 hours). **NFDMOF-3** crystallizes in the monoclinic space group $P2_1/c$ with two cadmium(II) cations, two complete 2.2'-bipyridine-4.4'-dicarboxylate anion, two DMF molecules coordinated to the metal centre and two uncoordinated DMF molecules in the asymmetric unit (Fig 3.15). Lig4 did not coordinate, instead it remained in the solution, hence not part of the structure. The packing diagram of **NFDMOF-3** viewed in the *ab* plane shows channels running along the crystallographic *c* axis (Fig 3.16). A diagram showing the guest accessible voids is presented in Fig 3.17. **NFDMOF-3** displays solvent accessible volume of 26.1% calculated using probe radius of 1.2Å and grid spacing of 0.7Å.

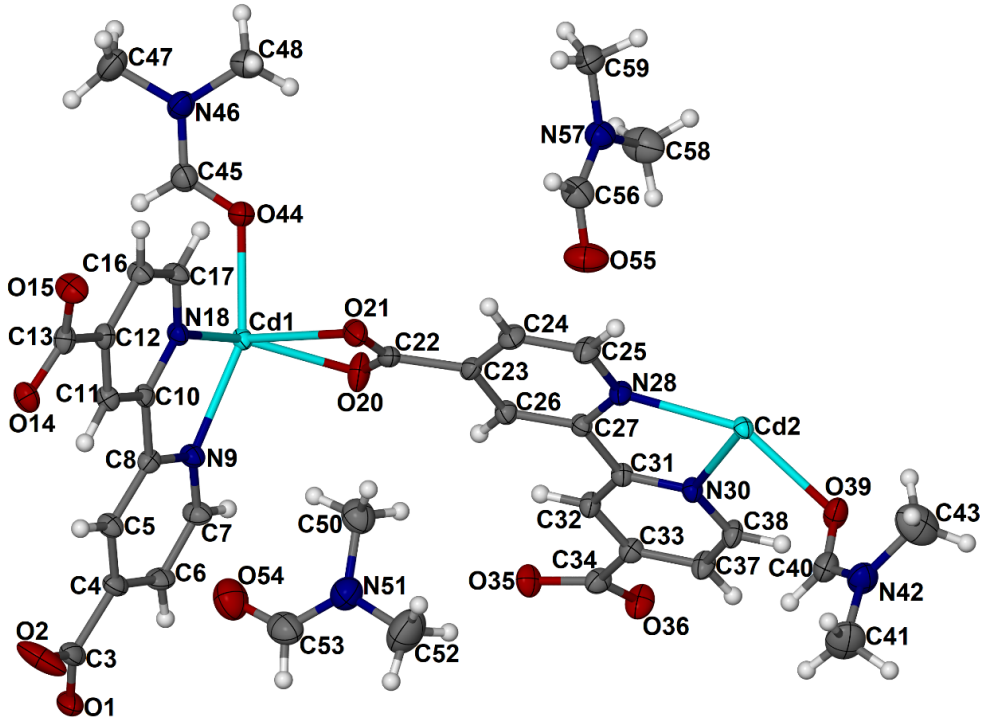

Figure 3.15. The asymmetric unit of NFDMOF-3 showing crystallographic labelling scheme. Ellipsoids are shown at the 70% probability level.

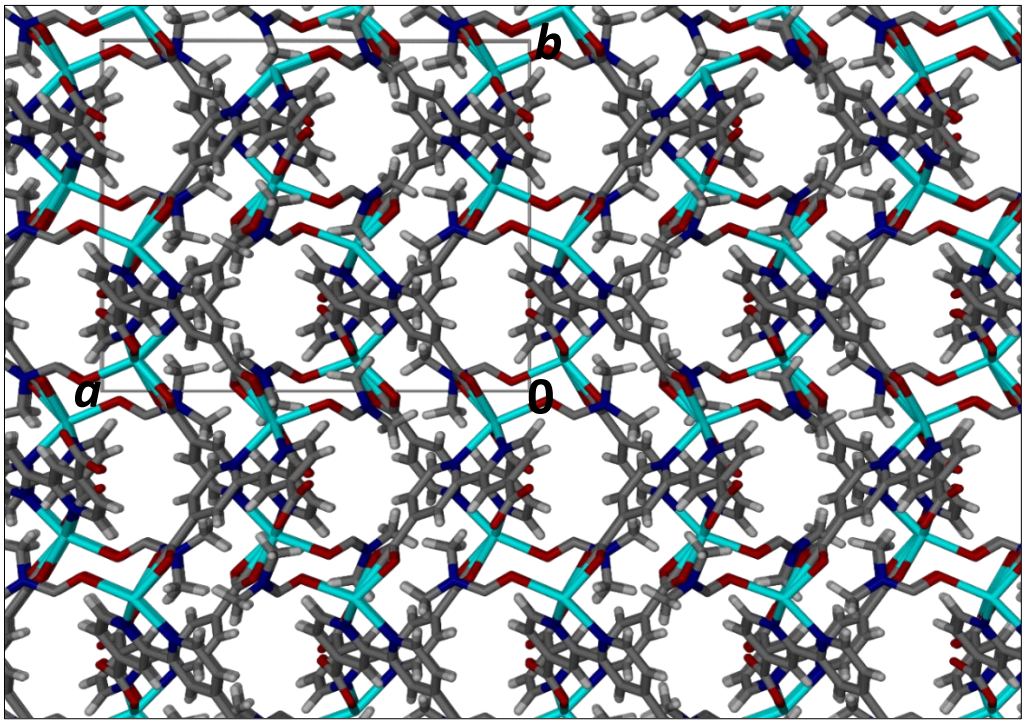

Figure 3.16. The packing diagram of NFDMOF-3 viewed in the *ab* plane. The DMF molecules are in channels running along the *c* axis.

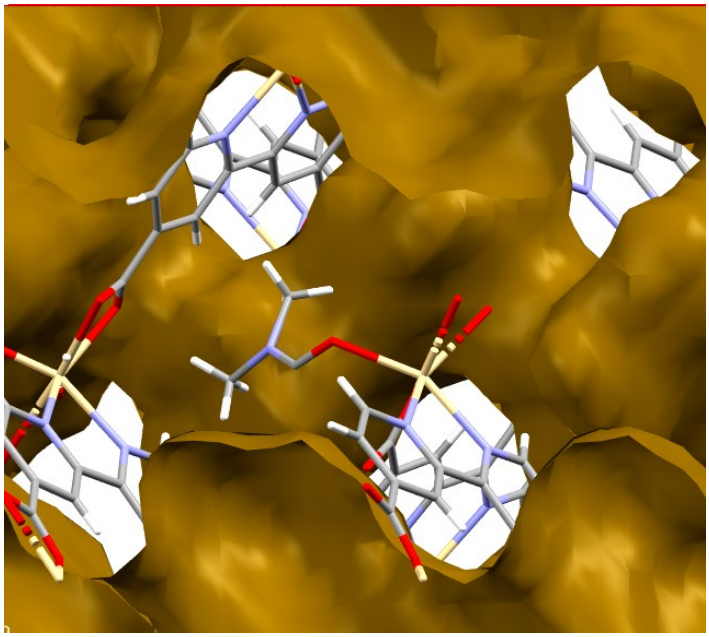

Figure 3.17. The guest accessible voids diagram of **NFDMOF-3** generated using the Mercury program.

3.3.2. Thermogravimetric Analysis (TGA)

The thermal profile of the as-synthesized **NFDMOF-3** shows a weight loss of 30.04 % (calculated 31.52%) within the temperature range of 16.26 °C to 260.58 °C. This is attributed to the loss of four DMF molecules; two coordinated DMF molecules (calculated 15.76%) and two uncoordinated DMF molecules (calculated 15.76%). The framework remains stable with no significant changes from 260.58 °C until 355.36 °C after which decomposition commences. The TGA trace of **NFDMOF-3** is presented in Fig 3.18.

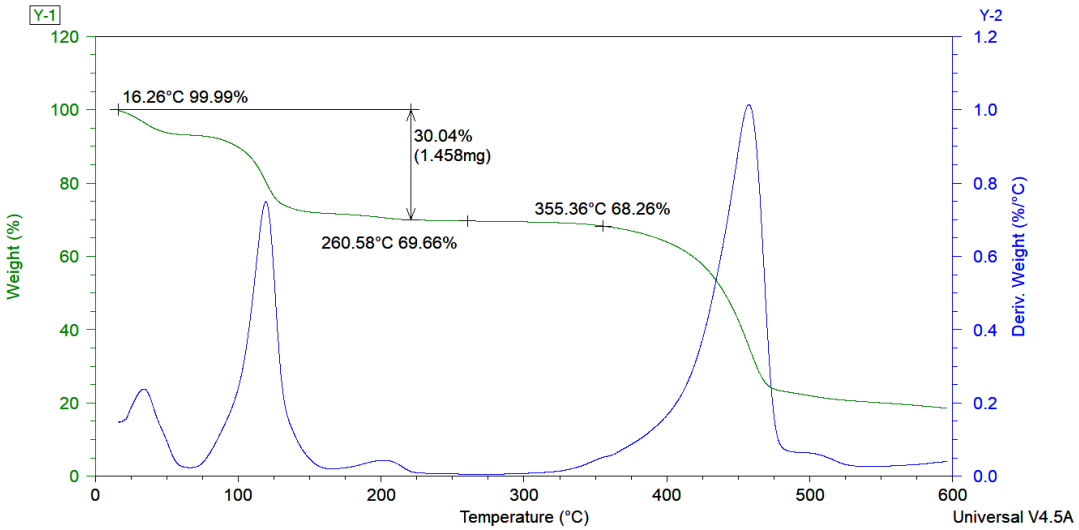

Figure 3.18. TGA profile of the as-synthesized **NFDMOF-3** (green) and its first derivative of the weight % plot (blue).

3.4. NFDMOF-4

3.4.1. Single Crystal X-Ray Diffraction (SCXRD)

NFDMOF-4 was prepared from a solvothermal reaction of Lig2 (20 mg; 0.045 mmol), 4,4'-oxybis (benzoic acid) (11.62 mg; 0.045 mmol) and cobaltous(II) nitrate hexahydrate (13.09 mg; 0.045 mmol in 10 mL DMF. **NFDMOF-4** crystallises in the monoclinic space group *C2/c* with one 4.4'-oxybis (benzoic acid) anion, one cobalt(II) cation, and half Lig2 molecule sitting on a centre of the symmetry and three uncoordinated DMF molecules in the asymmetric unit. The third DMF molecule is disordered and could not be modelled (Fig 3.19). The packing diagram viewed in the *ac* plane shows channels running along the crystallographic *b* axis occupied by the DMF molecules (Fig 3.20). A diagram displaying the potential solvent accessible volume within the channels of the compound is presented in Fig 3.21. The solvent accessible volume was found to be 10.8% determined using a probe radius of 1.2Å and a grid spacing of 0.7Å. The structure has one dimensional channels.

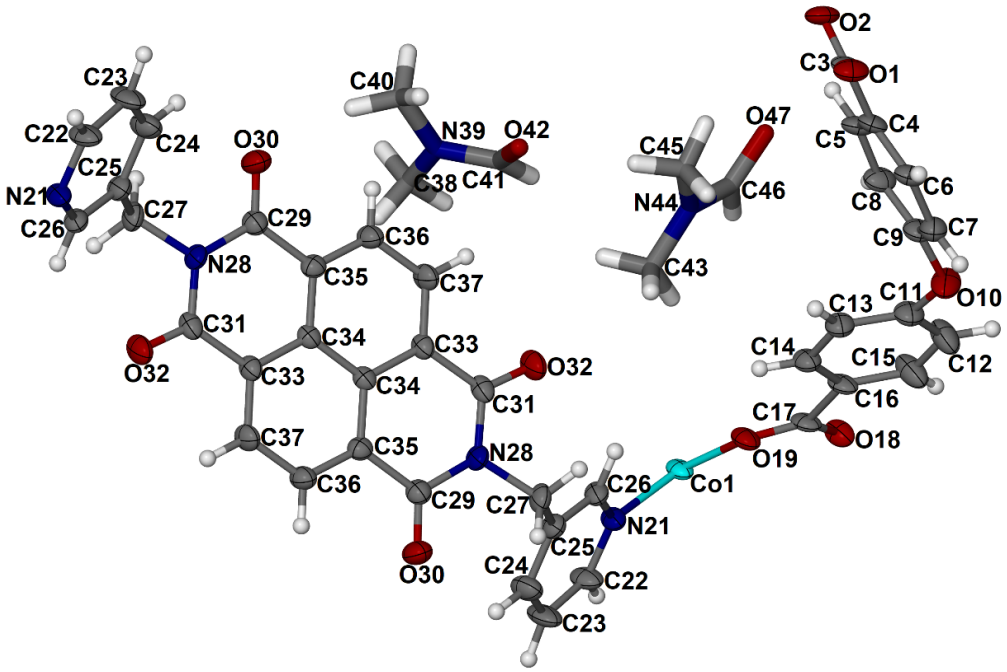

Figure 3.19. The molecular structure of **NFDMOF-4** showing the crystallographic labelling scheme for the asymmetric unit. Ellipsoids are shown at the 50% probability level.

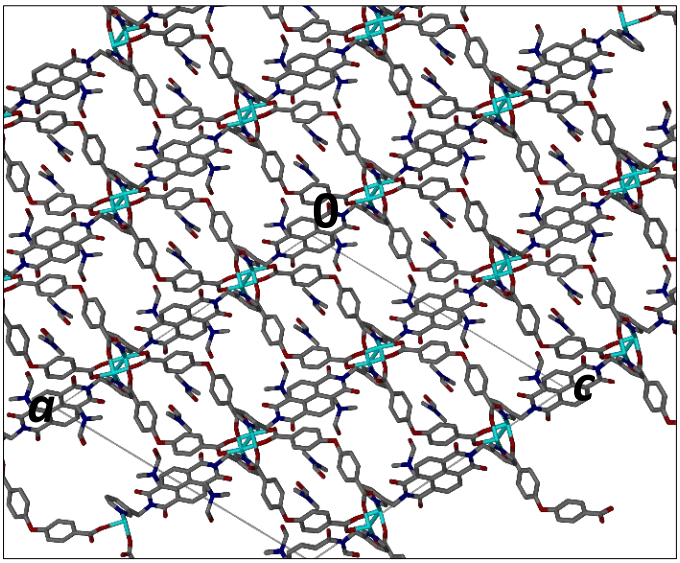

Figure 3.20. The packing diagram of **NFDMOF-4** viewed in the *ac* plane. The DMF molecules are in channels running along the *b* axis.

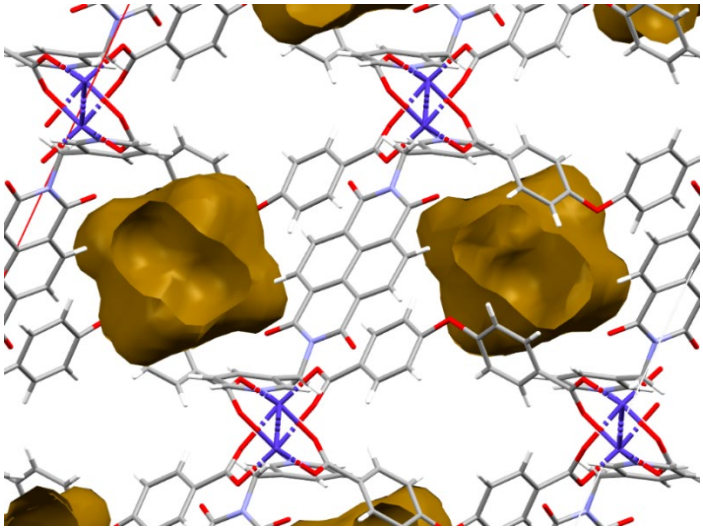

Figure 3.21. The guest accessible voids m of **NFDMOF-4** generated using the Mercury program.

3.4.2. Thermogravimetric Analysis (TGA)

The TGA trace of the as-synthesized **NFDMOF-4** (Fig 3.22) shows a weight loss of 19.68% within the temperature range of 19.68 °C to 147.25 °C. This weight loss is attributed to the loss of three DMF molecules (calculated 19.32%). The framework remains stable with no further significant changes within the temperature range of 147.25 °C to 338.09 °C. Decomposition commences at 338.09 °C. Activated **NFDMOF-4** (Fig 3.22) was prepared by heating the as-synthesized crystals at 100 °C for 24 hours under vacuum. The TGA profile of the activated phase shows no weight loss until 338.09 °C after which the framework begins to decompose. This confirms that the activation process was a success.

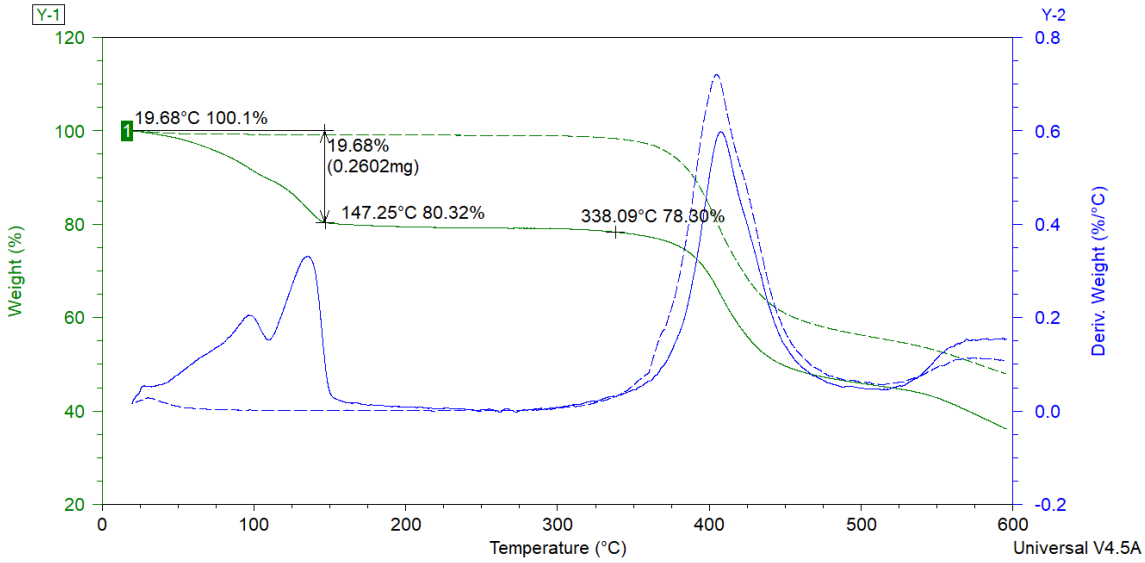

Figure 3.22. TGA profiles of the as-synthesized **NFDMOF-4** (solid green) and the activated **NFDMOF-4** (dashed green) as well as the first derivatives of the weight %: as-synthesized (solid blue) and activated (dashed blue).

3.4.3. Powder X-Ray Diffraction (PXRD)

PXRD was used to confirm bulk phase purity of **NFDMOF-4** and the stability of the compound after the activation process. The PXRD patterns of **NFDMOF-4** (as-synthesised), **NFDMOF-4** (activated) and **NFDMOF-4** (simulated) are presented in Fig 3.23. The PXRD of the as- synthesized and activated plots are similar which indicates that the MOF does not lose crystallinity and maintains its framework structure during desolvation. The PXRD of the as-synthesized and the simulated graphs are similar which indicates that the single crystal selected for SCXRD has the same crystal structure as the bulk material.

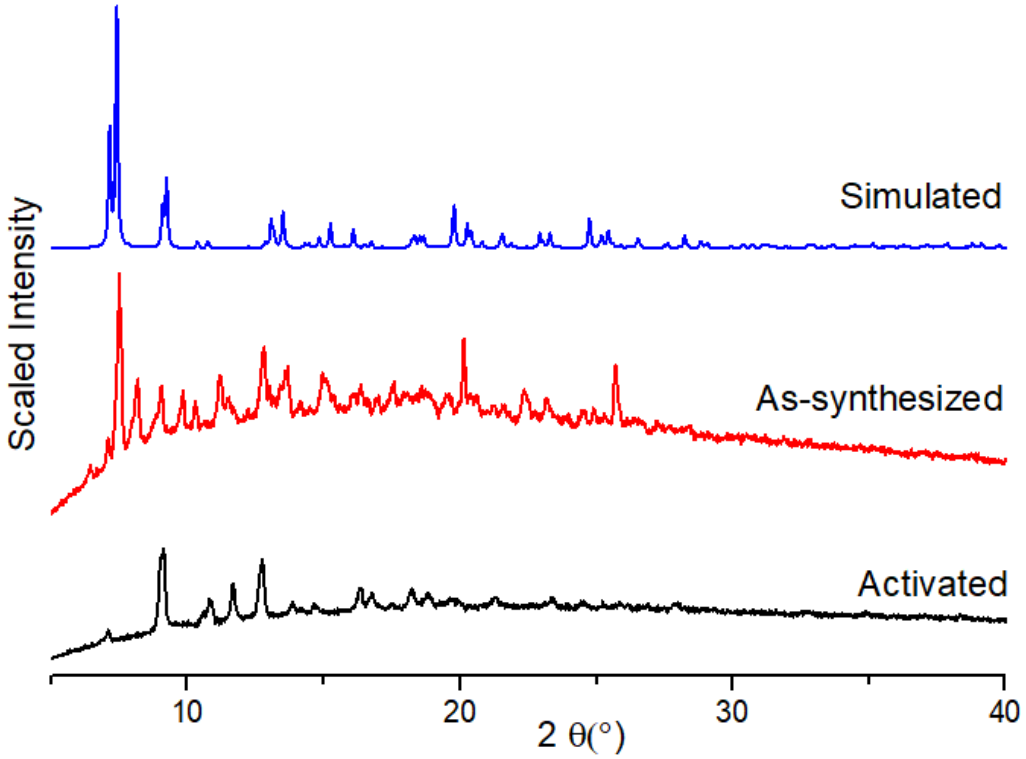

Figure 3.23. The PXRD patterns of as-synthesized **NFDMOF-4** (red), activated **NFDMOF-4** (black) and simulated **NFDMOF-4** (blue).

3.4.4. Xylene-Inclusion

Xylene inclusion was achieved by immersing **NFDMOF-4** in the three isomers of xylene on separate vials for five days and characterized using SCXRD, TGA and PXRD.

(a). Single Crystal X-Ray Diffraction (SCXRD)

Crystals of **NFDMOF-4** were exposed to the three xylene isomers separately and the resulting inclusion compounds were analysed using SCXRD. **NFDMOF-4-px** consists of half a Lig2 molecule, deprotonated 4.4'-oxybis (benzoic acid), Co(II) cation, one DMF molecule and one *para*-xylene isomer in the asymmetric unit (Fig 3.24). The packing diagram of **NFDMOF-4-px** viewed in the *ac* plane showing continuous channels running along the crystallographic *b* axis is presented in Fig 3.25. **NFDMOF-4-ox** is made up of dimeric 'paddle- wheel' consisting of two carboxylate bridges (two deprotonated 4.4'-oxybis (benzoic acid)), two metal-metal bonds (Co-- Co), and two independent halves of Lig2 molecules, four uncoordinated DMF molecules and one *ortho*-xylene isomer in the asymmetric unit (Fig 3.26). The

packing diagram of NFDMOF-4-ox viewed in the *ac* plane is presented in Fig 3.27. NFDMOF-4-mx consists of half a Lig2 molecule, deprotonated 4.4'-oxybis (benzoic acid), Co(II) cation, one DMF molecule and one *meta*-xylene isomer in the asymmetric unit (Fig 3.28). The packing diagram of NFDMOF-4-mx viewed in the *ac* plane showing continuous channels running along the crystallographic *b* axis is presented in Fig 3.29.

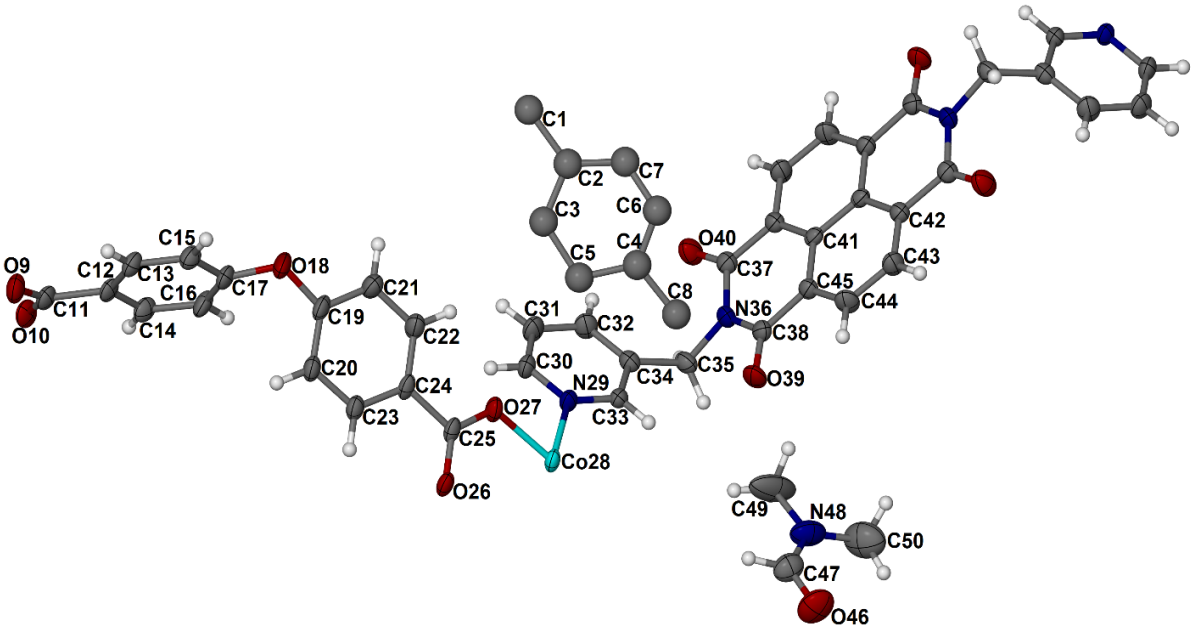

Figure 3.24. The molecular structure of NFDMOF-4-px showing the crystallographic labelling scheme for the asymmetric unit. Ellipsoids are shown at the 70% probability level.

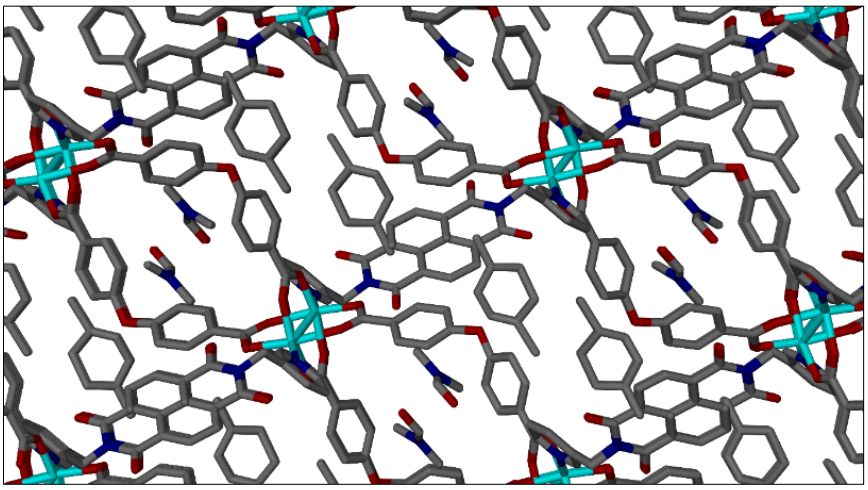

Figure 3.25. The packing diagram of NFDMOF-4-px viewed in the *ac* plane. The *para* xylene isomer and DMF molecules are in channels running along the *b* axis. Hydrogen atoms are omitted for a clear view.

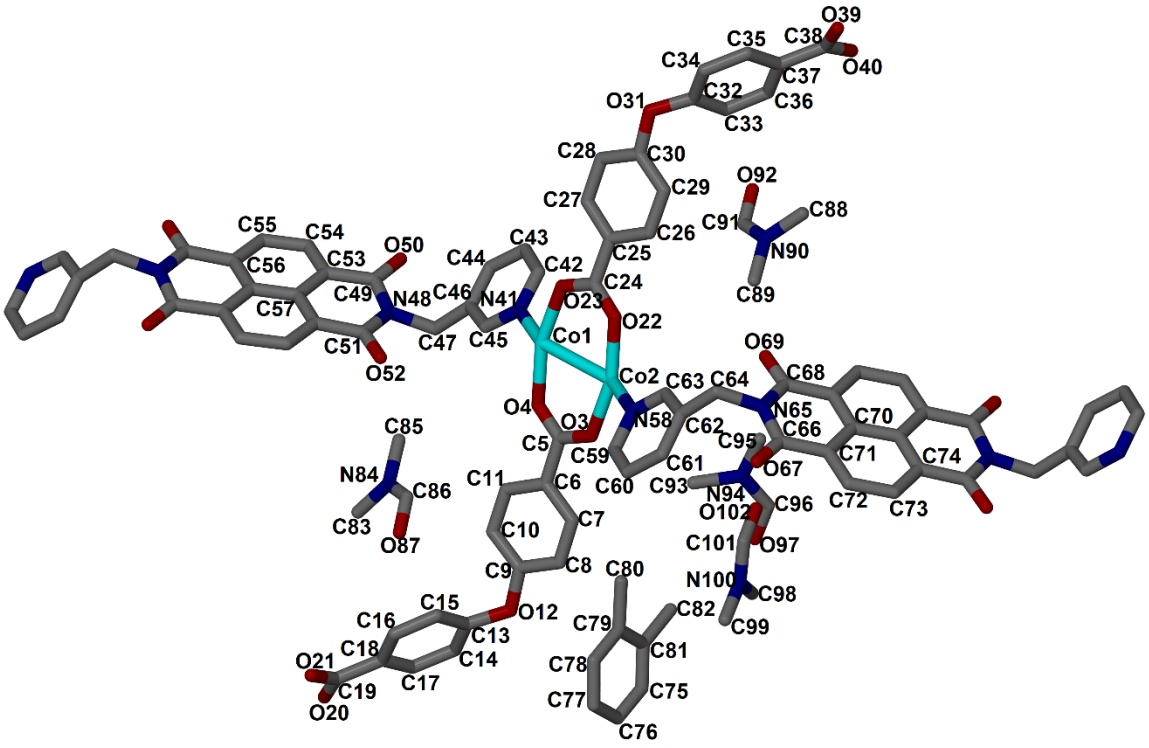

Figure 3.26. The molecular structure of NFDMOF-4-ox showing the crystallographic labelling scheme for the asymmetric unit. Hydrogen atoms are omitted for a clear view.

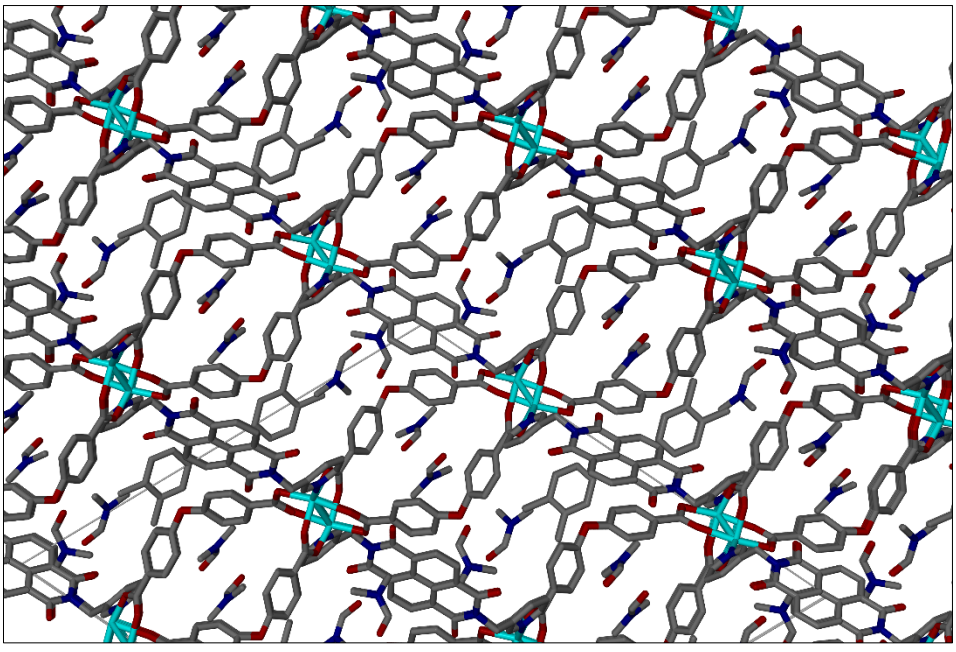

Figure 3.27. The packing diagram of NFDMOF-4-ox viewed in the *ac* plane. The DMF molecules are in channels running along the *b* axis. Hydrogens omitted for clear view.

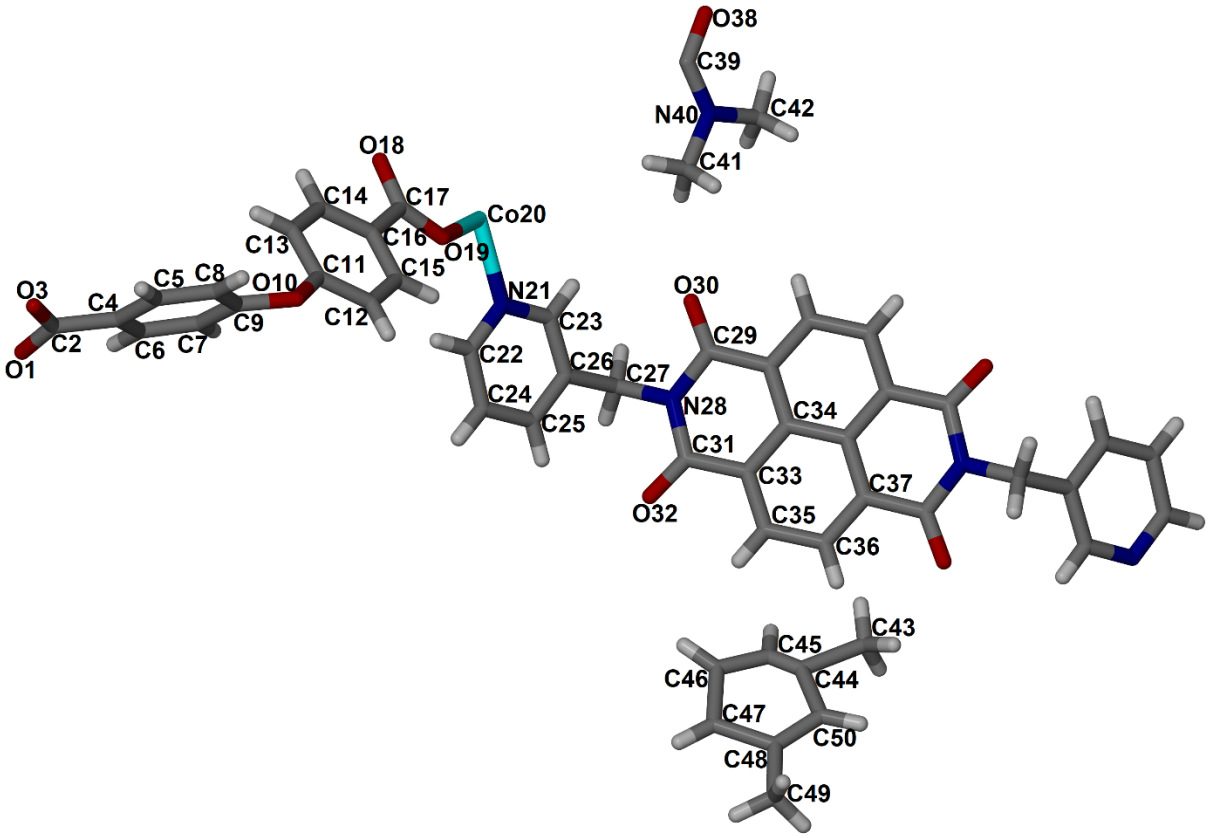

Figure 3.28. The molecular structure of NFDMOF-4-mx showing the crystallographic labelling scheme for the asymmetric unit.

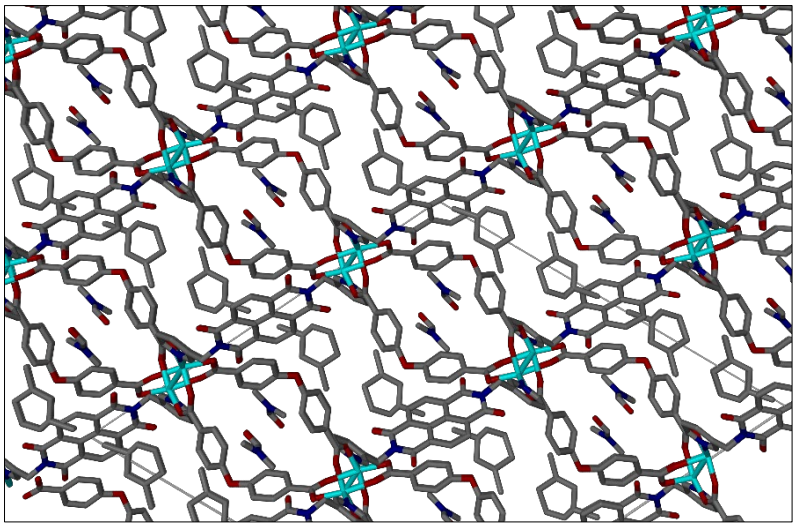

Figure 3.29. The packing diagram of NFDMOF-4-mx viewed in the *ac* plane. The *meta* xylene isomer and DMF molecules are in channels running along the *b* axis. Hydrogens are omitted for a clear view.

(b). Thermogravimetric Analysis (TGA)

The TGA profiles of **NFDMOF-4-ox,** and **NFDMOF-4-px** exchange (Fig 3.30) show significant weight loss from 100 °C, indicating the removal of trapped xylene. The thermal profile of **NFDMOF-4-ox** shows a weight loss of 24.84%, while a weight loss of 24.73% was observed for **NFDMOF-4-px** and a significant weight loss of 20.58% was recorded for **NFDMOF-4-mx.** These losses are attributed to at least one xylene molecule, and they are not included in the plot below for clarity. Decomposition of the framework commences at around 352.13 °C.

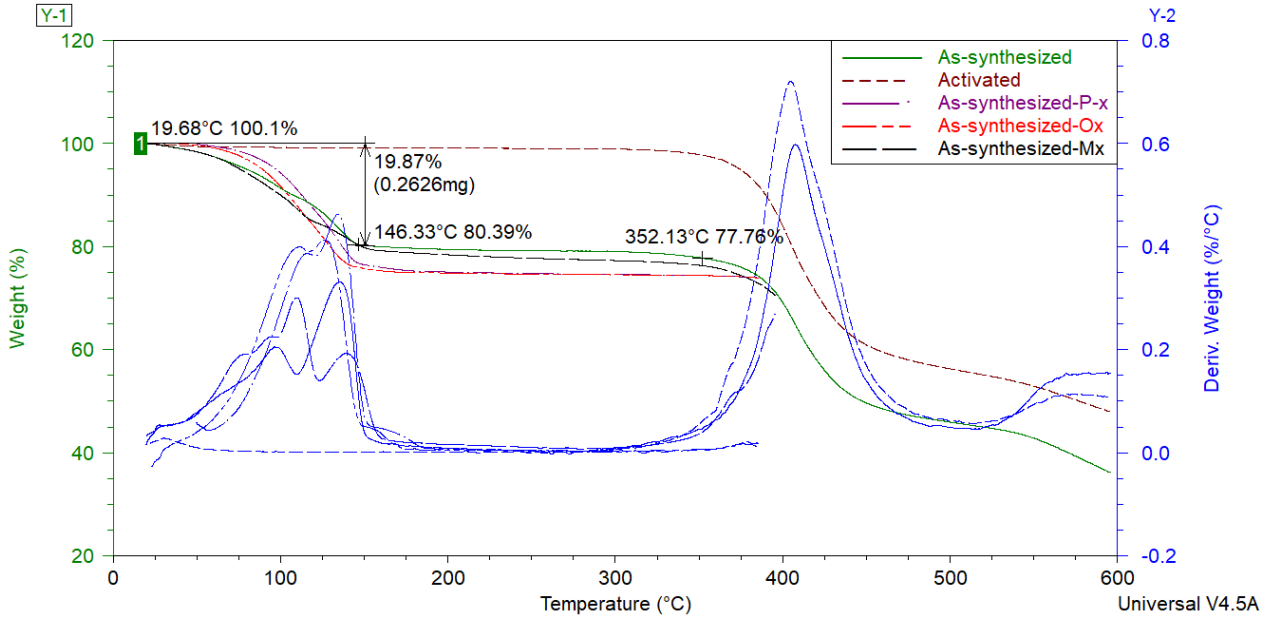

Figure 3.30. TGA profiles of the as-synthesized **NFDMOF-4** (solid green), the activated **NFDMOF-4** (dashed maroon) and the as-synthesized with xylenes exchanged: **NFDMOF-4-px** (purple), **NFDMOF-4-ox** (red) and **NFDMOF-4-mx** (black) as well as the first derivatives of the weight %.

(c). Powder X-Ray Diffraction (PXRD)

PXRD was used to check for structural changes of **NFDMOF-4** upon guest exchange. The PXRD patterns of the **NFDMOF-4-mx**, **NFDMOF-4-px** and **NFDMOF-4-mx** show that the as-synthesized **NFDMOF-4** maintains crystallinity during guest exchange. The PXRD patterns are presented in Fig 3.31. The powder patterns of **NFDMOF-4-mx**, **NFDMOF-4-px** and **NFDMOF-4-mx** are different from the as-synthesized **NFDMOF-4**, indicating a structural transformation after the guest exchange.

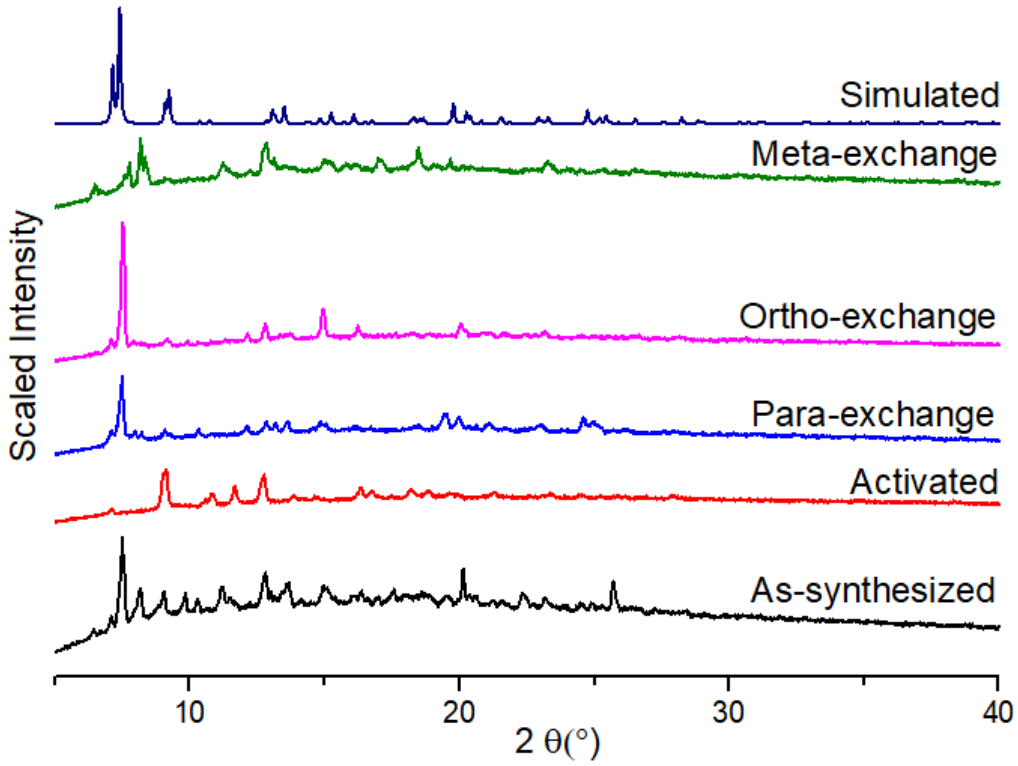

Figure 3.31. The PXRD patterns of as-synthesized **NFDMOF-4** (black), activated **NFDMOF-4** (red), simulated **NFDMOF-4** (navy) and the as-synthesized **NFDMOF-4** with xylenes exchanged: **NFDMOF-4-px** (blue), **NFDMOF-4-ox** (purple) and **NFDMOF-4-mx** (green).

(d). Dynamic Vapour Sorption (DVS)

Dynamic vapour sorption of **NFDMOF-4** was investigated to test for permanent porosity and sorption performances of the compound. Vapour sorption measurements were carried out using the activated **NFDMOF-4**. A continuous significant uptake was observed for *para* -xylene vapor with up to 24mg adsorbed. A constant uptake was also observed for *ortho*-xylene vapor with up to 15mg adsorbed. The adsorption analysis of *meta*-xylene vapor showed negligible uptake with only 0.002mg adsorbed. These results evidently indicate that **NFDMOF-4** adsorbs both *para*- and *ortho*-xylene vapour inside the channels over *meta*-xylenes, though it adsorbs more of the *para*-xylene (Fig 3.32).

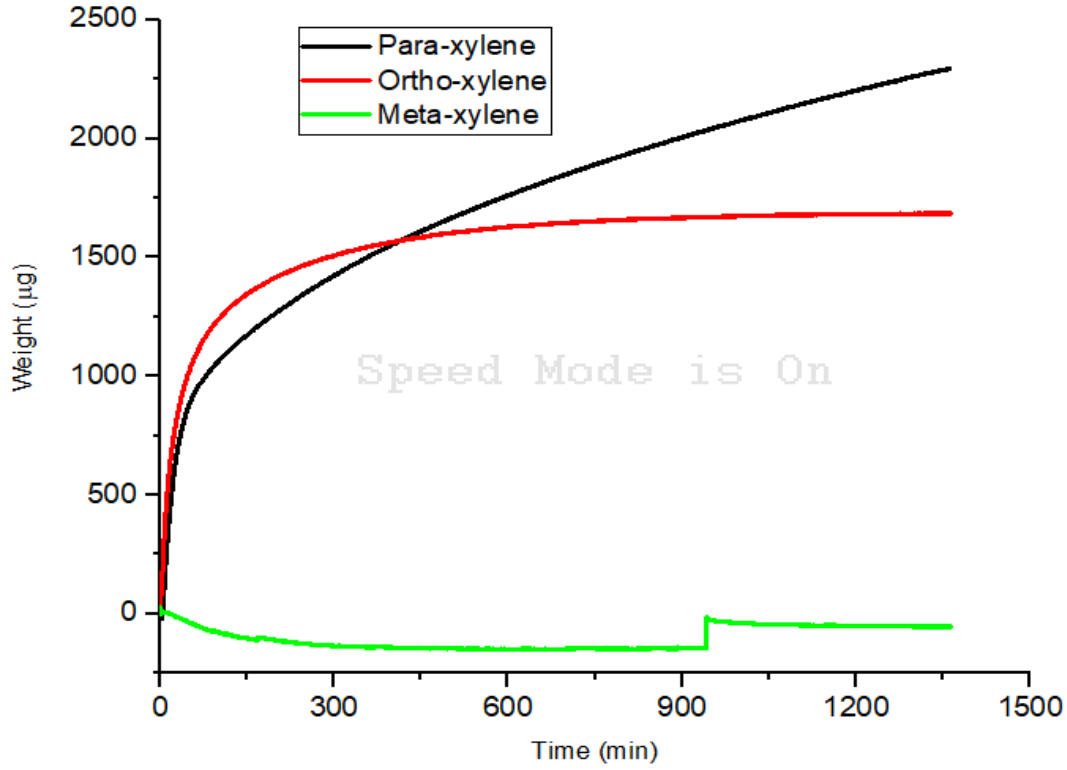

Figure 3.32. Dynamic vapour sorption for NFDMOF-4 displaying the extent of reaction as a function of time for the uptake of the three xylene isomers; **NFDMOF-4-px** (black), **NFDMOF-4-ox** (red), and **NFDMOF-4-mx** (green).

3.5. NFDMOF-5

3.5.1. Single Crystal X-Ray Diffraction (SCXRD)

NFDMOF-5 was prepared from a solvothermal reaction of Lig2 (20 mg; 0.045 mmol), 4,4'-oxybis (benzoic acid) (11.62 mg; 0.045 mmol) and zinc(II) nitrate hexahydrate (13.39 mg; 0.045 mmol) in 10 mL DMF. **NFDMOF-5** crystallizes in the monoclinic space group *C2/c* with one deprotonated 4.4'-oxybis (benzoic acid), one zinc(II) cation, half a molecule of Lig2 and three DMF molecules in the asymmetric unit (ASU) (Fig 3.33). The two DMF molecules could not be modelled. The Zn(II) centre is six-coordinate, exhibiting a zinc paddle wheel coordination environment composed of two nitrogen atoms and four oxygen atoms. The packing diagram viewed in the *ab* plane shows continuous channels running along the *c* axis (Fig 3.34). The potential guest accessible voids are found to be 34.0% using a probe radius of 1.2Å and grid spacing of 0.7Å (Fig 3.35). The structure has 3D channels.

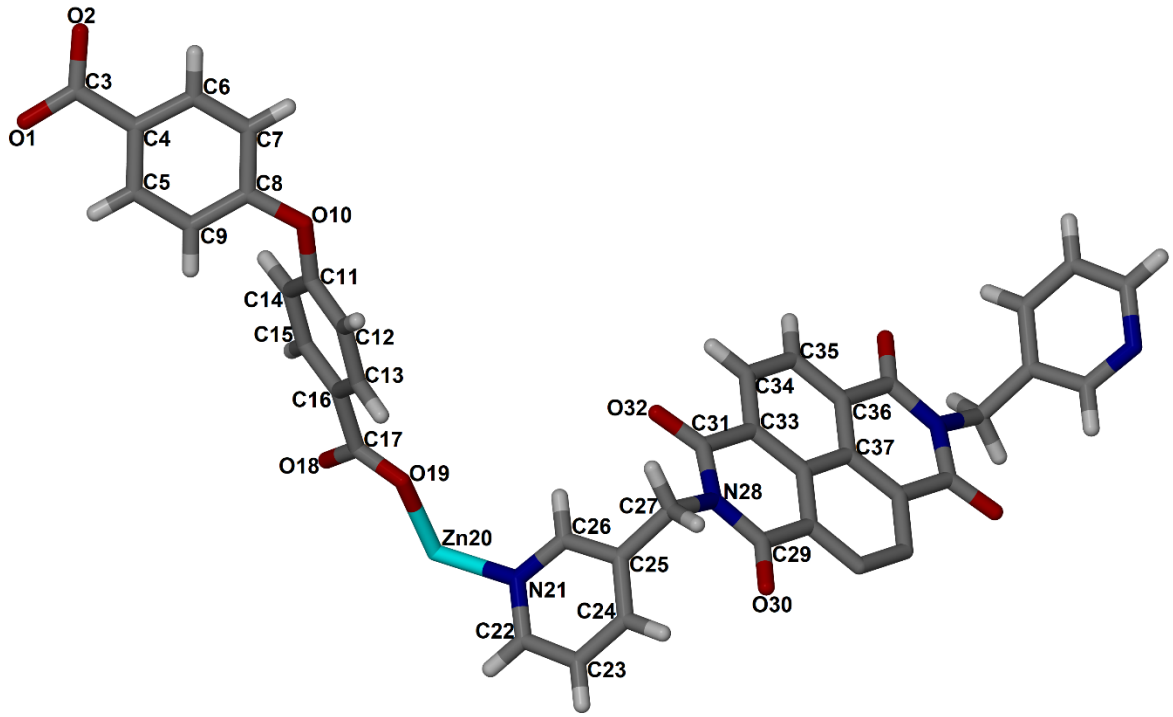

Figure 3.33. The molecular structure of NFDMOF-5 showing the crystallographic labelling scheme for the asymmetric unit.

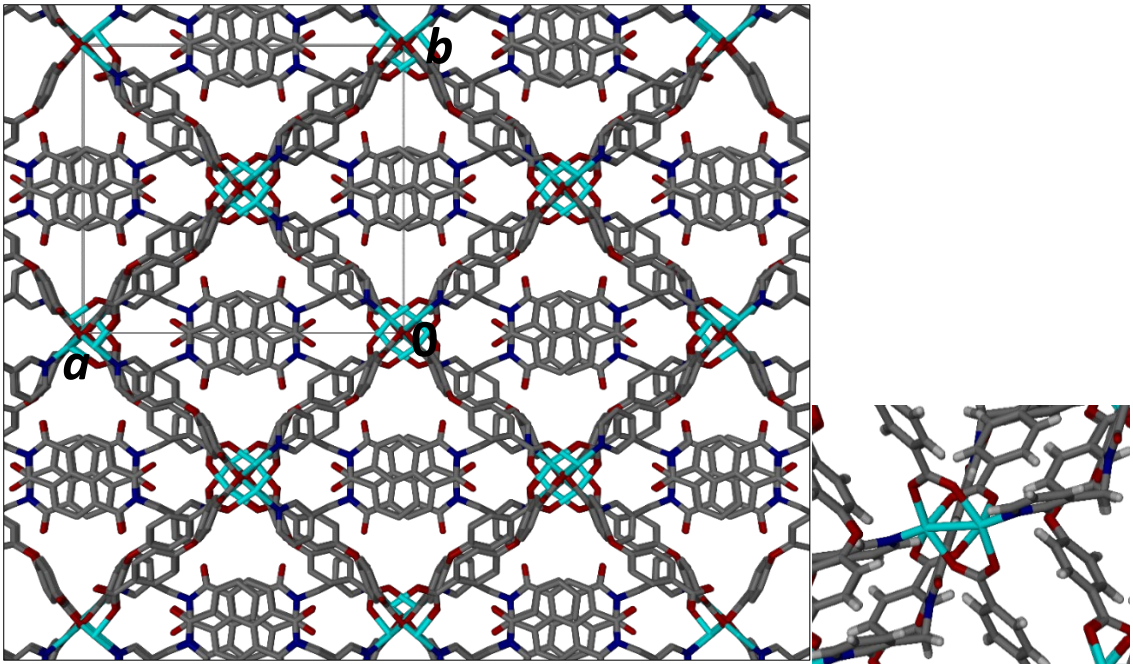

Figure 3.34. The packing diagram of NFDMOF-5 viewed in the *ab* plane and a coordination environment around Zn(II) centre . The DMF molecules are in channels running along the *c* axis.

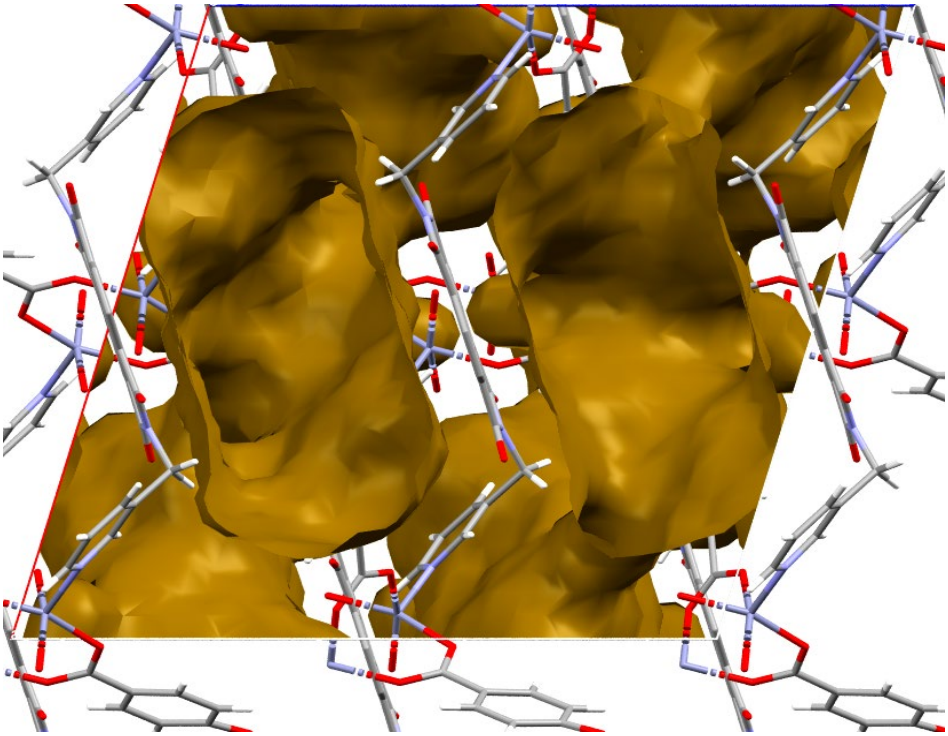

Figure 3.35. The guest accessible voids of **NFDMOF-5** generated using the Mercury program.

3.5.2. Thermogravimetric Analysis (TGA)

The thermal profile of the as-synthesized **NFDMOF-5** (Fig 3.36) shows a weight loss of 17.48% (calculated 23.62%) within the temperature range of 21.54 °C to 153.74 °C. This weight loss is attributed to the loss of two DMF molecules. The framework remains stable with no significant changes from 153.74 °C until 359.01 °C after which decomposition commences. The activated **NFDMOF-5** was prepared by heating the as-synthesized crystals at 100 °C for 24 hours under vacuum. The TGA profile of the activated phase shows no weight loss from 21.54 °C to 359.01 °C which confirms that the activation process was a success (Fig 3.36).

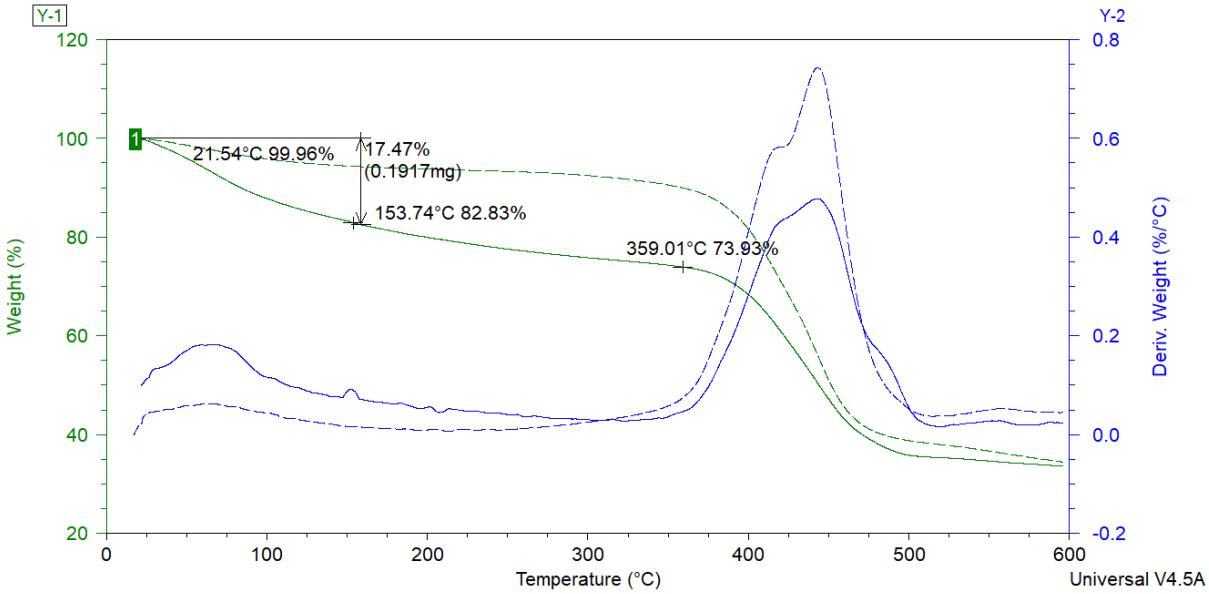

Figure 3.36. TGA profiles of the as-synthesized **NFDMOF-5** (solid green) and the activated phase (dashed green) as well as the first derivatives of the weight %: as-synthesized (solid blue) and activated (dashed blue).

3.5.3. Powder X-Ray Diffraction (PXRD)

PXRD was conducted on the crystals of **NFDMOF-5** (as-synthesized), and **NFDMOF-5** (activated) and the PXRD patterns were compared to the **NFDMOF-5** (simulated) pattern (Fig 3.37). The PXRD pattern of the activated **NFDMOF-5** shows that the compound loses crystallinity, as evidenced by the broad peaks (Fig 3.37). The PXRD patterns of the as-synthesized **NFDMOF-5** and the simulated graphs match indicating that the single crystal selected for SCXRD is a representative of the bulk crystals and it further confirms that the compound is pure. There is also evidence of loss of monocrystallinity on the PXRD pattern of the as-synthesised **NFDMOF-5.**

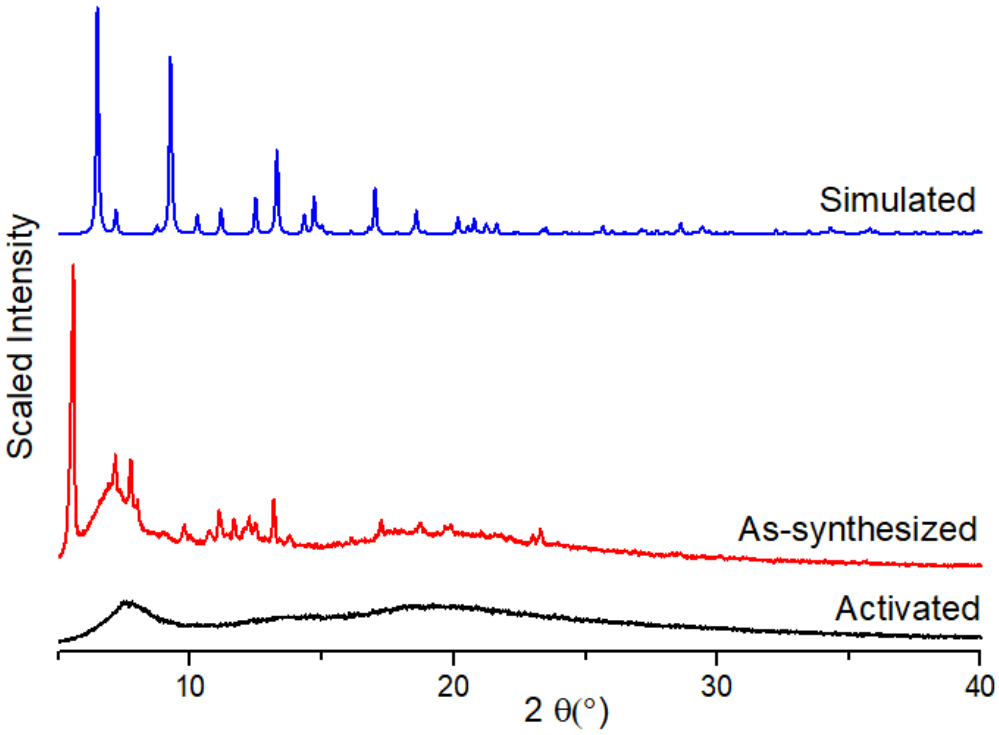

Figure 3.37. The PXRD patterns of as-synthesized **NFDMOF-5** (red), activated **NFDMOF-5** (black) and simulated **NFDMOF-5** (blue).

3.5.4. Xylene-Inclusion

(a). Single Crystal X-Ray Diffraction (SCXRD)

The **NFDMOF-5** was exposed to all three xylene isomers separately by immersing the as-synthesised crystals in the liquid xylene isomers. The resultant clathrates were characterized using SCXRD. **NFDMOF-5-mx** consists of two independent halves of Lig2 molecules, two deprotonated 4.4'-oxybis (benzoic acid), two Zn(II) cations, four DMF molecules and one *meta*-xylene isomer in the asymmetric unit (Fig 3.38). The packing diagram of **NFDMOF-5-mx** viewed in the *ac* plane showing continuous channels running along the crystallographic *b* axis is shown in Fig 3.39.

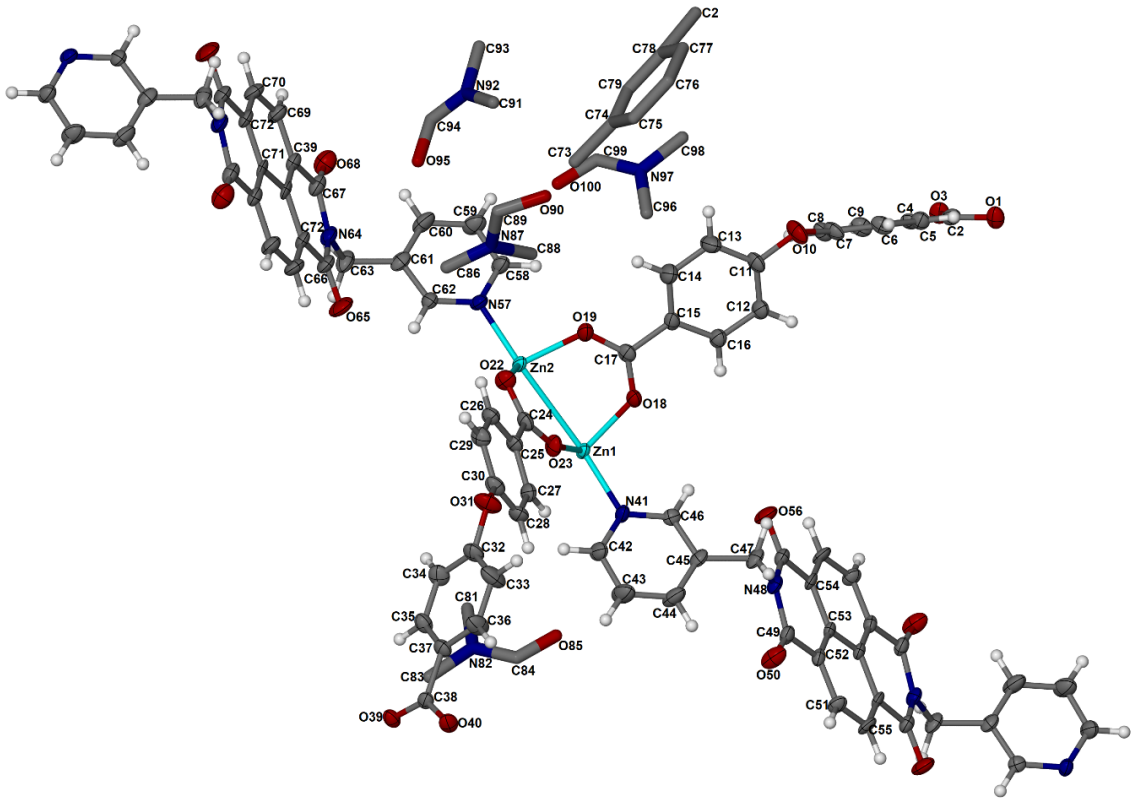

Figure 3.38. The molecular structure of NFDMOF-5-mx showing the crystallographic labelling scheme for the asymmetric unit.

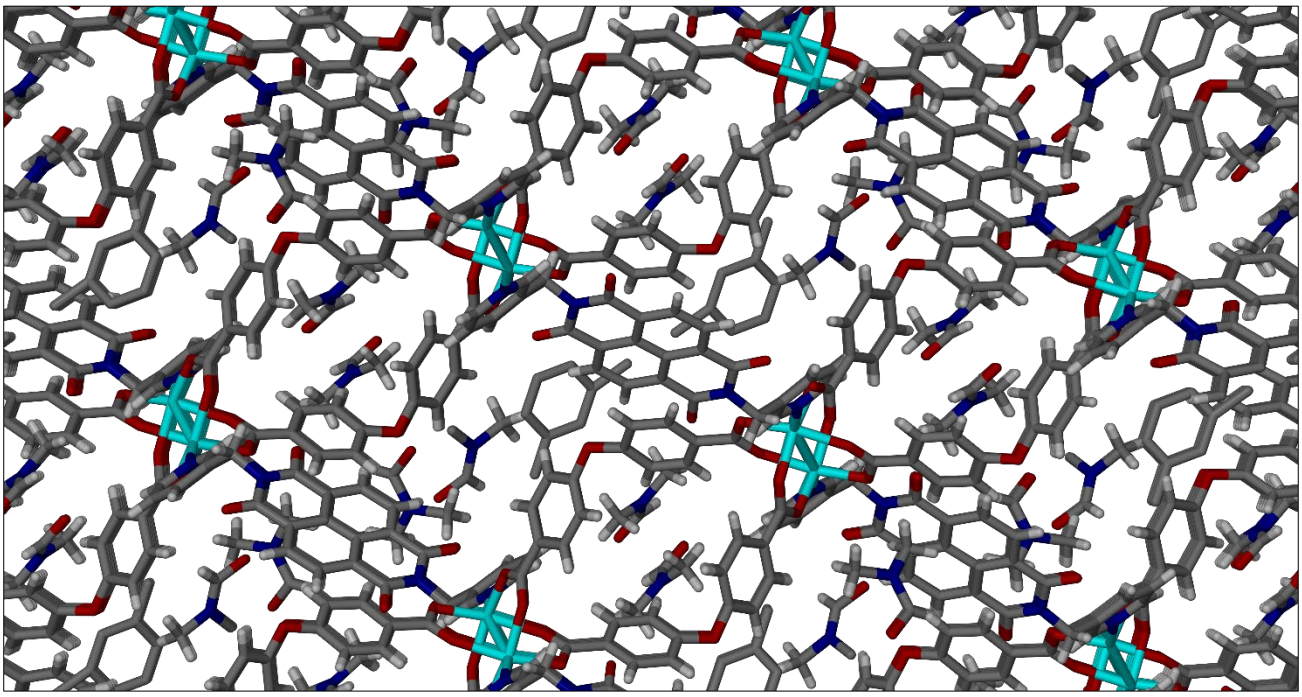

Figure 3.39. The packing diagram of NFDMOF-5-mx viewed in the ac plane. The *meta* xylene isomer is in channels running along the *b* axis.

3.6. NFDMOF-6

3.6.1. Single Crystal X-Ray Diffraction (SCXRD)

NFDMOF-6 was synthesized from the solvothermal reaction of Lig5 (20 mg; 0.055 mmol), 2,2-bipyridine (8.59 mg; 0.055 mmol) and zinc(II) nitrate hexahydrate (32.7 mg; 0.109 mmol) in 5 mL DMF. NFDMOF-6 crystallizes in the orthorhombic space group *Pbca*. The asymmetric unit of this MOF consist of a Lig5 molecule, one DMF molecule, 2.2'-bipyridyl molecule and zinc(II) cation (Fig 3.40). The packing diagram showing the overall arrangement of the molecules viewed in the *ac* plane is presented in Fig 3.41.

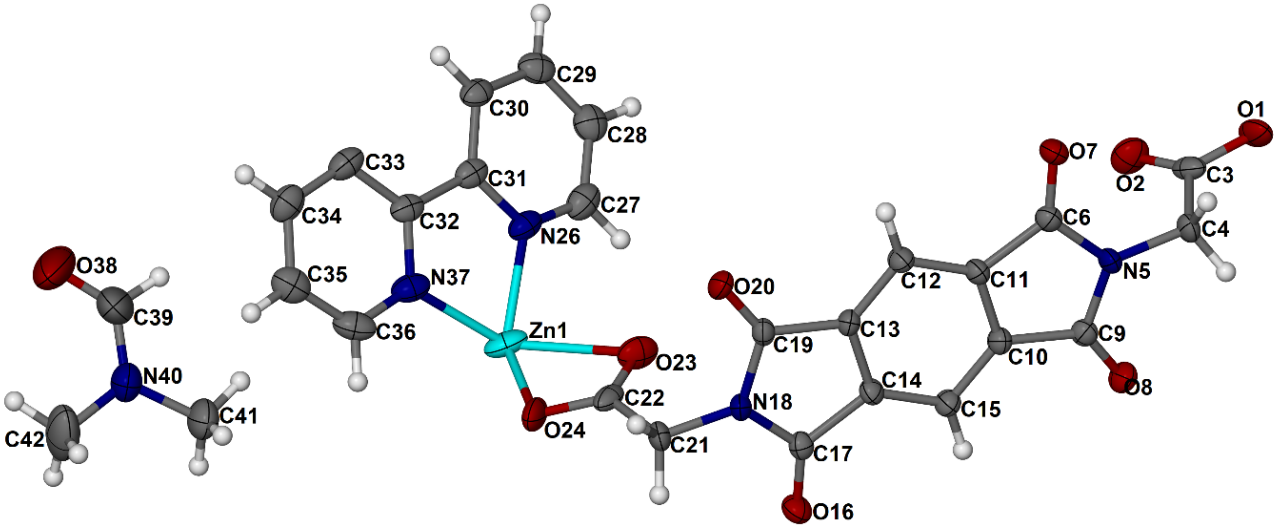

Figure 3.40. The asymmetric unit of NFDMOF-6 showing the crystallographic labelling scheme. Ellipsoids are shown at the 70% probability level.

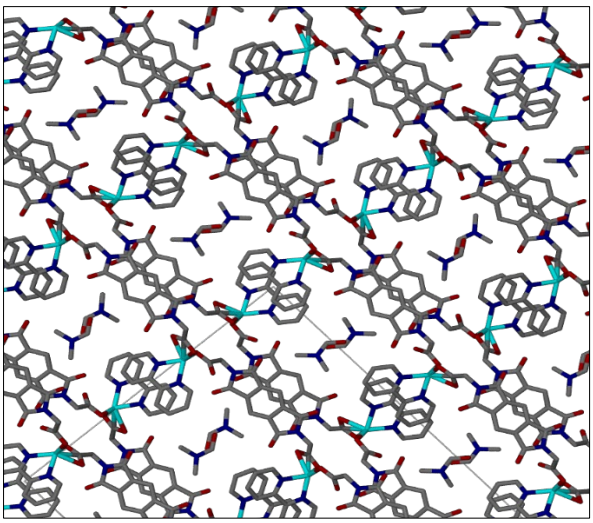

Figure 3.41. The packing diagram of NFDMOF-6 viewed in the *ac* plane. The DMF molecules are in channels running along the *b* axis.

3.6.2. Thermogravimetric Analysis (TGA)

The thermal profile of the as-synthesized **NFDMOF-6** shows a weight loss of 13.28 % within the temperature range of 21.54 °C to 246.60 °C which is attributed to the loss of one DMF molecule (calculated 10.50%). The framework remains stable with no significant changes from 246.60 °C to 339.11 °C after which decomposition commences. The activated phase of **NFDMOF-6** was prepared by heating the as-synthesized crystals at 100 °C for 24 hours under vacuum. The TGA profile of the activated phase shows no weight loss from 21.54 °C to 375.02 °C which confirms that the activation process was successful. The TGA traces of the as-synthesized and activated **NFDMOF-6** are presented in Fig 3.42.

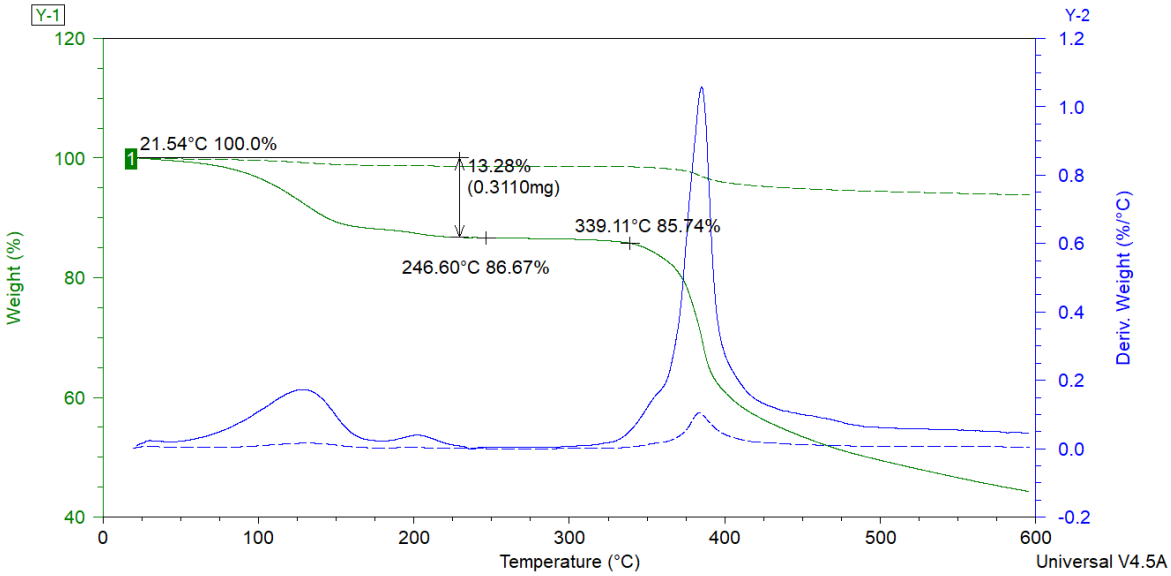

Figure 3.42. TGA profiles of the as-synthesized **NFDMOF-6** (solid green) and the activated phase (dashed green) as well as the first derivatives of the weight %: as-synthesized (solid blue) and activated (dashed blue).

3.6.3. Powder X-Ray Diffraction (PXRD)

PXRD was used to confirm bulk phase purity of **NFDMOF-6** and the stability of the MOF after activation process. The PXRD patterns are presented in Fig 3.43. The PXRD patterns of the as-synthesized and activated plots are similar which indicates that the framework remains intact, it does not collapse during the activation process, and that the framework maintains crystallinity. The PXRD of the as- synthesized and the simulated graphs match confirming that the compound is pure.

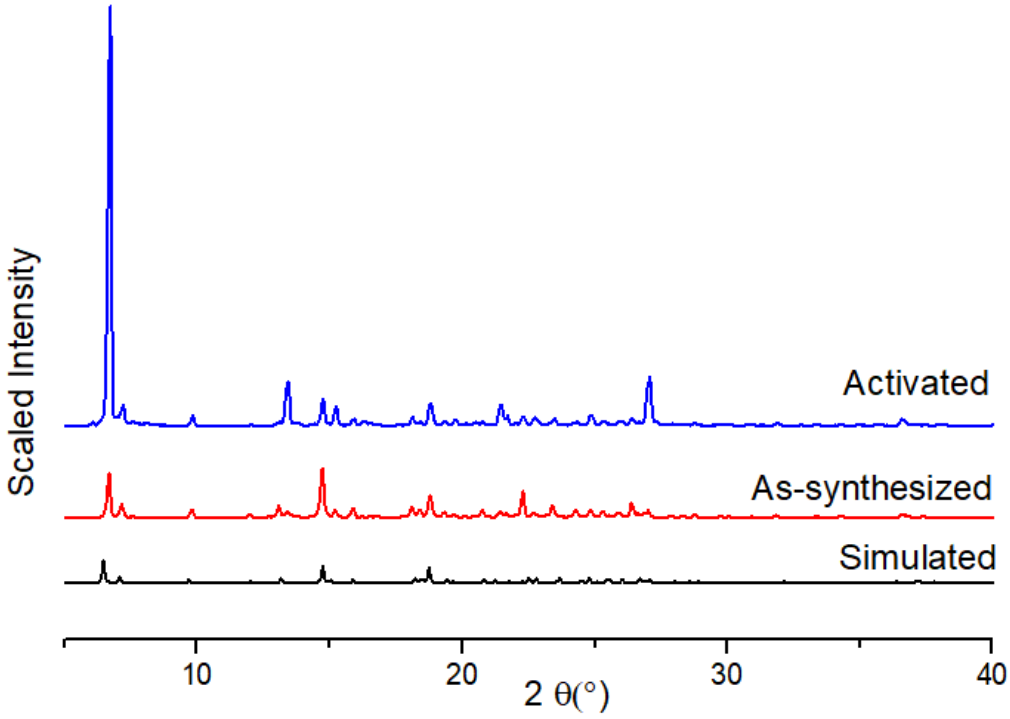

Figure 3.43. The PXRD patterns of as-synthesized **NFDMOF-6** (red), activated **NFDMOF-6** (blue) and simulated **NFDMOF-6** (black).

3.7. SUMMARY

Six (6) novel metal organic frameworks were successfully synthesized and characterized using SCXRD, TGA, and PXRD. TGA was used to determine the thermal stability of the MOFs and the amount of guest included in the channels. The most thermally stable MOF as revealed by TGA is **NFDMOF-5** (decomposes at 359 °C) and the least thermally stable MOF is **NFDMOF-2** (decomposes at 312 °C). The MOFs that maintain crystallinity during the activation process are **NFDMOF-2, NFDMOF-4** and **NFDMOF-6. NFDMOF-1** and **NFDMOF-5** do not maintain crystallinity as they have broad peaks in the PXRD of the activated phases. The MOF with the largest amount of solvent accessible space is **NFDMOF-5** with 34% of the unit cell volume. Xylene inclusion experiments revealed that only four MOFs could exchange the as-synthesized guest for a xylene isomer. The MOFs that included liquid phase xylene are **NFDMOF-1**, **NFDMOF-2**, **NFDMOF-4**, and **NFDMOF-5**. **NFDMOF-4** also adsorbed the xylene vapour.

3.8. CRYSTALLOGRAPHIC DATA

Table 3.1. Crystallographic data for **NFDMOF-1**, **NFDMOF-2,** and **NFDMOF-3**

Compound	NFDMOF-1	NFDMOF-2	NFDMOF-3
Empirical formula	C_{28} H_{16} Co N_5 O_{11}	C_{28} H_{18} N_3 0_7 Zn	C_{30} H_{25} Cd_2N_6 O_{10}
Formula weight	657.39 g/mol	573.82 g/mol	854.36 g/mol
Temperature	173(2) K	173(2) K	173(2) K
Wavelength	0.71073 Å	0.71073 Å	0.71073 Å
Crystal system, space group	Monoclinic, *C* 2/*c*	Monoclinic, *P* 2(1)/*c*	Monoclinic, *P* 2(1)/*c*
Unit cell dimensions	a = 36.708(2) Å, alpha = 90 °	a = 10.1786(6) Å, alpha = 90 °	a = 18.3523(30) Å, alpha = 90 °
	b = 14.5480(8) Å, beta = 105.837(2) °	b = 19.7427(11) Å, beta = 100.133(1) °	b = 15.0131(25) Å, beta = 113.594(3) °
	c = 14.6965(9) Å, gamma = 90 °	c = 17.0460(9) Å, gamma = 90 °	c = 15.9372(27) Å, gamma = 90 °
Volume	7550.4(7) A^3	3372.0(3) A^3	4024.2(12) A^3
Z, Calculated density	8, 1.044 g/cm^3	43, 12.15 g/cm^3	4, 1.410 g/cm^3
Absorption coefficient	0.508 mm^{-1}	8.263 mm^{-1}	1.110 mm^{-1}
F(000)	2672	12599	1692
Theta range for data collection	1.153 to 25.080 °	1.593 to 28.453 °	1.211 to 29.602 °
Reflections collected / unique	57180 / 6705 [R(int) = 0.0865]	94669 / 6393 [R(int) = 0.0489]	122008 / 8565 [R(int) = 0.0577]
Data / restraints / parameters	6705 / 0 / 370	8481 / 0 / 159	11320 / 0 / 201
Goodness-of-fit on F^2	2.029	2.587	2.289
Final R indices [I>2sigma(I)]	R1 = 0.1475, wR2 = 0.4539	R1 = 0.1838, wR2 = 0.5157	R1 = 0.1616, wR2 = 0.4741
Largest diff. peak and hole	5.623 and -0.888 e.A^{-3}	5.455 and -1.294 e.A^{-3}	12.665 and -1.839 e.A^{-3}

Table 3.2. Crystallographic data for **NFDMOF-4**, **NFDMOF-5,** and **NFDMOF-6**

Compound	NFDMOF-4	NFDMOF-5	NFDMOF-6
Empirical formula	C_{33} H_{28} Co N_4 O_9	C_{27} H_{16} N_2 O_7 Zn	C_{27} H_{19} N_5 0_9 Zn
Formula weight	683.52 g/mol	545.79 g/mol	622.84 g/mol
Temperature	173(2) K	173(2) K	173(2) K
Wavelength	0.71073 Å	0.71073 Å	0.71073 Å

Crystal system, space group	Monoclinic, *C* 2/*c*	Monoclinic, *C* 2/*c*	Orthorhombic, *Pbca*
Unit cell dimensions	a = 27.2474(23) Å, alpha = 90 °	a = 19.2348(45) Å, alpha = 90 °	a = 24.2173(10) Å, alpha = 90 °
	b = 10.5807(9) Å, beta = 114. 707(1) °	b = 18.3220(43) Å, beta = 106.322(4) °	b = 7.9045(3) Å, beta = 90 °
	c = 26.2858(22) Å, gamma = 90 °C	c = 19.2553(45) Å, gamma = 90 °	c = 26.4110(11) Å, gamma = 90 °
Volume	6884.4(10) A^3	6512(3) A^3	5055.7(4) A^3
Z, Calculated density	8, 1.319 g/cm^3	8, 1.113 g/cm^3	101, 20.662 g/cm^3
Absorption coefficient	0.555 mm^{-1}	0.792 mm^{-1}	13.131 mm^{-1}
F(000)	2824	2224	32118
Theta range for data collection	1.645 to 28.321 °	1.566 to 29.594 °	2.282 to 28.302 °
Reflections collected / unique	94353 / 6951 [R(int) = 0.0487]	84546 / 7427 [R(int) = 0.0500]	230371 / 5509 [R(int) = 0.0640]
Data / restraints / parameters	8542 / 0 / 428	9143 / 0 / 149	6288 / 0 / 171
Goodness-of-fit on F^2	1.826	2.410	1.070
Final R indices [I>2sigma(I)]	R1 = 0.1266, wR2 = 0.3795	R1 = 0.1820, wR2 = 0.4829	R1 = 0.1319, wR2 = 0.3270
Largest diff. peak and hole	4.510 and -1.388 $e.A^{-3}$	7.737 and -1.742 $e.A^{-3}$	7.725 and -5.771 $e.A^{-3}$

Table 3.3. Crystallographic data for **NFDMOF-4-px**, **NFDMOF-4-ox, NFDMOF-4-mx** and **NFDMOF-5-mx**

Compound	NFDMOF-4-px	NFDMOF-4-ox	NFDMOF-4-mx	NFDMOF-5-mx
Empirical formula	C_{43} H_{33} Co N_3 O_8	C_{74} H_{70} Co_2 N_8 O_{18}	C_{40} H_{26} Co N_4 O_9	C_{45} H_{28} N_4 O_{14} Zn_2
Formula weight	778.7 g/mol	1477.24 g/mol	765.58 g/mol	1087 g/mol
Temperature	173(2) K	173(2) K	173(2) K	173(2) K
Wavelength	0.71073 Å	0.71073 Å	0.71073 Å	0.71073 Å
Crystal system, space group	*C* 1(2)/*c*1	*P* 2(1)/*n*	*C* 2/*c*	*P* 2(1)/*n*
Unit cell dimensions	a = 27.131(3) Å, alpha = 90 °	a = 26.234(4) Å, alpha = 90 °	a = 27.332(4) Å, alpha = 90 °	a = 26.162(11) Å, alpha = 90 °
	b = 10.6009(13) Å, beta = 114.636(2) °	b = 10.555(15) Å, beta = 115.163(3) °	b = 10.577(14) Å, beta = 115.468(2) °	b = 10.709(4) Å, beta = 115.971(10) °
	c = 26.336(3) Å, gamma = 90 °	c = 27.157(4) Å, gamma = 90 °	c = 26.3138(3) Å, gamma = 90 °	c = 27.4045(11) Å, gamma = 90 °
Volume	6885.09(15) A^3	6806.8(17) A^3	6868.04(15) A^3	6852.6(5) A^3
Z, Calculated density	8, 1.502 g/cm^3	8, 2.883 g/cm^3	8, 1.4810 g/cm^3	8, 2.108 g/cm^3

Absorption coefficient	0.563 mm^{-1}	1.135 mm^{-1}	0.566 mm^{-1}	1.505 mm^{-1}
F(000)	3224	6144	3144	4416
Theta range for data collection	1.651 to 27.501 °	1.423 to 28.290 °	1.650 to 28.325 °	1.440 to 27.132 °
Reflections collected / unique	76560 / 6421/ [R(int) = 0.0633]	80035 / 11835/ [R(int) = 0.0760]	89043 / 7330/ [R(int) = 0.0416]	147843 / 11983/ [R(int) = 0.0629]
Data / restraints / parameters	7904 / 0 / 479	16865 / 0 / 17	8549 / 0 / 9	15114 / 0 / 331
Goodness-of-fit on F^2	1.046	8.106	12.470	2.673
Final R indices [I>2sigma(I)]	R1 = 0.08331, wR2 = 0.1935	R1 = 0.6249, wR2 = 0.8704	R1 = 0.6036, wR2 = 0.8839	R1 = 0.2191, wR2 = 0.5479
Largest diff. peak and hole	1.207 and -1.144 $e.A^{-3}$	23.510 and -7.669 e.A^-3	5.587 and -1.110 $e.A^{-3}$	9.643 and -2.025 $e.A^{-3}$

CHAPTER 4

CONCLUSION AND FUTURE WORK

4.1. CONCLUSION

In conclusion, five (5) pyridine N donor ligands were successfully designed from a variety of chemical compounds and amino acids. The ligands were characterized using nuclear magnetic resonance (NMR). Six (6) metal-organic frameworks (MOFs) were successfully synthesized from the designed pyridine N donor ligands and carboxylate O donor co-ligands. The MOFs were characterized using single crystal X-ray diffraction (SCXRD), thermogravimetric analysis (TGA) and powder X-ray diffraction (PXRD). The SCXRD revealed that **NFDMOF-1**, **NFDMOF-4** and **NFDMOF-5** have channels extending in three dimensions, while **NFDMOF-2** has 2D channels and **NFDMOF-6** possesses 1D channels. The Mercury program was utilized to estimate the guest accessible volume in the MOFs. It was revealed that **NFDMOF-5** possess the largest guest accessible space accounting for 34 % of the total volume while **NFDMOF-1** has 17.3 %, **NFDMOF-2** has 31.4%, **NFDMOF-3** has 26.1%, and **NFDMOF-4** possess the least guest accessible space amounting to 10.8% of the total volume.

Xylene inclusion experiments were performed whereby the as-synthesized MOFs were immersed into solution of xylenes for about five (5) days. The resultant clathrates were characterized using SCXRD, TGA and PXRD. Four MOFs showed framework adjustability and flexibility to adsorb the xylene isomers inside pores. **NFDMOF-1** and **NFDMOF-2** presented liquid phase adsorption of all xylene isomers as confirmed by TGA and PXRD. However, due to the large channels, the guest molecules could not be modelled in the crystal structures. SCXRD revealed that **NFDMOF-4** partially exchanged DMF for *ortho*, *meta* and *para* xylene, in separate experiments**.** The dynamic-vapour reactions of the activated MOF with the three xylene isomers were recorded separately at room temperature. Sorption kinetics of **NFDMOF-4** were investigated to evaluate its suitability for practical separations. Dynamic vapour sorption of **NFDMOF-4** displayed preferable adsorption of *para*-xylene and *ortho*-xylene over *meta*-xylene isomer. **NFDMOF-5** also presented partial exchange of DMF for *meta*-xylene isomer. Further characterization regarding **NFDMOF-5** *ortho*- and *para*-xylene isomers will be performed in future.

4.2. FUTURE WORK

Due to challenges associated with Covid-19, some of the characterization work could not be completed. Therefore, future work planned for this project includes the characterization of NFDMOF-2-ox, NFDMOF-2-mx, NFDMOF-2-px using SCXRD. Sorption kinetics experiments of activated NFDMOF-1 and NFDMOF-2 and, characterization of the resulting clathrates using TGA and PXRD. Lastly, the clathrates of NFDMOF-5-ox and NFDMOF-5-px will be characterized using SCXRD, TGA and PXRD and, NFDMOF-5-mx will be characterized using TGA and PXRD. Vapour sorption experiments will be done on the activated NFDMOF-5 with all three xylene isomers. The resulting clathrates will be characterized using TGA and PXRD.